REPUBLIQUE ALGERIENNE DEMOCRATIQUE ET POPULAIRE
MINISTERE DE L'ENSEIGNEMENT SUPERIEUR ET DE LA RECHERCHE SCIENTIFIQUE

UNIVERSITE FERHAT ABBAS-SETIF1
UFAS1 (ALGERIE)

THESE

Présentée à

L'institut d'optique et de mécanique de précision

Pour l'obtention du diplôme de

DOCTORAT EN SCIENCES

Option : Optique et mécanique de précision

Présentée par: **GUECHI ABLA**

STUDY OF OPTICAL, ELECTRONIC AND STRUCTURAL PROPERTIES OF ZINTL PHASE KAsSn

Soutenu le : 10/12/ 2015

Devant la commission d'examen :

Président	R. LOUAHDI	Professeur	Université de Sétif 1
Rapporteur	A. MERABET	Professeur	Université de Sétif 1
Examinateurs :	N. BOUARISSA	Professeur	Université de M'Sila
	Z. ROUABAH	MCA	Université de B.B.A

PEOPLE'S DEMOCRATIC REPUBLIC OF ALGERIA
MINISTRY OF HIGHER EDUCATION AND SCIENTIFIC RESEARCH

UNIVERSITY FERHAT ABBAS-SETIF1
UFAS1 (ALGERIA)

THESIS

Presented to

The Institute of Optics and Precision Mechanics

For the abstention of the degree of

DOCTOR OF SCIENCES

Option: Optics and Precision Mechanics

Presented by: **GUECHI ABLA**

STUDY OF OPTICAL, ELECTRONIC AND STRUCTURAL PROPERTIES OF ZINTL PHASE KAsSn

Submited: 10 /12 /2015

Members of the assessment committee:

President	R. LOUAHDI	Professor	University of Setif 1
Supervisor	A. MERABET	Professor	University of Setif 1
Examiners:	N. BOUARISSA	Professor	University of M'Sila
	Z. ROUABAH	MCA	University of B.B.A


بسم الله الرحمن الرحيم

TABLE OF CONTENTS

Chapter III: Results and Discussion

Appendix

LIST OF FIGURES

CHAPTER I

CHAPTER II

CHAPTER III

APPENDIX

LIST OF TABLES

ACKNOWLEDGEMENTS

First and foremost I want to thank by god for all things

I am also very grateful to my advisor Prof Merabet Abdelali, the person without whom this thesis would never have come to life. It has been an honor to be his Ph.D. student. I appreciate his continuous support, his patience and useful critiques of this research work.

I would like to thank my Prof Chegaar Mohamed for supporting me during these past years. I will be thankful to him forever. First, he has provided insightful and fruitful discussions, comments and advices about research. When discussing with him, you can feel his solid background on physics and mathematics. I am very grateful for his scientific advice and knowledge and many insightful discussions and suggestions. He is my primary resource for getting my science questions answered.

I present my sincere thanks to Prof Louahdi Rachid and Prof Nadir Bouarissa for kindly accepting to referee this thesis and Dr Rouabah Zahir equally for accepting to be a member of my thesis committee. I am grateful for their thoughtful and detailed comments

Finally, many thanks to my mother for her encouragement and constant support and unconditional love

I would like to dedicate this thesis to, the memory of my father, To Mouna, Noura, Ahmed chocho, Sara, Melouk,, Omaima and Alae.

GENERAL INTRODUCTION

The fascination for solid state chemistry and the more applied field of material science not only arises from the structural diversity and the curiosity driven research but also from the often exciting physical properties of the compounds. In general solid state chemistry is truly interdisciplinary as it borders solid state physics, crystallography, quantum theory, metal science and inorganic chemistry.

Exploration of the alkali metal, alkaline-earth metal systems has revealed a vast array of new chemistry and novel structure types. The structures and properties of these new materials have been studied in an attempt to understand the chemistry of these and other related systems.

Most of these materials possess a metallic luster indicative of an intermetallic compound, which is correct in some cases, but upon further analysis, a majority of these compounds exhibit closed shell bonding along with the corresponding semiconducting and diamagnetic properties [1-3].

Alloys and intermetallic compounds are among the oldest and most important man made materials, being subject of constant interest for inorganic chemists, physicists and material scientists [4-10]. Intermetallics are phases composed of two or more metallic or semi-metallic elements with stoichiometry that displays little or no phase width. Unlike alloys, they are typically formed by elements with significantly different sizes and electro-negativities which results in atoms with preferred crystallographic sites, limiting site mixing between elements. There is an electronegativity difference which results in some charge transfer; however, the valence electrons are still largely delocalized resulting in metallic or semi-conducting phases and most do not follow electron-counting rules. Intermetallics then are in a middle ground between localized, charge balanced salts and conducting delocalized metals which can lead to interesting magnetic and electronic properties.

Today, the important research areas of intermetallic compounds are very broad and range from refractory high-strength super alloys [11-13], magnetic compounds [14-16] and superconductors [17-18], to metallic glasses for possible applications in fuels cells [19], Furthermore, the possibility of functional intermetallic materials has been validated by several discoveries of polar intermetallics and Zintl phases that display complex combinations of structural, electronic, thermal, magnetic, and transport properties.[20-21].

A large number of new intermetallic compounds have been synthesized, and their structural and electronic characterizations have given tremendous information about their structure property relationship [22-29], e.g. Yb_3CoSn_6 and $Yb_4Mn_2Sn_5$, $La_{11}Li_{12}Ge_{16}$, and Zr_3Co, InPd, $A_3In_2Ge_4$ and $A_5In_3Ge_6$ (A=Ca, Sr, Eu, Yb), $U_{34}Fe_{4-x}Ge_{33}$ and $Yb_3Pd_2Sn_2$.

The properties are typically more consistent with valence (salt-like) compounds and therefore these materials can be viewed as a link between typical intermetallic phases on one hand, and normal valence compounds on the other. This category of materials has become known as *Zintl phase*. It is the merit of Eduard Zintl (1930) [4-6], and others that some easily applicable rules exist for this subgroup of intermetallic compounds.

Zintl phases are a special class of intermetallic compounds in which one of the components is far more electropositive than the other(s). They are at the extreme polar end of intermetallics, featuring complete or nearly complete charge transfer between atoms resulting in a charge balanced structure with localized electrons similar to a salt.

The structural peculiarities of Zintl phases are explained by assuming the presence of both ionic and covalent parts in the bonding picture. Within the Zintl-Klemm concept [30], all valence electrons can be assigned, at least formally, to the electronegative main group elements. The electrons are then localized either in two-center-two-electron (2c-2e) bonds between post-transition metal atoms or in the form of lone pairs located at these atoms. In that sense, the fundamental difference between Zintl phases and all other intermetallic phases is the role played by the electronegative components, which accept the electrons from their more electropositive partners to form polyanions. Between Zintl phases and intermetallic phases a further class is situated, which is denoted as “polar intermetallic compounds”.

Interest in the study of these compounds has increased markedly in recent decades, deriving mainly from the rich structural variety shown by these compounds, as well as the evident or prospective simplicity of their bonding schemes among polar intermetallic compounds. Examples include K_2ACdSb_2 (A= Sr, Ba), $Ba_3T_2As_4$ (T=Zn, Cd), $A_{21}Zn_4Pn_{18}$ (A=Ca, Eu; Pn=As, Sb), Na_2ACdSb_2 and K_2ACdSb_2 (A=Ca, Sr, Ba, Eu, Yb), $KBa_2Cd_2Sb_3$, AM_2Sb_2 (A=Ca, Sr, Ba, Eu, Yb; M=Zn, Cd), $Ba_3Al_3P_5$ and $Ba_3Ga_3P_5$ [31-37] and the specific ternary Zintl compound mentioned in this work is KAsSn which despite being isoelectronic, adopts the structure of KSnSb and crystallizes in the space group P 63/mc (No. 186) [38]. From the crystal structure, it is known that KSnAs contains three bonded Sn and As /Sb atoms which consist of puckered sheets with the potassium cations between the sheets. The structures KAsSn can be interpreted in terms of the Zintl concept [39-40] which is isovalent and isostructural with KSnSb [38]. Using the Zintl concept to interpret the chemical bonds in KAsSn, the arrangement of the atoms in this compound suggests that the almost free valence electrons of K are transferred to the Sn/As substructures to form saturated covalent bonds between Sn and As according to the octet rule.

The fundamental basis of understanding the different properties of materials and phenomena relies upon understanding their electronic structure. Indeed, developing theoretical approaches that can accurately describe a system of interacting particles, electrons and nuclei, emerged as a serious challenge encountering theoretical physics. An exact theory for a system of ions and interacting electrons is intimately quantum mechanical based on solving a many body Schrödinger equation which is evidently complex.

The large computational complexity of calculations involving modified structures does not permit a comparable progress in the field of modeling as in the experimental counterpart. This complexity arises from the need to include a large number of atoms in the computer simulation, as well as from the accuracy required to treat systems in a realistic manner.

Ab-initio calculations have become an efficient tool to understand characteristic properties of materials and which provides interpretation for experimentally observable phenomena. In the framework of density functional theory [41] it is now possible to calculate the geometry, the electronic structure, and the excitations of systems with hundreds of electrons starting from first principles. No empirical parameters have to be included, in principle, in these numerical simulations and the results can be directly compared with experiment.

There is an abundance of program packages to calculate the properties of materials from first principles. The DFT (Density Functional Theory) tool chosen for this work was the CASTEP (Cambridge Serial Total Energy Package) [42] simulation package codes which is an electronic minimization code that uses calculates optimal geometry, total energy, force, stress as well as band structures and optical spectra, etc... In particular it has a wide range of spectroscopic features that link directly to experiment, such as infra-red, Raman spectroscopies, and core level spectra.

In the context of investigating the realization of specific structural patterns and changes of chemical bonding in solids, high pressure is one of the fundamental state variables which can be varied in order to uncover factors governing stability fields of structure and bonding types as well as to separate electronic effects from packing aspects. Simultaneously, it is a useful parameter in quantum chemical investigations since the compression can be easily simulated in the calculations by a corresponding reduction of unit cell parameters.

The main objective of this thesis is a study of optical, electronic and structural properties of ternary Zintl phase KAsSn compound using density-functional theory (DFT) method within the generalized gradient approximation developed by Wu-Cohen (GGA-Wc).

Layout of the Dissertation

In what follows, this PhD work is presented, firstly, a brief introduction to intermetallic and Zintl phase compounds is given, followed by a discussion of *Ab-initio* calculations, within the framework of density functional theory (DFT) using the CASTEP code.

This dissertation consists of three chapters with one appendix, all of which include experimental and theoretical studies as well as physical properties of the Zintl phases KAsSn. A brief summary of each chapter is described below:

In ***Chapter I***, we describe the progress of studies on intermetallic compounds especially Zintl phase. We show the remarkable success of the Zintl concept in rationalizing crystal structure, stoichiometry, and chemical bonding of the main group intermetallics.

The experimental and theoretical studies of structural and electronic properties of Zintl phase KAsSn, are presented in ***Chapter II*****.** We summarize previous theoretical works on these compounds. Then, we present our contribution to investigate physical properties of Zintl phase KAsSn and the method of calculation used in this work.

The last chapter (***Chapter III*****)** is devoted to the presentation of our results for the ternary Zintl phase KAsSn compound including structural, electronic, elastic and optical properties.

Finally, we give conclusions of this work. This manuscript is completed by an annex on the Density Functional Theory DFT

References

[1] M. R. Castillo et al., Theoretical study of the closed-shell d10–d10 Au(I)–Cu(I) attraction in complexes in extended unsupported chains, Computational and Theoretical Chemistry, 965(1), pp 163-167, 2011.

[2] X.H Chen et al., Generation of curved or closed-shell carbon nanostructures by ball-milling of graphite, Journal of Crystal Growth, 218 (1), pp57-61, 2000.

[3] S. F. Matar et al., Electronic and magnetic structures and bonding properties of Ce_2T_2X (T = nd element; X = Mg, Cd, Pb or Sn) intermetallics from first principles, Intermetallics, 51, pp 18-23, 2014.

[4] E. Zintl, Dullenkopf, W. Z. Phys. Chem., B16, 183, 1932.

[5] E. Zintl, Brauer, G. Z. Phys. Chem. B20, 245, 1933.

[6] E. Zintl, Angew. Chem., 52, 1, 1939

[7] W. Hume-Rothery, J Inst Metals 35:296, 1926.

[8] H. Schäfer, B. Eisenmann, W. Müller, Zintl Phases: Transitions between Metallic and Ionic Bonding. Angew. Chem. Int. Ed., 12, 694–712, 1973.

[9] Nesper. R, Chemical bonding-intermetallic compounds. Angew. Chem.,103 (7):805-34 1991.

[10] R. Demchyna et al., High-pressure crystal chemistry of binary intermetallic compounds, Z. Kristallogr, 221,420–434, 2006.

[11] F. Zhang et al., Effect of welding parameters on microstructure and mechanical properties of friction stir welded joints of a super high strength Al–Zn–Mg–Cu aluminum alloy, Materials & Design, 67, pp 483-491, 2015.
[12] M. Sadeghian, M. Shamanian, A. Shafyei, Effect of heat input on microstructure and mechanical properties of dissimilar joints betweensuper duplex stainless steel and high strength low alloy steel,Materials & Design, 60, pp 678-684, 2014.
[13] Y. Zuo et al., Effect of low frequency electromagnetic field on the constituents of a new super highstrength aluminum alloy, Journal of Alloys and Compounds, 402, 1–2, pp 149-155, 2005.
[14] L. Cui et al., Effect of Cu doping on the magnetic and magnetocaloric properties in the HoNiAlintermetallic compound, Journal of Alloys and Compounds, 622, pp 24-28, 2015.
[15] R. Mondal, R. Nirmala, J. A. Chelvane, A.K. Nigam, Magnetic and magnetocaloric properties of rare earth intermetallic compounds $HoCo_{2-x}Ni_x$(x=0.75 and 1.25), Physica B: Condensed Matter, 448, pp 9-12, 2014.
[16] B.V. Neamţu, influence of wet milling conditions on the structural and magnetic properties of Ni_3Fe nanocrystalline intermetallic compound, Intermetallics, 19 (1), pp 19-25, 2011
[17] C. Mazumdar, R. Nagarajan, Quaternary boro carbides: Relatively high Tc intermetallic superconductors and magnetic superconductors, Physica C: Superconductivity and its Applications, Volume 514, pp173-183, 2015.
[18] R.J. Cava, et al., Good news from an abandoned gold mine: A new family of quaternary intermetallic superconductors, Physica C: Superconductivity, 235–240, Part 1, pp 154-157, 1994.
[19] F. Smeacetto et al., Electrophoretic deposition of $Mn_{1.5}Co_{1.5}O_4$ on metallic interconnect and interaction with glass-ceramic sealant for solid oxide fuel cells application, Journal of Power Sources, 280, pp 379-386, 2015
[20] B. Penc, A. Winiarski, A. Szytuła, D. Kaczorowski, Magnetic, transport and electronic properties of $CeAu_{1-x}Ni_xIn$ intermetallics, Journal of Alloys and Compounds, 569, pp 22-28, 2013.
[21] N. Guechi et al., First-principles prediction of the structural, elastic, electronic and optical properties of the Zintl phases MIn_2P_2 (M = Ca, Sr), Journal of Alloys and Compounds, 577, pp 587-599, 2013.
[22] J. H. Kim, M. Nakamichi, Synthesis of Be–Ti–V ternary beryllium intermetallic compounds, Journal of Alloys and Compounds, 640, 15 , pp 285-289,2015.
[23] Y. Jung et al, Crystal structure and chemical bonding of novel Li-containing polar intermetallic compound $La_{11}Li_{12}Ge_{16}$, Journal of Solid State Chemistry, 196, pp 543-549, 2012.
[24] A. H. Moghadam et al., Development of a nanostructured Zr_3Co intermetallic getter powder with enhanced pumping characteristics, Intermetallics, 57, pp 51-59,2015.
[25] M. Hahne, P. Gille, Single crystal growth of the intermetallic compound InPd, Journal of Crystal Growth, 401, pp 622-626, 2014.
[26] T.S You, S. Bobev, Synthesis and structural characterization of $A_3In_2Ge_4$ and A_5In_3Ge6 (A=Ca, Sr, Eu, Yb)—New intermetallic compounds with complex structures, exhibiting Ge–Ge and In–In bonding, Journal of Solid State Chemistry, 183,(6), 2010, pp 1258-1265.
[27] M.S. Henriques et al., A novel ternary uranium-based intermetallic $U_{34}Fe_{4-x}Ge_{33}$: Structure and physical properties, Journal of Alloys and Compounds, 606, pp154-163, 2014.

[28] P. Solokha,et al., Structural and physical properties of the new intermetallic compound $Yb_3Pd_2Sn_2$, Journal of Solid State Chemistry, 184 (9), pp 2498-2505, 2011.
[29] X.W. Lei et al, Yb_3CoSn_6 and $Yb_4Mn_2Sn_5$: New polar intermetallics with 3D open-framework structures, Journal of Solid State Chemistry, 181(9), pp 2448-2455,2008.
[30] W. Klemm, and E. Busmann, Z. Anorg. Allg. Chem.,319,297,1963.
[31] S. Azam, A.H. Reshak, Theoretical study of the new zintl phases compounds K_2ACdSb_2 (A= (Sr, Ba)), Physica B: Condensed Matter, 464, pp 9-16, 2015.
[32] J. Wang et al., Syntheses, crystal structure and physical properties of new Zintl phases $Ba_3T_2As_4$ (T=Zn, Cd), Journal of Solid State Chemistry, 198, 2013, Pages 6-9
[33] N. T. Suen et al, Synthesis, crystal structures, and physical properties of the new Zintl phases $A_{21}Zn_4Pn_{18}$ (A=Ca, Eu; Pn=As, Sb) Versatile arrangements of [ZnPn4] tetrahedra, Journal of Solid State Chemistry, 227, pp 204-211, 2015.
[34] B. Saparov, M. Saito, S. Bobev, Syntheses, and crystal and electronic structures of the new Zintl phases Na_2ACdSb_2 and K_2ACdSb_2 (A=Ca, Sr, Ba, Eu, Yb): Structural relationship with Yb_2CdSb_2 and the solid solutions $Sr_{2-x}A_xCdSb_2$, $Ba_{2-x}A_xCdSb_2$ and $Eu_{2-x}Yb_xCdSb_2$, Journal of Solid State Chemistry, 184, I2, pp 432-440, 2011.
[35] S. A. Khan, A.H. Reshak, Optoelectronic and transport properties of Zintl phase $KBa_2Cd_2Sb_3$ compound, Computational Materials Science, 95, pp 328-336, 2014.
[36] K. Guo et al., Zintl phase compounds AM_2Sb_2 (A=Ca, Sr, Ba, Eu, Yb; M=Zn, Cd) and their substitution variants: a class of potential thermoelectric materials, Journal of Rare Earths, 31 (11), pp 1029-1038, 2013.
[37] Z. Feng, Origin of different thermoelectric properties between Zintl compounds $Ba_3Al_3P_5$ and $Ba_3Ga_3P_5$: A first-principles study, Journal of Alloys and Compounds, 636, pp 387-394, 2015.
[38] K.H. Lii, R.C. Haushalter, J. Solid State Chem., 67, pp. 374–378, 1987.
[39] J. Klein, B. Eisenmann, Mater. Res. Bull., 23 pp. 587–594, 1988.
[40] A. Guechi et al., Pressure effect on the structural, elastic, electronic and optical properties of the Zintl phase KAsSn, first principles study, Journal of Alloys and Compounds, 623, pp 219–228, 2015.
[41] P. Geerlings, F. D. Proft, and W. Langenaeker, Chem. Rev. 103, 1793, 22, 2003.
[42] Segall, M. D.; Lindan, P. J. D.; Probert, M. J.; Pickard, C. J.; Hasnip, P. J.; Clark, S. J.; Payne, M. C.: First-principles simulation: ideas, illustrations and the CASTEP code. J. Phys. Cond. Matter. 14 , 2717–2744,2002.

CHAPTER I
ZINTL PHASES

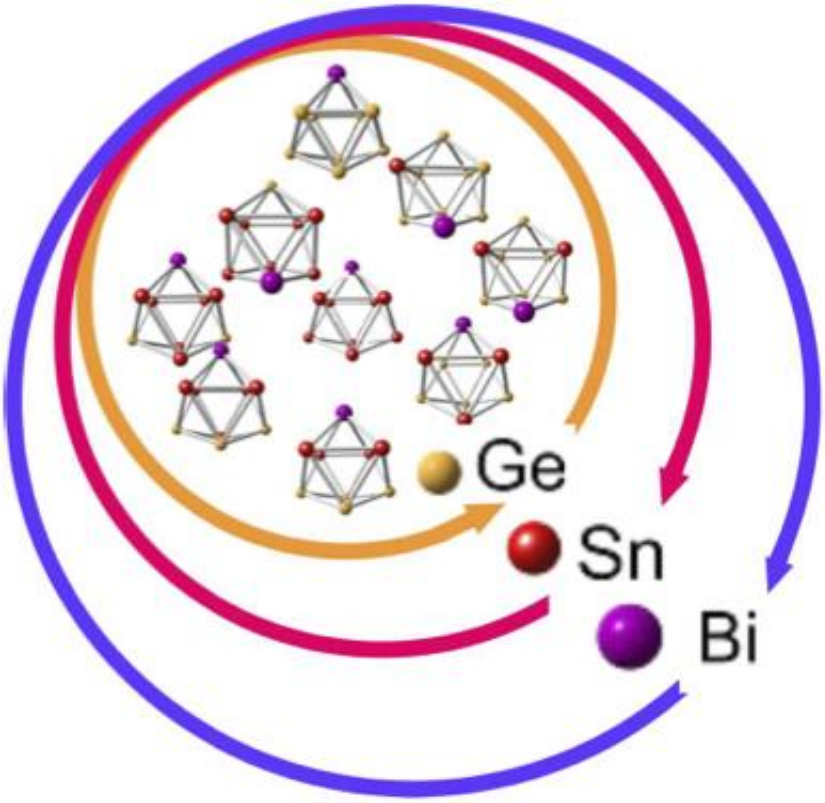

CHAPTER I
ZINTL PHASES

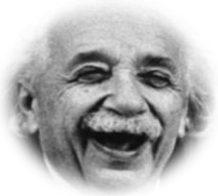

" Know where to find the information and how to use it- that´s the secret of success. "

Albert Einstein

Contents

Preamble

Since the Zintl phase is the main chemical compound around which this doctoral thesis is developed, it is appropriate to devote a chapter to describing their most physical properties. To cope with this work, we present first an overview of concepts and developments revealing the potential of intermetallic and Zintl phase compounds in fundamental as well as applied research. After briefly discussing the generalized 8-N rules, the Zintl-Klemm model and related ideas are discussed. Then the progress in the field of Zintl phases from Zintl's original ideas to the application of these compounds in materials science is outlined. We have also shown the remarkable success of the Zintl concept in rationalizing crystal structure, stoichiometry, and chemical bonding of many main group intermetallics. Finally this study has shown that Zintl phase compounds exhibit a rich diversity of crystal structures like cluster, clathrate, etc.

I.1 Introduction

In recent decades, a large number of inorganic compounds have been synthesized and their study has given much information about structure - property relationships in the field of semiconductor cluster or Zintl compounds. On the other hand, the structures and properties associated with main group intermetallics found in the boundary region between metals and non metals have generated interest within the solid state community [1]. In the course of time, intermetallic chemistry has become what it is today, namely one of the most diverse research areas which can be viewed as the staging area of different scientific fields; mainly chemistry, physics, metallurgy, material science and engineering (Fig I.1)

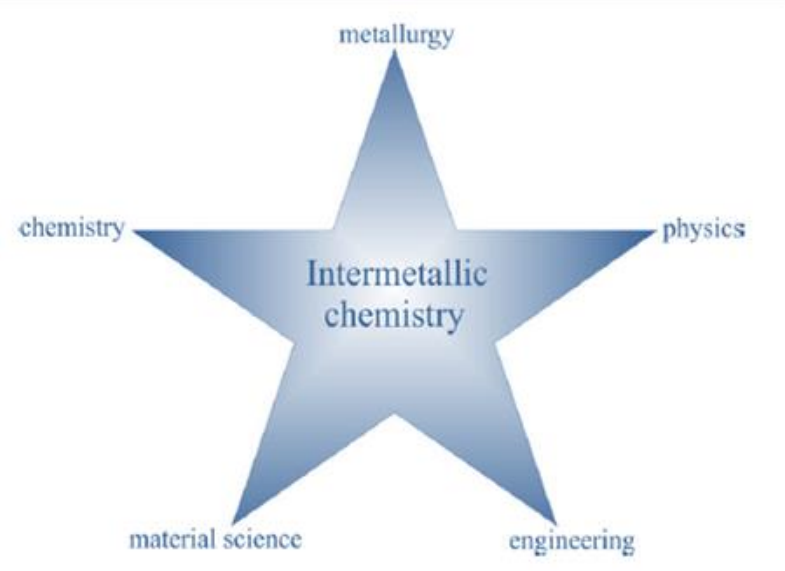

Fig I.1 Components of intermetallic chemistry

Intermetallic phases comprise a realm of staggering structural diversity. One of the best compasses for navigating this realm is the grouping of compounds according to the electronegativity differences of their component elements. At one extreme are the Zintl phases, whose large electronegativity values allow for the conceptual division of their structures into cationic and anionic components, which individually satisfy molecular bonding schemes [2-3]. At the other extreme are the Hume-Rothery phases in which the low electronegativity value result in the vanishing of clear charge assignments or localized bonds [4]. Nevertheless, we still know much less about structure and chemical bonding in Zintl phases and intermetallic compounds than in other classes of chemical compounds. However, the chemical bonding exhibited by these compounds is complex and cannot be classified according to classical bonding theories.

A representation of the correlation between classes of chemical compounds, electron counts, and structural elements can be seen in Fig. I.2. Among the earliest systems to be understood electronically were the salt-like compounds, in which cationic and anionic components attain a complete octet or an 18-electron shell [5-7].

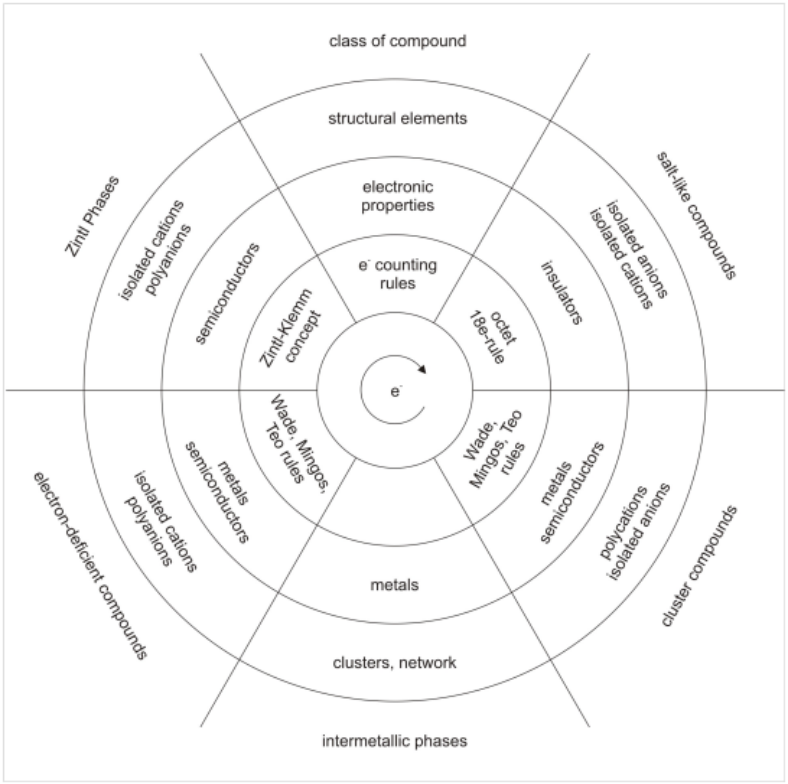

Fig I.2 Relations between classes of chemical compounds through the comparison of structural elements, electronic properties, and electron-counting rules [8].

The Zintl phases, with their various anion frameworks, now form a large family of compounds whose electron structures mostly conform to the 8-N rule. They are a special class of intermetallic compounds, which are composed of the alkali, alkaline-earth metals, and rare earth metals in combination with the early post-transition metals and semi-metals [9]. In that sense, the fundamental difference between Zintl phases and all other intermetallic phases is the role played by the electronegative components, which accept the electrons from their more electropositive partners to form polyanions. Borderline cases of Zintl phases, that is, those exhibiting "locally delocalized electrons" and not conforming to either the 8-N rule or the Zintl-Klemm concept, mark the transition to the intermetallic phases. With the great expansion of Zintl concept and intermetallic compounds recently, a large number of these compounds are synthesized and these diverse structures also bring abundant physical properties, such as, magnetism [9-13] semiconducting, [15-16] mixed-valence [14] and so on. Since Zintl phases provide structural and electronic connections among the traditional classes of metallic, covalent, and ionic compounds, these three classifications can be demonstrated using a van Arkel–Ketelaar triangle, illustrated in Fig. 1.3 [17-18]. This triangle is constructed quantitatively, using as the horizontal coordinate the sum of configuration energies [19-21], and as the vertical axis, their difference for binary compounds. The classical metals are found around the lower left vertex of the triangle. Here, both the average *CE* and Δ*CE* are small, and the valence electrons are largely delocalized.

In reciprocal space, valence electrons populate continuous energy bands without band gaps around the Fermi level. As we deviate from the metallic region, valence electrons tend to localize. At the top vertex, around which ionic compounds are found, Δ*CE* is large, and the valence electrons tend to localize around the atoms with higher *CE*. Toward the lower right vertex, the average *CE* increases while Δ*CE* remains small, and, thus, valence electrons tend to localize between atoms. Along the base of the triangle, therefore, metals transform to covalent crystals. Due to the different behaviors of valence electrons in metallic, ionic, and covalent solids, each of them typically employs its own structural rationalization. Zintl phases can be assigned to a region between the metallic and ionic corners, but they merge with the covalent region as well. Recently, significant research effort has focused on so-called *polar intermetallics*, which show many features of Zintl phases except that their structures typically do not follow the 8-N rule [22-23].

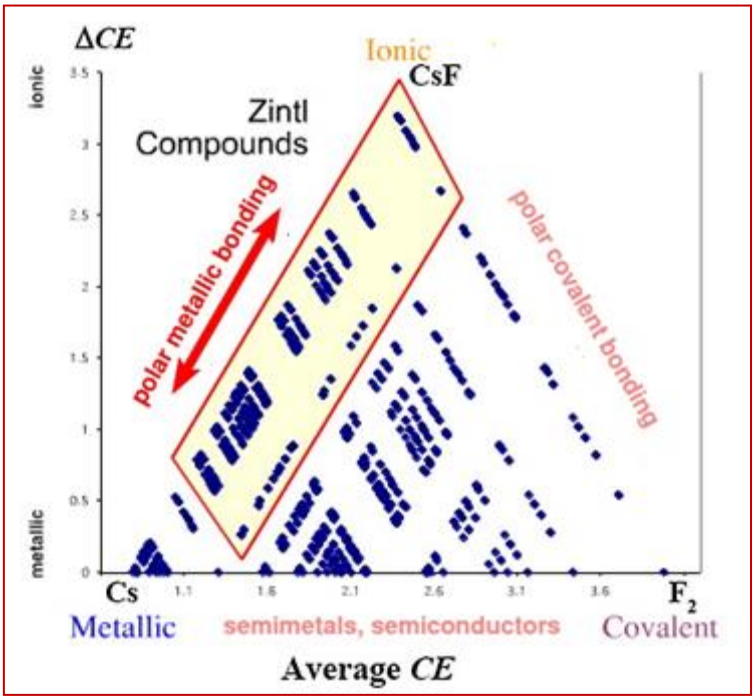

Fig I.3 Van Arkel–Ketelaar triangle for binary compounds. The base of the triangular map consists of elements ranging from Cs to F and the apex is the most "ionic" compound, CsF [17-18].

I.2 Electron Counting Rules

I.2.1 Generalized 8-N Rule

The octet principle can be expressed as a formula by the *generalized 8-N rule* according to E. Mooser & W.B. Pearson [24-25]. We restrict our considerations to binary compounds M_mX_x, and propose the following:

1. X is element of 4th to 7th main group of the periodic table. An X atom has $e(X)$ valence electrons.
2. The electrons needed to fill up the electron octet at X are supplied by the more electropositive M electron. An M atom has e (M) valence electrons.

The compound M_mX_x can be called a normal valence compound if the number of valence electrons of cations e *(M)* and anions $e(X)$ correspond to the relation:

$$m.\ e(M) + x\ .\ e(X) = 8x \quad (\textit{normal valence compound rule, octet rule}) \qquad \text{(I.1)}$$

If covalent bonds exist between M atoms, then not all of the *e(M)* electrons of M can be turned over to X, and the number *e(M)* in equation (I.1) must be reduced by the number *b(MM)* of covalent bonds per M atom. If the M atoms retain nonbonding, then *e(M)* must also be reduced by the number E of these electrons. On the other hand, the X atoms require fewer

electrons if they take part in covalent bonds with each other; the number $e(X)$ can be increased by the number $b(XX)$of covalent bonds per X atom:

$$M\,[e(M) - b(MM) - E] + x\,[e(X) + b\,(XX)] = 8x \qquad (I.2)$$

In several compounds, the so-called Valence-Electron Concentration (*VEC*) proved to be a parameter relevant to their composition, structure and stability [26-27].

For a compound M_mX_x, the *VEC* parameter is defined by:

$$VEC = (m.\ e\ (M) + x.\ e(X))/\ (m+ x) \qquad (I.3)$$

We define the valence electron concentration per anion, *VEC(X)*, as the total number of all valence electrons in relation to the number of anionic atoms:

$$VEC(X) = [m\ .e(M) + x.\ e(X)]/\ x \qquad (I.4)$$

I.2.2 Tetrahedral structures: In a more limited field than that of the previously considered general octet rule, it may be useful to mention the 'tetrahedral structures' which form a subset of the general valence compounds. According to Parthe [28-29], if each atom in a structure is surrounded by four nearest neighbours at the corner of a tetrahedron, the structure is called *normal tetrahedral structure*.

The general formula of the normal tetrahedral structure, for the compound M_mX_x is:

$$(m.\ e\ (M)\ + x.\ e(X)) = 4(m + x) \qquad (I.5)$$

That may be considered a formulation of the so-called Grimm and Sommerfeld Rule [30].

The following specialized cases are of importance:

❖ **Elements**. For pure elements that belong to the right side of the Zintl line, we have m = 0, $VEC(X) = e(X) = N$, and equation (I.2) becomes:

$$b\ (XX) = 8\text{-}VEC(X) = 8\text{-}N \qquad (I.6)$$

This is other than the simple *8-N* rule.

❖ **Polyanionic compounds**. The *M* atoms lose all their valence electrons to the *X* atoms, no cation–cation bonds occur and no nonbonding electrons remain at the cations, $b(MM) = 0$ and $E = 0$. Equation (I.2) then becomes:

$$b\ (XX) = 8\text{-}VEC(X) \qquad (I.7)$$

This is again the 8-N rule, but only for the anionic component of the compound.

According to this concept, put forward by E. Zintl and further developed by W. Klemm and E. Busmann [31], the more electronegative partner in a compound is treated like that element

which has the same number of electrons. This statement is therefore a specialized case of the general rule according to which isoelectronic atom groups adopt the same kind of structures.

❖ **Polycationic compounds**. Provided that no covalent bonds occur between the anionic atoms, *b(XX)*=0, equation (I.2) becomes:

$$b(MM) + E = (x/m)\,(VEC(X)-8) \qquad \text{(I.8)}$$

When applying this equation, we can note that for the calculation of *VEC(X)* according to equation (I.4) all valence electrons have to be considered, including those that take part in *M–M* bonds.

❖ **Simple ionic compounds**: compounds having no covalent bonds, $b(MM) = b(XX) = E = 0$. Equation (I.2) becomes:

$VEC(X) = 8$, this is the octet rule.

According to the conventional simple chemical definition, the valence compounds are those in which individual atoms are assumed to reach a 'filled valence shell' by accepting, donating or sharing electrons. This definition was first applied to the compounds (normal valence compounds) where the cations may donate the exact number of electrons to complete the valence shells (particularly the octet shells) of every anion.

We thus deduce the criterion:

$VEC(X) = 8$, simple ionic **(***normal valence compound*)

This concept was then extended to include compounds having anion-anion or cation-cation bonds, that is, the so-called polyanionic or polycationic valence compounds, assuming:

$VEC(X) < 8$ (*polyanionic valence compounds*)

and

$VEC(X) > 8$ (*polycationic valence compounds*)

I.3 Intermetallic compounds

Distinguishing between metals and non-metals is one of the first things that pupils learn in chemistry. Intermetallic compounds are materials composed of two or more metallic elements, with optionally one or more non metallic elements, which exist as homogeneous, composite substances and differ discontinuously in structure from that of the constituent metals. They are also called, preferably, intermetallic phases. Their properties cannot be transformed continuously into those of their constituents by changes of composition alone, and they form distinct crystalline species separated by phase boundaries from their metallic components and mixed crystals of these components. It is generally not possible to establish formulas for intermetallic compounds on the sole basis of analytical data, so formulas are

determined in conjunction with crystallographic structural information. In most cases, intermetallic compounds solidify at a fixed temperature and composition, and have thus a narrow domain of existence. Under this definition the most important intermetallic phases are [26-32]:

- Electron (or Hume-Rothery) compounds.
- Size packing phases. e.g. Laves phases, Frank–Kasper phases and Heusler phases.
- Zintl phases

Often, intermetallic compounds are hard, i.e. they exhibit high hardness, brittleness and strength and usually have a relatively high chemical resistance. Moreover, they are characterized by a high melting point and high electrical conductance which is generally one order of magnitude greater than that of pure transition metals.

There are intermetallic compounds with stoichiometric compositions according to the usual metal valencies and there are intermetallic phases having more or less extensive ranges of homogeneity in the phase diagram.

Intermetallic phases could be classified following the most important factor which controls their crystal structure (Pearson 1958, Girgis 1983, Hafner 1989, Westbrook and Fleischer 1995, Cahn and Haasen 1996) [33-36]. As a recapitulation of these points we may again refer to Pearson (1972), who underlined the role of the following factors in the classification of intermetallic phases:

- Geometrical factor, Size factor
- Chemical bond factor.
- Electrochemical factor (electronegativity difference).
- Energy band factor (electron concentration).

According to W.B. Pearson [37], there are five groups of intermetallic phases depending on their building principles and physical properties:

1. Intermetallics with geometrical close packing: These include most intermetallic phases. Compounds exhibit dense packing and the volume of the unit cell is less than the sum of the elemental atomic volumes of the atoms in the cell. Accordingly, inter-atomic distances are closer than those expected from the number of valence electrons available.

2. Intermetallics which only occur for certain valence electron concentrations (VEC):

(VEC = valence electrons/number of atoms). Examples include the α, β, and γ phases of the group B metals of copper, silver, and gold. According to Hume-Rothery rules [26-37, 38]: the

phase (fcc) occurs for VEC = 1.40; β -brasses (bcc) occur for VEC = 1.50 and the γ -brasses (defect bcc) occur for VEC = 1.61 [39-40].

3. Intermetallics with framework structures: In these compounds, all atoms form a common framework in which the distances to the nearest neighbors adhere to Pauling's formula [41]:

$$d_n = d_1 - 0.3 \log n \quad \text{(I.9)}$$

n: bond order (n = valence/coordination number),

d_1: the single-bond length.

4. Intermetallics with hybrid framework structures: Examples of these compounds are $BaAl_4$ [42-43] or $ThCr_2Si_2$, [44-46] in which atoms on certain sites form a framework and the remaining atoms are accommodated in the large voids according to the geometrical packing principles.

5. Intermetallics that follow the valence rules. Valence compounds include Zintl phases such as NaPb[47] and normal valence compounds like Mg_2Sn [48-49] with stoichiometric compositions, these phases are usually insulating or semiconducting, while non stoichiometry may result in a metallic behavior.

I.4 Zintl Border

Many published periodic tables highlight distinction between metals and nonmetals with a bold faced zigzag line as demarcation between metals lying to the left and nonmetals to the right. The Zintl border, which represents the limits of the Zintl concept, lies between group 13 and 14 of the periodic table when combined with the electropositive metals, post-transition elements of groups 13 and 14 provide structures that generally differ greatly in physical behavior (shown as a red line in Fig. 1.4). Along the border, the Zintl phases can be viewed as intermediate in bonding, situated between the electron precise valence compounds and the normal intermetallic compounds. Compounds of group 13 elements adopt numerous compositions and follow no simple chemical rules. Whereas those involving group 14 elements resemble salts and normally adhere to the simple octet or Zintl rule. Attention has therefore been dedicated to compounds of alkali metals with the elements of the 13th, 14th and 15^{th} groups (without B, Al, C, N and P) [26-50].

However, Klemm points out that some compounds to the right of the Zintl border show metallic properties and suggests that crystal structures are a more useful tool in separating metallic from non-metallic elements [51-52].

We turn our attention to the classification introduced by Klemm, and based on the tetra-partition of the elements into metals (true metals), meta-metals, semimetals and non-metals. True metals (alkali, alkaline earth metals, Al, Cu, Ag, Au, etc.) having a high specific electrical conductivity and crystal structures of high coordination numbers. Whereas Non-metals (N, O, S, Se, Halogens, etc) have a lower coordination number, While Meta-metals (Be, Zn, Cd, Hg, In, TI, Pb, etc.) have crystal structures with small deviations from high symmetry.

Thus Klemm has called the group 12 metals, as well as In, α-Tl, and ß-Sn, meta-metals [51], some others named them metalloids. To the right of the meta-metals the semimetals and semiconductors are found, to the left the classical metals [53].

Elemental tin occupies the borderline position between semiconductors and meta-metals due to the occurrence of both α (grey)-*Sn* (diamond structure; semiconducting) and *ß* (white)-*Sn* (tetragonal distortion of diamond; metallic). In fact, the *ß* modification may be considered as a border case between semimetals and meta-metals. Furthermore, Al mostly resembles the normal metals, but, like all of the meta-metals, it becomes superconducting at temperatures below 10 K. Gallium behaves in many compounds like a semimetal but melts at 28°C.

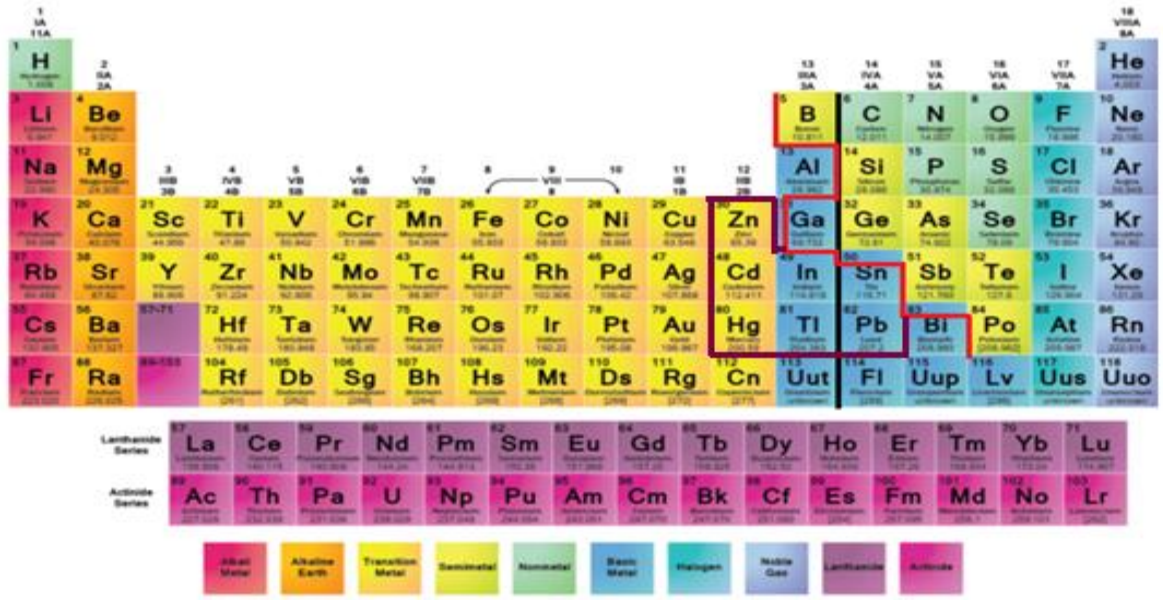

Fig I.4 Various boundaries in the periodic table. The metalloids are shown in blue; the distinction between metals and non-metals according to Zintl (-); the distinction between metals and non-metals according to Klemm (-); the metals Klemm designated meta-metals (-).

Alloys are formed when two or more metallic elements are mixed whilst molten and then cooled to form a solid which also exhibits metallic properties. Such alloys can be divided into two classes, those which are homogeneous solid solutions and those which have a definite composition and internal structure. Those in this second class are called intermetallic compounds and have a clear structure, usually unrelated to that of the individual metals. A compound formed from a metal with a much higher electronegativity than the second metal is defined as a Zintl phase. Following are some examples of Zintl phases and intermetallic compound.

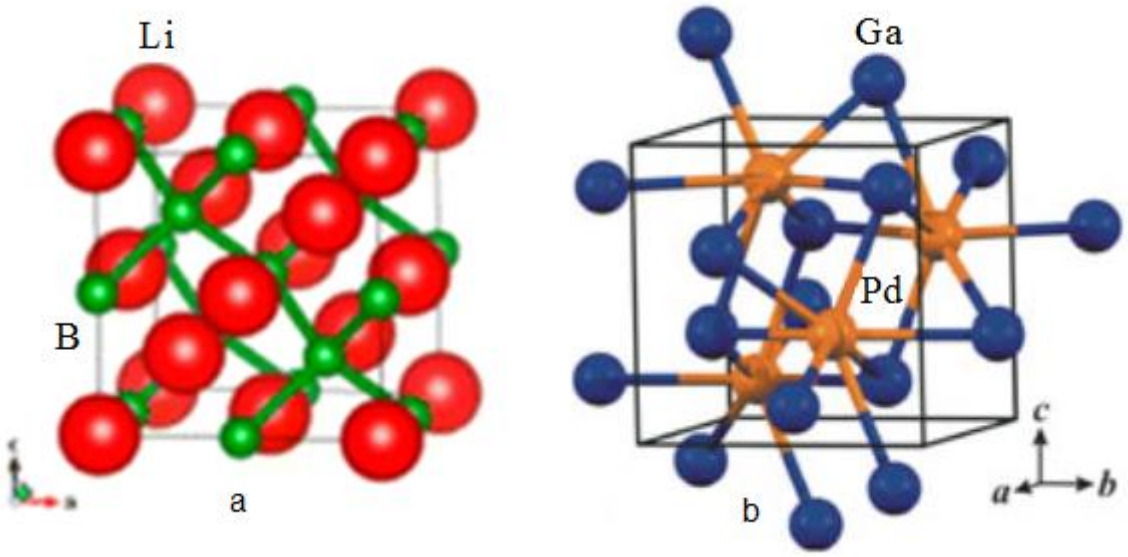

Fig. 1.5 Crystal structure of: a) The Zintl Phase LiB [54]
b) The Intermetallic PdGa [55]

I.5 Zintl Klemm concept and Zintl phases

The term "Zintl phases" entered the chemists' vocabulary more than 60 years ago to reflect the merits of Edward Zintl, who had discovered and studied a large number of substances which in a way may represent a bridge, a transition, between the valence compounds (molecule and salt) on the one hand and the intermetallic compounds on the other hand [56-58].

They are especially interesting because of their extraordinary structural variety. Upon examination of the atomic volumes of the elements, Zintl observed significant contractions in the unit cell volumes that did not follow the Hume-Rothery rule [4-57]. Rather than evaluate a total valence electron concentration (VEC), Zintl proposed electron transfer from the electropositive component to the electronegative component.

In these phases, covalent polyanionic networks are formed if the electrons received from the electropositive atoms do not fulfill the octet requirements of the electronegative elements. Hence the terms Zintl phases and Zintl concept were introduced.

In binary compounds AB consisting of electropositive cations A and post-transition elements B, the cation A transfers its electrons to the element B, which thus achieves a closed electron shell. The electron octet of element B appears due to the formation of two electron covalent *B-B* bonds and localization of lone electron pairs. A significant consequence of the fulfillment of the octet rule is the appearance of properties typical of most of Zintl phases. The fact that element B reaches a closed-shell electronic configuration implies that all the bonding and nonbonding (lone electron pairs) states in the covalent anionic sublattice are occupied, while all the anti-bonding states are vacant. As the number of electrons provided by element A strictly correlates with the number of B-B bonds and lone pairs of element B, the Zintl phases possess a very narrow homogeneity region. Consequently, it was clear that it is more convenient to apply the term Zintl phases to intermetallic compounds which display a pronounced heteropolar bonding construction and agreement with an ionic formulation in their anion partial lattices that obey the (8-N) rule [2]. Klemm and Busmann took this one step further. They pointed out a relationship between the anion structure and the electron count [31].

W. Klemm and E. Busmann (ZKB) stated: *"In Zintl's idea the formally negatively charged atoms that possess the same electron number as the neutral atoms of the next group elements, form polyanions with similar structures to the corresponding elements".* The strength of the concept is the connection between structure and electron distribution; if the structure is known, the atomic charges can be estimated [51-31].

Another important refinement of the Zintl phase concept was made by Schäfer and Eisenmann, where it was going beyond the concept of isostructural relationship to structure of the elements with the same number of valence electrons [2]

On the other hand, there exists a vast group of compounds formed by electropositive elements and Group 13-15 elements that exhibit properties characteristics of Zintl phases but, have an electronic structure not conforming to the octet rule. As an example, note metal-rich lithium silicides and germanides, whose electronic structures and properties are due to the occupation of the "cage" orbitals of Li clusters, as well as alkali and alkaline earth metal aluminides. Furthermore there are a number of liquid alloys (K–Pb, Rb–Pb, Cs–Pb, K–Sn, Rb–Sn, Cs–Sn,

K–Te) that behave as if all the anions were in the form of perfect simple *Zintl anions* like tetrahedra and dumbbells.

For example in Fig I.6, the structure NaSi contains regular tetrahedra of Si atoms between which the Na atoms are situated. So we have the overall composition $Na^{-}Si^{-}$ in which, however, the silicon ions have a discrete (molecular like) tetrahedral isoelectronic structure Si_4^{4-}. The NaSi structure may also be compared with that of NaGe in which tetrahedra of Ge atoms are contained (and Na in the intervening space) even if there is a somewhat different arrangement of the tetrahedra.

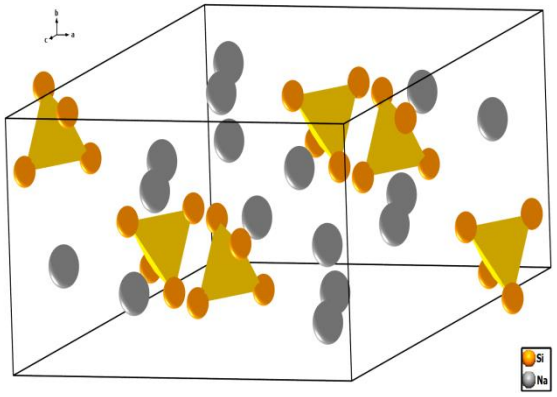

Fig I.6 Crystal structure of NaSi with Si_4^{4-} tetrahedra [60]

More complex examples of Zintl phases are given by ternary compounds in which the anionic part of the structure may be compared for instance to molecular halides. This point is illustrated by Ba_4SiAs_4 which can be described as $(Ba^{2-})_4(SiAs_4)^{8-}$ in which the $(SiAs_4)^{8-}$group is isostructural to the tetrahedral molecule $SiBr_4$.

In recognition of the work done by Zintl, Corbett et al [61-63] named the anions *Zintl ions*, later defining them as "homo-polyatomic anions of the post-transition metals" [64]. Corbett suggested two conditions; '(empty) clusters and related polyhedral species, often with non classical bonding, of the character first broadly illuminated by zintl' and polyanionic clusters and rings that require some unusual care or condition for their stabilization. The second condition proposes that in order to retain the ions in solid state, complexing of the cations or special organic solvents have to be utilized. This has been referred to as 'anti-coordination chemistry'. Just as for the Zintl phases the group of Zintl ions has been extended and several definitions coexist [21-65]. Parallel to the work of Corbett et al. on the Zintl anions, different groups strived to rationalize the topology of boranes (boron-hydrides) based on the number of

valence electrons included in the bonding and together these efforts resulted in what has become known as the Wade's rules [66].

As the close relationship between boranes and post-transition metal clusters already had been noticed, the Wade's rules could easily be extended to Zintl anions as well. Therefore, the structure of the polyanions can in many cases be predicted by counting the valence electrons. In addition, compounds containing transition metals in which the octet rule cannot be fulfilled but so-called completed electron configurations can be formed are classified as nontraditional Zintl phases. A specific case of nontraditional Zintl phases is represented by compounds that we call *"inverted" Zintl phases* [21-65]. In these compounds, the cationic sub-lattice consists of post-transition elements having an electron octet and transferring excess electrons to electronegative elements, usually halogens. As examples, one can cite $BiTeCl_7$ isotypical to the traditional Zintl phases KSnAs and K_8Sn_{44} respectively.

The term Metallic Zintl phase is not being used uniformly. In general in such metallic salts, the connectivity of the atoms forming the anionic substructure can be well rationalized by the (8–N) rule. However, on one hand few extra electrons are present that occupy the conduction band. Those extra electrons are often delocalized across the whole anion or in cation–anion bonding states. The appropriate term 'submerged continent' by Nesper [5] can be understood as polyanions buried in a sea of electrons. Prominent examples are the phases A_5Pn_4 (A = K, Rb, Cs; Pn = As, Sb, Bi), K_3Bi_2, $Ba_3Sn_4As_6$. On the other hand metallic conduction can also be obtained by electron deficiency in polar intermetallics at the Zintl boundary, such as Sr_3In_5, leading to an open and incompletely filled valence band.

I.5.1 Example of traditional Zintl phase NaTI

A traditional example of a Zintl phase is represented by NaTI which may be considered as a prototype of the Zintl rules. Zintl observed a curious arrangement of Na and TI atoms in the crystal structure which has also been observed in several other element combinations such as LiAl, LiGa and NaIn. The structure of this compound can be described as resulting from two interpenetrating diamond type lattices corresponding to the arrangements of the Na and Tl atoms respectively (see Fig I.7). NaTI assumes complete electron transfer from the more electropositive sodium (Na) to the more electronegative thallium (TI), just as in real ionic salts such as NaCl.

The difference is that the resulting anions do not necessarily achieve an electronic octet as isolated species but may rather bond to each other in order to do so. Each TI atom forms four homo nuclear bonds with a tetrahedral arrangement of neighbors. Thus, the TI atom forms an

electron octet. The Na^- ions, owing to their small dimensions can be considered isolated and inserted in the holes of the TI framework. Since the TI-TI bond is two electrons, to form four bonds, the TI atom must acquire one more electron, which is provided by the Na atom. TI^- in Na^+TI^- behaves like an element of the group to the right, group 14, and forms a diamond network, typical for the elements of that group, that is stuffed by the Na^+ cations. Thus, the characteristic ionic character of such phases, Na^+TI^-, gave them the name polar intermetallic phases.

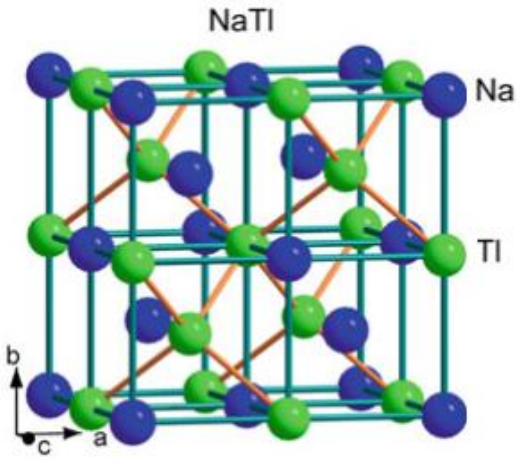

Fig I.7 Crystal structure of NaTI [21]

I.5.2 Characteristics of Zintl phases

In a more detailed description and according to Nesper (1990), the criteria for defining the Zintl phases may be summarized in the following points [5]:

1. The Zintl phases can be described within the group of normal valence compounds and a well-defined relationship can be assumed within their electronic and chemical structures (certain aspects of their structures satisfy electron counting rules).

2. Zintl phases are closed-shell compounds, for most of these compounds short interatomic contacts represent two centers two electrons bonds and the octet rule is fulfilled for both isolated cations and polyanions.

3. Zintl phases are semiconductors. The band gap limit is taken at 2.0 eV, or, at least, they show increasing electrical conductivity with increasing temperature.

4. Most Zintl-phase compounds are brittle.

5. Zintl phases are mostly diamagnetic, but can be paramagnetic. However, they should not show temperature independent Pauli paramagnetism, as is observed for normal metals.

Criteria (**1**) provide the connection to the general class of intermetallics. Requirement (**2**) needs to be explained in some more detail, especially the meaning of number of electrons needed for covalent bonding. For structures with normal 2- center-2-electron localized bonds all atoms follow the octet rule. While for compounds with delocalized bonding, on the other hand, the valence rules are different. The bonding electrons in compounds with deltahedral clusters are calculated by Wade's rules [66] that have been developed for the borane cages but also work equally well for naked main-group clusters. Moreover, there are combinations of the two compounds that contain networks of deltahedral clusters bonded to each other via localized bonds, and the sum of bonding electrons for such systems will include the electrons for cluster bonding, those for inter-cluster bonding, and the lone pairs.

In addition to the "observable" criteria, the calculated electronic structures of Zintl phases typically show that the bonding and nonbonding states are completely occupied and separated from the empty, anti-bonding states by not more than 2 eV. As the electronegative component progresses from the right to the left of the Zintl border, this energy gap approaches zero, but the chemical system retains important characteristics of Zintl phases, "metallic Zintl phases" [50]. See Fig I.8

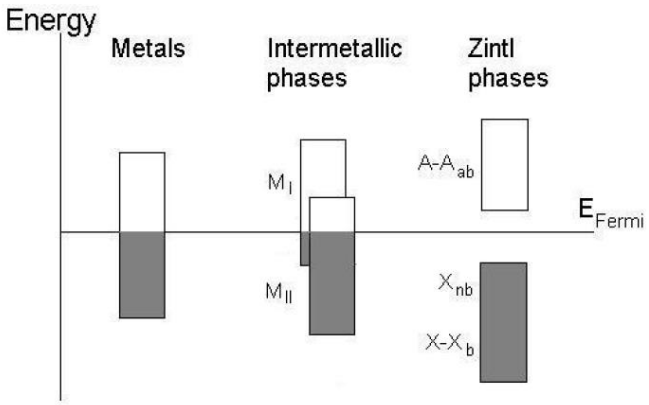

Fig I.8 Idealized density of states (DOS) of metals, conventional intermetallic phases and Zintl phases. Shaded regions represent occupied states [50].

I.5.3 Different groups of Zintl phases

Sevov [86] presented typical groups of Zintl phases, these are:

- Zintl phases with delocalized bonding
- Zintl phases with interconnected (Homo- and hetero-atomic) clusters
- Zintl phases with localized bonding

I.5.3.1 Zintl phases with delocalized bonding:

- **Isolated Clusters:** corresponding to isolated deltahedral clusters, mainly of the elements of the 13th and 14th groups, associated with the borane cages and their derivatives type $B_{12}H^{-2}_{12}$, $B_{10}H^{-2}_{10}$ (see Fig I.9) [67-68].

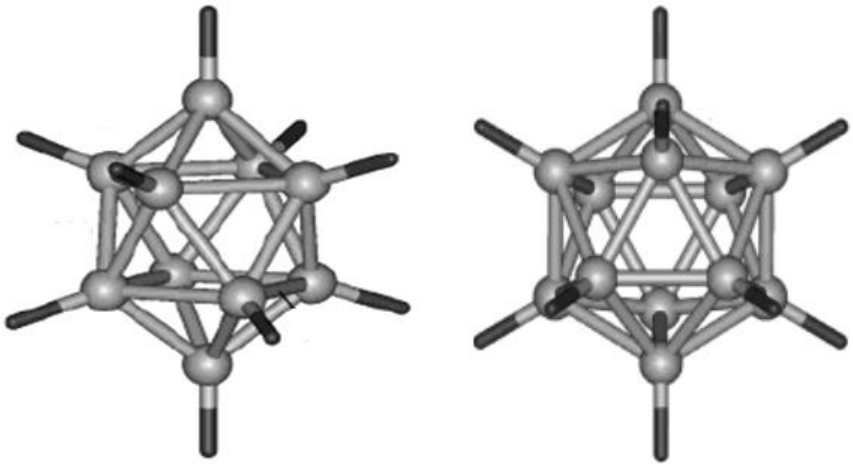

Fig I.9 Structures of $B_{12}H_{10}^{2-}$ and $B_{12}H^{2-}_{12}$ famous boron hydride clusters [68]

The bonding electrons in such species are delocalized. Consequently, the electronic requirements in such species cannot be rationalized with simple 2-center-2- electron bonds but rather that it is achieved through delocalized electrons that follow Wade's rules. This resulted in the structural characterization of E_9^{3-}, E_9^{4-}, and E_5^{2-} (E = Ge, Sn, Pb), As_7^{3-}, Sb_7^{3-}, As_{11}^{3-}, Sb_{11}^{3-}, Sb_4^{2-}, and Bi_4^{2-}, as well as several other species (Fig I.10).

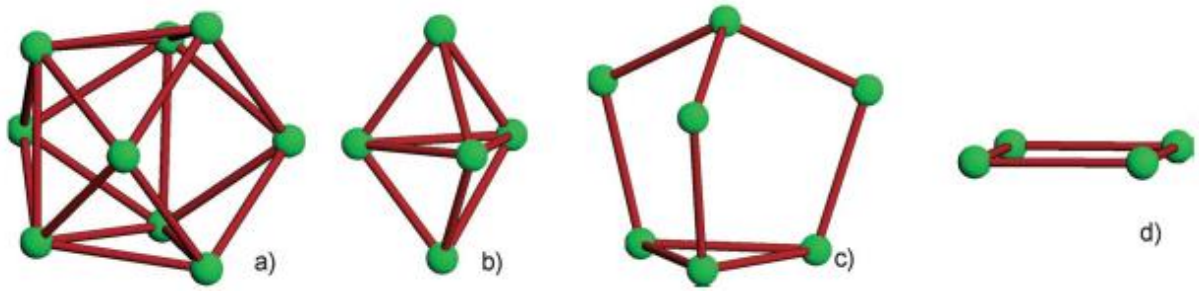

Fig I.10 Some of the main-group anionic clusters crystallized from solutions with sequestered alkali-metal cations: (*a*) $E_9^{3-}$and E_9^{4-} for E =Ge, Sn, Pb; (*b*) E_5^{2-} for E =Ge, Sn, Pb; (*c*) As_7^{3-} and Sb_7^{3-} ; (*d*) Sb_4^{2-} and Bi_4^{2-}. Clusters of silicon with shapes that correspond to those in (a) and (*b*) were isolated recently [69-71].

As shown in Fig I.11, the relation between the total electron count and the number of skeletal electrons require 2n+2 (closo "cage"), 2n+4 (nido "nest"), and 2n+6 (arachno "spider web") electrons for bonding, respectively, where n is the number of vertices of the cluster. For example, E_9^{4-} species are nido clusters with 2n+4 = 22 cluster-bonding electrons (each group

14 vertex provides 2 electrons) that can be described either as monocapped square antiprisms or as distorted tricapped trigonal prisms [72-74].

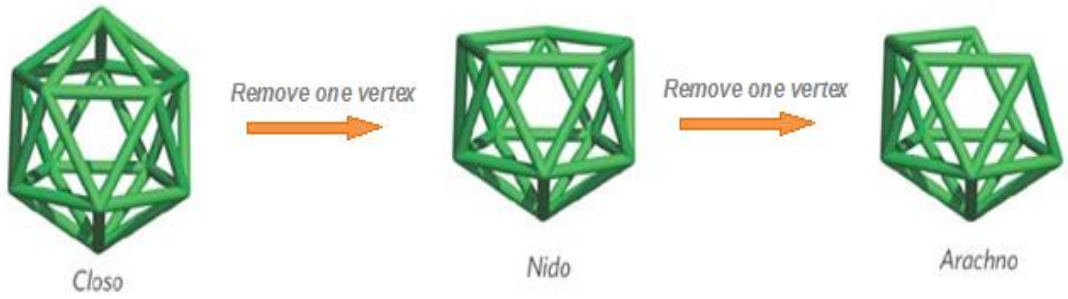

Fig I.11 Borane-type clusters held together by 13 electron pairs have shapes based on the icosahedron. This is complete (closo) with 12 skeletal atoms, as in $C_2B_{10}H_{12}$or $[B_{12}H_{12}]^{2-}$: nest-like (nido, one vacancy) with 11 skeletal atoms, as in $[C_2B_9H_{11}]^{2-}$; and cobweb-like (arachno, two vacancies) with 10 skeletal atoms, as in $[B_{10}H_{14}]^{2-}$ [72-74].

- **Example: Elements of group 14:**

As shown in Fig I.12, structure Cs_4Ge_9, was the first zintl phase with isolated 9-atom deltahedral clusters. The clusters Ge_9^{4-} are mono-capped square anti-prismatic, nido deltahedra. It combines the largest cation, Cs, and the smallest element of this group, Ge, for which a 9-atom cluster has been characterized from solution [75].

E_9^{4-} clusters cannot exist in neat solids due to the mismatch of large clusters and small cations, and therefore the best chance for formation of such species had the smallest clusters combined with the largest cations. With the knowledge that at least Ge_9^{4-} exist in neat solids it was more than logical to test the possibilities for similar clusters of the heavier analogs Sn and Pb. Zintl phase Cs_4Pb_9, Rb_4Ge_9, and K_4Pb_9 are Zintl cluster anions of the same type and geometry [76-80].

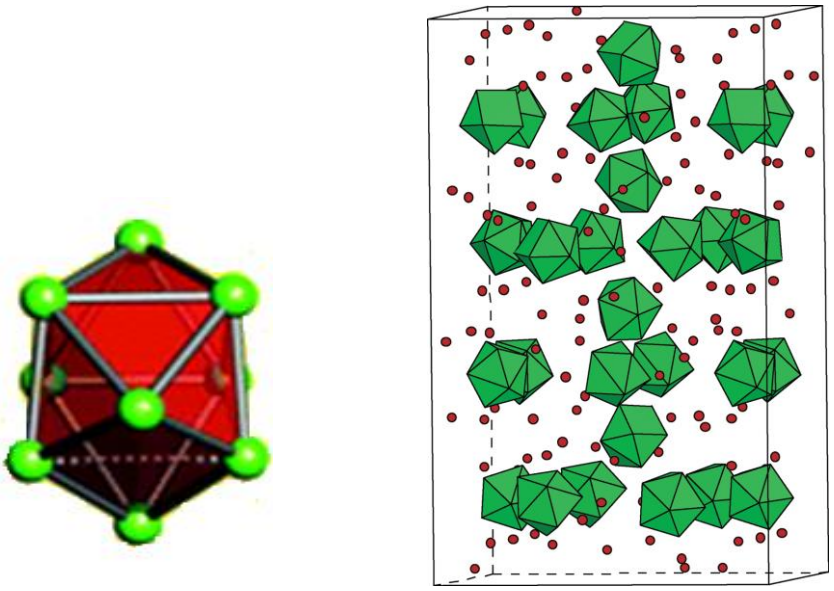

(b) (a)

Fig I.12 a- The structure of Cs_4Ge_9. b-The clusters Ge_9^{4-} are nido delta-hedra with the shape of mono-capped square anti-prisms [71-75].

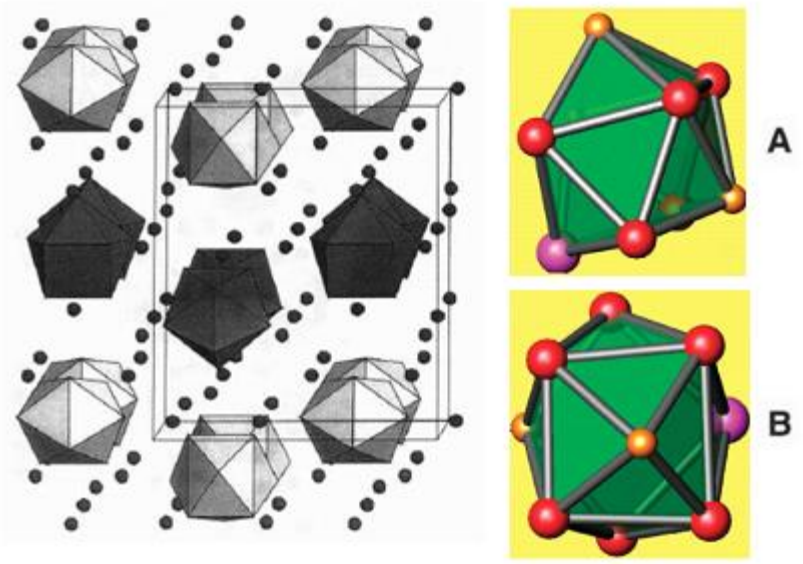

Fig I.13 General view of the structure of zintl phase K_4Pb_9, showing the two type of Pb_9^{4-} clusters: (a) the A-type, a monocapped square antiprism, and (b) the B-type, an elongated tricapped trigonal prism [80].

- **Example: elements of group 13:**

The first cluster of this group was found in a phase which is not exactly a true Zintl phase ('almost Zintl phases' or 'metallic Zintl phases) and the cluster itself is not of borane-type geometry. The important entrée into new hypoelectronic clusters that are achieved through distortion, and the most common example among the trielides, is In_{11}^{-7}. It is an 11 atom

cluster of indium, In_{11}^{7-} found in the compound K_8In_{11}, shown in Fig I.14 [69-84]**.** A general view (Fig I.13) of the structure of zintl phase K_4Pb_9, showing the two type of Pb_9^{4-} clusters: (a) the A-type, a monocapped square antiprism, and (b) the B-type, an elongated tricapped trigonal prism [95].

The discrepancy between charge and number of cations means that there is an extra electron per formula. So, it is not a true Zintl phase. Nevertheless, the cluster is deltahedral and exhibits delocalized bonding. Another example is K_8 $[In_{10}Hg]$ with the same 11-atom cluster as in K_8In_{11}, but with one indium atom substituted by Hg [81]. Due to the substitution the cluster $[In_{10}Hg]^{8-}$ assumes charge 8-, and the compound is a true Zintl phase. Another example, the substituted, hetero-atomic, 11-atom clusters represented by $[Tl_9Au_2]^{9-}$, $[Tl_8Cd_3]^{10-}$

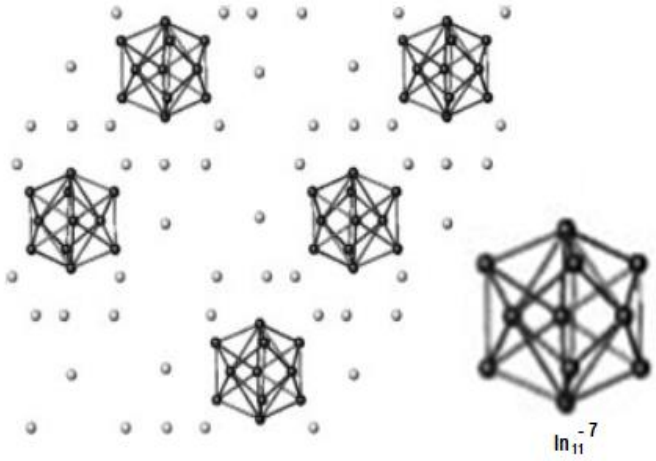

Fig I.14 [110] section of the rhombohedral structure of K_8In_{11} [82-83]

I.5.3.2 Zintl phases with interconnected (Homo- and hetero-atomic) clusters:

Mainly given by alkali metals and 13th group elements. Generally in these compounds two types of bonding are combined: delocalized within the clusters (endo-bonds) and localized (2c,2e exo-bonds) between them. The intercluster bond distances (ero-bonds) are shorter than those within the clusters (endo-bonds) since the former are 'normal' 2-center-electron bonds while the latter is delocalized bonding. Many of the network compounds have a few extra electrons (or holes) relative to those needed for the bonding. Such compounds can be referred to as 'metallic Zintl phases'.

- **Exemple of elements Group 13**

A good example of a gallium network is the structure of KGa_3, which contains 8-atom clusters of gallium, each with 8 exo-bonds, and isolated 4-bonded gallium atoms, the two

species in equimolar ratio; see Fig I.15. The clusters are of the closo-type and therefore require 18 electrons for skeletal bonding. As well each exo-bond is a normal (2c, 2e) bond, half of the electrons needed for them. The total number of electrons required for the endo- and exo-bonding of the cluster is therefore 26. The eight gallium atoms of the cluster bring 24 electrons and the charge of the cluster is - 2 (Ga_8^{2-}). The 4-bonded isolated gallium is in tetrahedral coordination and therefore has a formal charge of 1 -, (Ga^{-1}), in order to achieve an octet [84].

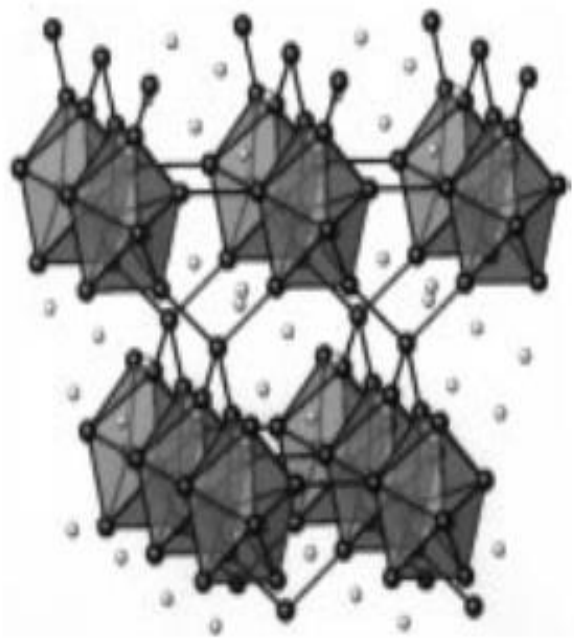

Fig I.15 The structure of KGa_3 made of interconnected gallium (dark spheres) 8-atom cioso deltahedra and isolated atoms [84].

More complex structures Rb_2In_3, are also indium networks made up of interconnected deltahedral clusters, layers of 4-bonded octahedra made of indium (Fig I.16). The electron count is straight forward: 14 for skeletal bonding, 4 for lone pairs on the two non-exo-bonded vertices, and 4 for the 4 exo-bonds. This totals 22 electrons required for bonding while the 6 indium atoms of the cluster provide only 18 electrons. The additional 4 electrons come from the 4 rubidium atoms, and the compound is electronically balanced [85].

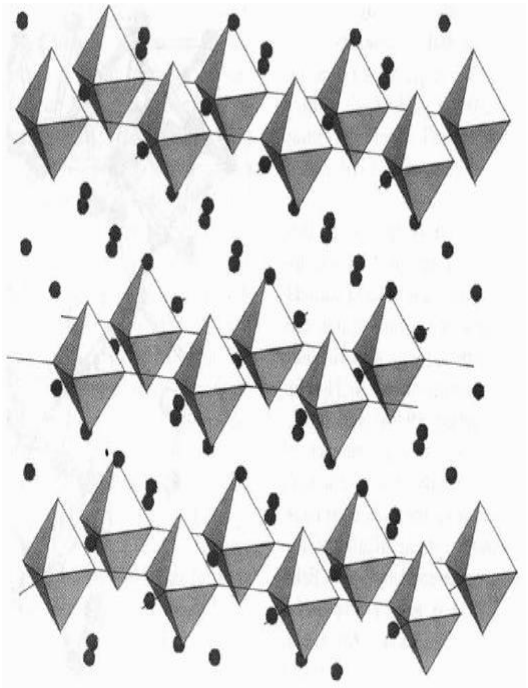

Fig I.16 The structure of Rb_2In_3 made of layers of 4-bonded closo octahedra of indium and separated by the rubidium cations (isolated spheres) [85-86].

I.5.3.3 Zintl phases with localized bonding:

The compounds in this category contain only regular 2-center-2-electron bonds between the p-elements. The majorities of compounds involve at least two p-elements of different groups and alkali metals, and are therefore mostly ternaries. Many of the compounds contain tetrahedral units made of one of the p-elements and centered by the other, and often share corners or edges with each other. The basic structural feature of these compounds is the composition of weakly coupled $SnSb_4$ tetrahedra and intercalated alkali or alkaline earth cations as shown in Fig I.17-a. For example, isolated Sn centered tetrahedra of antimony, $[SnSb_4]^{8-}$, are found in Na_8SnSb_4. Chains and higher dimensional motifs of corner sharing tetrahedra are found in many compounds like Na_5SnSb_3 **(**Fig I.17-b**)**. All these compounds have simple bonding, are easily understood by simple octet rule consideration.

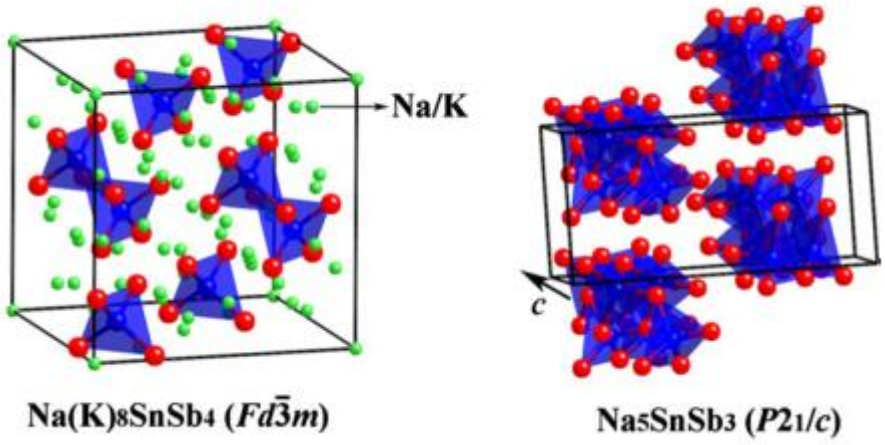

Fig I.17 Crystal structures of Zintl-phase compounds containing $SnSb_4$ tetrahedra [87]:
a- Na $(K)_8$ Sn Sb_4 b- Na_5SnSb_3.

The Sn atoms (blue spheres) sit at the centers of the tetrahedra formed by Sb atoms (red spheres). The interstitial Na, K cations are all depicted as smaller light spheres. For Na_5SnSb_3, the Na cations are not shown for clarity and the $SnSb_4$ tetrahedra are vertex shared to form chain like structures.

- **Exemple Group I4**

Most known clathrate compounds are based on the group 14 elements Si, Ge and Sn (Tetrel or Tt) and predominantly crystallize into two structure types [88]. These Tt-framework atoms are tetrahedrally coordinated and can be substituted by group 13 and 12 elements, as well as late transition metals (M), and the resulting cages are partially or fully occupied by guest atoms (A), such as alkali metals, alkaline-earth metals, or the rare-earth metals Ce and Eu [96]. The most common structure for the clathrates is type-I with the nominal composition A_8 $(M, Tt)_{46}$ followed by type-II with the general formula $A_{24}(M, Tt)_{136}$.

The structure of type-I boasts 20 and 24 atom cages (Fig I.18-b), while the structure of the type-II clathrates is based upon 20 and 28 atom polyhedral (Fig I.18-a). Due to these differences in their frameworks, for the type-I compounds, a complete occupation of all cages can be achieved either with one or two kinds of guest atoms, e.g., $(K \text{ or } Rb)_8Ga_8Si_{38}$ [90], $K_6Eu_2(Zn \text{ or } Cd)_5Ge_{41}$ [91], and $(Rb,Eu)_8In_xGe_{46-x}$ [92], while two types of different guest atoms will be preferred for the complete and ordered filling of both cavities in the type-II compounds. Some examples, illustrating this type of clathrates are $(Cs \text{ or } Rb)_8Na_{16}(Si \text{ or } Ge)_{136}$[89,93], $Cs_8Na_{16}Ga_{21}Si_{115}$ [94], $Cs_8Na_{16}Ag_{6.7}Ge_{129.3}$ [95-96], and $Cs_8Ba_{16}Ga_{39.7}Sn_{96.3}$ [97]. Four bonded atoms of group 14 should have zero formal charge, and therefore

both clathrates should be `metallic Zintl phases' considering a full transfer of electrons from the alkali metal atoms to the framework atoms.

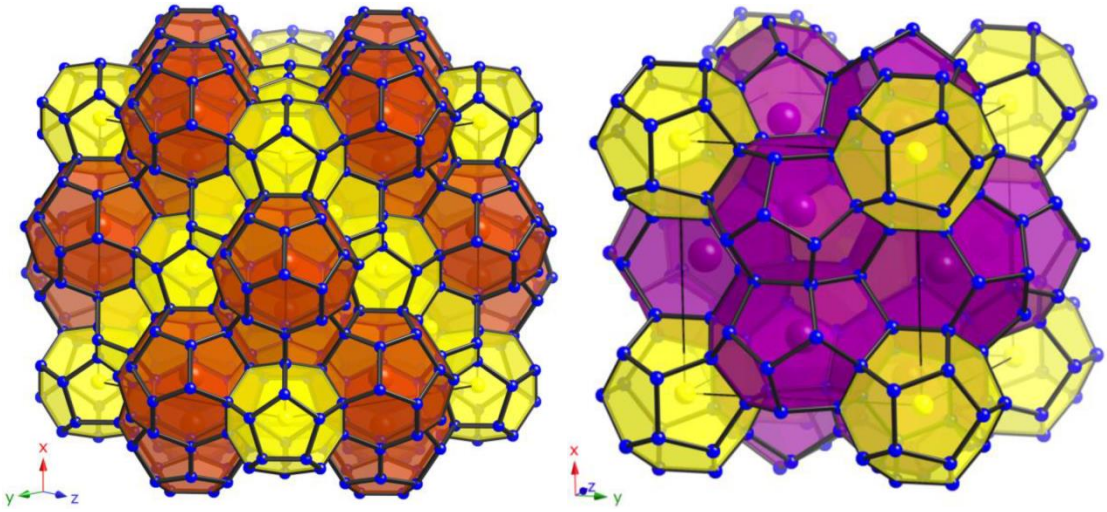

-a- -b-

Fig I.18 a- View of the polyanionic framework of clathrates with type-II structure (yellow: pentagonal dodecahedra; red: hexakaidecahedra).

b- View of the polyanionic framework of clathrates with type-I structure (yellow: pentagonal dodecahedra; purple: tetrakaidecahedra).

I.6 Conclusion

The Zintl phases form the link between classical valence compounds and intermetallic phases, the gradual change of chemical bonding passing from one chemical family to the other can be studied experimentally and theoretically in Zintl phases. At the border between Zintl phases and intermetallic compounds the typical properties of Zintl phases diminish smoothly and metallic conductivity appears. Brittleness, however, seems to be a good criterion for a Zintl phase. In other words, in a brittle substance most, if not all valence electrons, take part in chemical bonding according to the Zintl-Klemm concept. Hence, metallic conductivity based on a small number of charge carriers (electrons or holes) would not contradict the general chemical description of these compounds. Even if metallic properties occur and the basic or extended Zintl-Klemm concept do not apply exactly, most of the corresponding phases show electron counts very close to the Zintl-Klemm concept. Both the true Zintl phases and the 'metallic Zintl phases' are classes of fascinating compounds, some with clusters presenting delocalized bonding and some with normal localized bonds. The variety and structural

richness is quite obvious, and this is only a small percent of all possible combinations to be explored, so there are definitely many new and more exciting compounds to be found.

References

[1] S.M, Kauzlarich, Chemistry, Structure and Bonding of Zintl Phases and Ions; Ed., VCH Publishers: New York, 1996.

[2] H. Schäfer, B. Eisenmann, W. Müller, Zintl Phases: Transitions between Metallic and Ionic Bonding. Angew. Chem. Int. Ed., 12, 694–712, 1973.

[3] S.M. Kauzlarich, Chemistry, Structure, and Bonding of Zintl Phases and Ions; Wiley-VCH: New York, NY, USA, 1996

[4] W. Hume-Rothery, J Inst Metals 35:296, 1926.

[5] R. Nesper, Chemical bonding-intermetallic compounds. Angew. Chem., 103(7):805-34 1991.

[6] E. Zintl, Dullenkopf, W. Z. Phys. Chem., B16, 183, 1932.

[7] E. Zintl, Brauer, G. Z. Phys. Chem. B20, 245, 1933.

[8] E. Zintl, Angew. Chem., 52, 1, 1939.

[9] R. Ma et al., Theoretical study on the electronic structures and magnetism of Fe_3Si intermetallic compound, Journal of Alloys and Compounds,552, 5, pp 324–328 , 2013.

[10] M. Diviš, First-principles study of the structural properties and magnetism of R_2CoIn_8 (R=Y, Pr, Nd, and Dy) intermetallic compounds, Physica B: Condensed Matter, 407(13), pp 2524–2526, 2012.

[11] V.H. Tran et al., Magnetism of the series of intermetallic Ce_5CuM_3 compounds, where M = Sn, Pb and Bi, Journal of Alloys and Compounds, 451, (1–2), pp 457–460, 2008.

[12] L. Severinet et al., Mechanisms for itinerant magnetism in intermetallic compounds, Journal of Magnetism and Magnetic Materials, 104 (107), pp 745–746, 1992.

[13] D. S. Khoshnoud et al., Magnetostriction and thermal expansion of $HoFe_{11-x}Co_xTi$ intermetallic compounds, Journal of Magnetism and Magnetic Materials, 363, pp 188–194, 2014.

[14] S. Laksari et al., First-principle studies of the structural, electronic and optical properties of the intermetallics semiconducting compounds $RuAl_2$, $RuGa_2$ and $OsAl_2$,Computational Materials Science, 61, pp 20–26, 2012.

[15] U. Haussermann et al.,$FeGa_3$ and $RuGa_3$: Semiconducting Intermetallic Compounds, Journal of Solid State Chemistry,165 (1), pp94–99, 2002.

[16] S. C. Peter et al., Yb_4LiGe_4 – A Yb mixed valent Zintl phase with strong electronic correlations, Journal of Alloys and Compounds, 516, pp 126–133, 2012.

[17] A. E. van Arkel, Molecules and crystals in inorganic chemistry. Interscience Publishers Inc, New York, 1956.

[18] J.A.A Ketelaar, Chemical constitution: an introduction to the theory of the chemical bond, 2nd edition. Elsevier, Amsterdam, 1958.

[19] L.C. Allen, J. Am. Chem Soc., 111:9003, 1989.

[20] J. B Mann, T.L Meek, L.C Allen, J Am Chem Soc (JACS), 122:2780, 2000.

[21] T. F. Faissler, Zintl Phases, Principles and Recent Developments, Springer-Verlag Berlin Heidelberg, 2011

[22] H. Woo et al., Crystal Structure, Chemical Bonding and Magnetism Studies for Three Quinary Polar Intermetallic Compounds in the $(Eu_{1-x}Ca_x)_9In_8(Ge_{1-y}Sn_y)_8$ (x = 0.66, y = 0.03) and the $(Eu_{1-x}Ca_x)_3In(Ge_{3-y}Sn_{1+y})$ (x = 0.66, 0.68; y = 0.13, 0.27) Phases, Int. J. Mol. Sci. 16, 9017-9036, 2015.

[23] D. C. Fredrickson et al., Bonding Schemes for Polar Intermetallics through Molecular Orbital Models: Ca-Supported Pt–Pt Bonds in $Ca_{10}Pt_7Si_3$, Crystals 3, 504-516, 2013.
[24] E. Mooser, W. B. Pearson, Phys. Rev. 101, 1608 ,1956.
[25] E. Mooser, W.B. Pearson, Prog. in Semiconductors, Heywood and Co. Ltd ,5, p. 129,1960.
[26] R. Ferro and A. Saccone, Intermetallic Chemistry, Pergamon Materials Series, Elsevier, 2008.
[27] L. S. Darken and R. W. Gurry, Physical Chemistry of Metals, McGraw-Hill Book Co., 1953.
[28] E. Parthe, The Concept of a partial electron concentration value and its application to problems in crystal chemistry, In: Developments in the Structural Chemistry of Alloy Phases, ed., Giessen, B.C. (Plenum Press, New York), p 49, 1969.
[29] E. Parthe, Valence and Tetrahedral Structure Compounds, Ed., Parthe, E. (Summer School on Inorganic Crystal Chemistry, Geneva), 1980
[30] H.G. Grimm, A. Sommerfeld, Z. Physik, 36, 36, 1926.
[31] W. Klemm, and E. Busmann, Z. Anorg. Allg. Chem.,319,297,1963.
[32] R.W. Cahn, P. Haasen, Physical Metallurgy, North Holland; 4 th Ed, pp 267, 1996.
[33] R. W. Cahn, in: Ordered Intermetallics – Physical Metallurgy and Mechanical Properties: Liu, C. T., Cahn, R. W., Sauthoff, G. (Eds.). Dordrecht: Kluwer, pp 51 1-524, 1992.
[34] K. Girgis, in: Physical Metallurgy: Cahn, R. W., Haasen, P. (Eds.). Amsterdam: North-Holland, pp. 219-269, 1983.
[35] J. Hafner, in: The Structure of Binary Compounds: de Boer, F. R., Pettifor, D. G. (Eds.). Amsterdam: North-Holland, pp. 147-286, 1989.
[36] W. B, Pearson,. A Handbook of Lattice Spacing's and Structures of Metals and Alloys, International Series of Monographs on Metal Physics and Physical Metallurgy, London: Pergamon, 1958.
[37] W.B. Pearson, J. Less-Common Met., 109, L3, 1985.
[38] H. Rothery, R. E. Smallman and C. W. Haworth, The Structure of Metals and Alloys. 5 th Ed., Metals and Metallurgy Trust, 1969.
[39] W. Z. Ekman, Phys. Chem., B12, 57, 1931.
[40] J. H. Westbrook, Intermetallic Compounds, Wiley, 1966.
[41] L. Pauling, Die Natur der Chemischen Binding; Verlag Chemie: Weinheim, 1976.
[42] K.R. Andress, E. Z. Albertini, Metallkd, , 27, 126, 1935.
[43] N. N. Belyavina, , et al., Crystal structures and magnetic properties of the $BaAl_4$-type structure derivatives in Gd‑Al‑Ga system, Journal of Alloys and Compounds , 576, pp 114‑120, 2013.
[44] Z. Ban, M. Sikirica, Acta Crystallographica, 18, 594. 1965.
[45] V.V Sikolenko, Modulated spin-density waves in uranium intermetallic compounds with $ThCr_2S_{i2}$ structure Physica B: Condensed Matter, 350, 1‑3, pp E163‑E166, 2004.
[46] K. Kadir, D. Noréus, Structural determination of $NaAl_2Ga_2$ intermetallic compound having the $ThCr_2Si_2$ type structure, Journal of Alloys and Compounds, 477,1‑2, pp149‑151, 2009.
[47] P. Villars, Calvert, L.D. Pearson's Handbook of Crystallographic Data for Intermetallic Phases; 2nd Ed., ASM International: 1991.
[48] Glazov, V.M.; Glagoleva, N.N. Inorg. Mater, 1, 989, 1965.
[49] S. Kim, B. Wiendlocha, H. Jin, J. Tobola, J. P Heremans, Electronic structure and thermoelectric properties of p-type Ag-doped Mg_2Sn and $Mg_2Sn_{1-x}Si_x$ ($x = 0.05, 0.1$), J. Appl. Phys. 116, 153706, 2014.

[50] G.J. Miller, C.S Lee, and W. Choe, Structure and bonding around the Zintl border.In: Inorganic Chemistry highlights, Eds. Meyer, G., Naumann, D. and Wesemann, L., (Wiley VCH, Weinheim), p. 21, 2002.
[51] W. Klemm, Angew. Chem., 62, 133-142, 1950.
[52] G. J. Miller et al., Quantitative Advances in the Zintl–Klemm,Formalism, Springer-Verlag Berlin Heidelberg, Struct Bond 139: 1–55, 2011.
[53] R.B. King, The metallurgist's Periodic Table and the Zintl-Klemm concept. In: The Periodic Table into the 21st Century, eds. Rouvray, D.H. and King, R.B (Research Studies Press Ltd, Baldock, Hertfordshire), p. 189.2004.
[54] A. Hermann et al., From Wade–Mingos to Zintl–Klemm at 100 GPa: Binary Compounds of Boron and Lithium, J. Am. Chem. Soc., 134 (45), pp 18606–18618, 2012.
[55] M. Armbrüster et al, Pd−Ga Intermetallic Compounds as Highly Selective Semihydrogenation Catalysts, *J. Am. Chem. Soc.*, 132 (42), pp 14745–14747, 2010
[56] P. Atkins , T. Overton , J. Rourke, Shriver and Atkins' Inorganic Chemistry, OUP Oxford; Ed.,5, pp 347, 2009.
[57] J. Jiang, and S.M. Kauzlarich, Chem. Mater., 18, 435, 2006.
[58] M.W. Weiser , J. N. Lalena, Principles of Inorganic Materials Design, Wiley-Blackwell; Eds: 2nd Edition, 147-148, 2010.
[59] P. Jutzi , U. Schubert, Silicon Chemistry, Wiley VCH, pp 172-178, 2003.
[60] R. Q. Cabrera, A. Salamat, Pressure-Induced Structural Transformations of the Zintl Phase Sodium Silicide, Journal of Solid State Chemistry, Elsevier, 182 (9), pp.2535-2542, 2009.
[61] J. D. Corbett, D. G. Adolphson, D. J. Merryman, P. A. Edwards and F. J. Armatis, J. Am. Chem. Soc., 97, 6267-6268., 1975.
[62] J. D. Corbett, Polyanionic Clusters and Networks of the Early p-Element Metals in the Solid State: Beyond the Zintl Boundary, Angew. Chem., Int. Ed., 39, 670-690, 2000.
[63] J. D. Corbett, Exploratory synthesis: the fascinating and diverse chemistry of polar intermetallic phases, Inorg. Chem., 49, 13-28, 2010.
[64] S. Scharfe, F. Kraus, S. Stegmaier, A. Schier and T. F. Faessler, Angew. Chem., Int. Ed., 50, 3630-3670, 2011.
[65] T. F. Faissler, Zintl Ions, Principles and Recent Developments, Springer-Verlag Berlin Heidelberg, 2011
[66] K. Wade., Structural and bonding patterns in cluster chemistry. Adv. Inorg. Chem. Radiochem., 18:1-66, 1976.
[67] D. F. Shriver, P. W. Atkins, Inorganic Chemistry Third edition, Oxford University Press, 2001
[68] M. M. Balakrishnarajan, R. Hoffmann, Exohedral Multiple Bonding in Polyhedra. 2. Skeletal istortions in Ring-Stacked Boranes, Inorg. Chem., 43, pp 27-32, 2004
[69] F. Li and S. C. Sevov Synthesis, Structures, and Solution Dynamics of Tetra-substituted Nine-Atom Germanium Deltahedral Clusters, J. Am. Chem. Soc., 136, 12056, 2014.
[70] M. M. Gillett-Kunnath and S.C. Sevov, Synthesis of Nine-atom Deltahedral Zintl Ions of Germanium and their Functionalization with Organic Groups, Journal of Visualized Experiments,60, e3532, 2012
[71] S. C. Sevov and J.M. Goicoechea, Chemistry of Deltahedral Zintl Ions, Organometallics , 25, 5678-5692,2006
[72] M. A. Fox and K. Wade, Evolving patterns in boron cluster chemistry,Pure Appl. Chem., 75(9), pp. 1315–1323, 2003.
[73] K. Wade, Bonding with boron, Nature Chemistry 1, 92 ,2009.

[74] Miriam M. Gillett-Kunnath , Ivaylo Petrov and Slavi C. Sevov, Heteroatomic Deltahedral Zintl Ions of Group 14 and their Alkenylation, Inorg. Chem., 49 (2), pp 721–729, 2010.
[75] N. Chandrasekharan , Slavi C. Sevovz, Anodic Electrodeposition of Germanium Films from Ethylenediamine Solutions of Deltahedral Ge_9^{4-} Zintl Ions, J. Electrochem. Soc. 157, 4, C140-C145, 2010.
[76] V. Queneau , Slavi C. Sevov, Synthesis and Structure of the Zintl-Phase K_4Pb_9 Containing Isolated Pb_9^{4-} Clusters of Two Different Geometries, Inorg. Chem. , 37, 1358-1360, 1998.
[77] C. H, Marco Wendorff, C. Röhr, Synthesis and crystal structure of the tetrelides $A_{12}M_{17}$ (A=Na, K, Rb, Cs; M=Si, Ge, Sn) and A_4Pb_9 (A=K, Rb), , Journal of Alloys and Compounds, 361, 1–2, pp 206–221, 2003.
[78] Svilen Bobev, Slavi C. Sevov**,** Isolated deltahedral clusters of lead in the solid state: synthesis and characterization of Rb_4Pb_9 and $Cs_{10}K_6Pb_{36}$ with Pb_9^{4-}, and $A_3A'Pb_4$(A=Cs, Rb, K; A′=Na, Li) with Pb_4^{4-}, Polyhedron, 21, 5–6, pp 641–649, 2002.
[79] V. Queneau, E. Todorov, S. C. Sevov, Synthesis and Structure of Isolated Silicon Clusters of Nine Atoms, J. Am. Chem. Soc., 120, 3263-3264, 1998.
[80] Slavi C. Sevov, Tin-Based Organo-Zintl Ions: Alkylation and Alkenylation of Sn94- Donald J. Chapman and Inorg. Chem.,47, 6009-6013, 2008.
[81] Sevov, S. C., and Corbett, I. D, J. SolidSfate Chem., 103, 114,1993.
[82] S. C. Sevov, J. D. Corbett, Inorg. Chem. 1991, 30, 4875.
[83] J. D. Corbett, J. Alloys Compd. 1995, 229, 10.
[84] R. G. Ling, C. H. E. Belin, Z. Anorg. Allg. Chem., 480, 1981.
[85] S. C. Sevov, J. D. Corbett, Z. Anorg. Allg. Chem., 619, 128, 1993.
[86] R. L. Fleischer intermetallie Compounds: Vol. 3, Principles and Practice. Edited by H. Westbrook and John Wiley & Sons, Ltd.pp113-132, Chapter 6, Zintl Phases-Slavi C. Sevov, 2002.
[87] L. Zhang, M. H. Du, and D. J. Singh, Zintl-phase compounds with $SnSb_4$ tetrahedral anions: Electronic structure and thermoelectric properties, Physical Review B 81, 075117, 2010.
[88] G.A. Jeffrey, Hydrate Inclusion Compounds. In Inclusion Compounds; edited by J.L. Atwood, J.E.D. Davies, D.D. Mac Nicol, Academic Press: London; pp. 135–190, 1984.
[89] Bobev, S.; Sevov, S.C. Clathrates of group 14 with alkali metals: An exploration. J. Solid State Chem. 2000, 153, 92–105.
[90] Kröner, R.; Peters, K.; von Schnering, H.G.; Nesper, R. Crystal structure of the clathrates $K_8Ga_8Si_{38}$and $K_8Ga_8Sn_{38}$. Z. Kristallogr. 1998, 231, 667–668.
[91] Paschen, S.; Budnyk, S.; Köhler, U.; Prots, Y.; Hiebl, K.; Steglich, F.; Grin, Y. New type-I clathrates with ordered Eu distribution. Physica B 2006, 383, 89–92.

[92] M. C. Schäfer, S. Bobev. On the possibility for Rb- and Eu-cation ordering in type-I clathrates. Synthesis and homogeneity range of the novel compounds Rb_{8-x} Eu_x(In, Ge)$_{46}$ ($0.6 \leq x \leq 1.8$), Acta Crystallographica Section C, C_{69}, 1457–1461, 2013.

[93] G.S. Nolas, D.G.Vanderveer, A.P. Wilkinson, J.L. Cohn, Temperature dependent structural and transport properties of the clathrates $A_8Na_{16}E_{136}$ (A = Cs or Rb and E = Ge or Si). J. Appl. Phys., 91, 8970–8973, 2002.

[94] S. Bobev, J. Meyers, V. Fritsch, Y. Yamasaki, Synthesis and structural characterization of novel clathrate-II compounds of silicon. In Proceedings of the 25th International Conference on Thermoelectrics, Vienna, IEEE: New York, NY, USA, 25, pp. 48–52, 2006.

[95] M. Beekman, Wong-Ng, W.; Kaduk, J.A.; Shapiro, A.; Nolas, G.S., Synthesis and single-crystal X-ray diffraction studies of new framework substituted type II clathrates, $Cs_8Na_{16}Ag_xGe_{136-x}$ ($x < 7$), J. Solid State Chem., 180, 1076–1082,2007.

[96] M. C. Schäfer and S. Bobev, Tin clathrates with the type-II structure., J. Am. Chem. Soc.,135, 1696–1699, 2013.

[97] M. C. Schäfer and S. Bobev , New Type-I and Type-II Clathrates in the Systems Cs–Na–Ga–Si, Rb–Na–Ga–Si, and Rb–Na–Zn–Si, Inorganics , 2(1), 79-95, 2014.

CHAPTER II
Previous Studies of Zintl Phase KAsSn

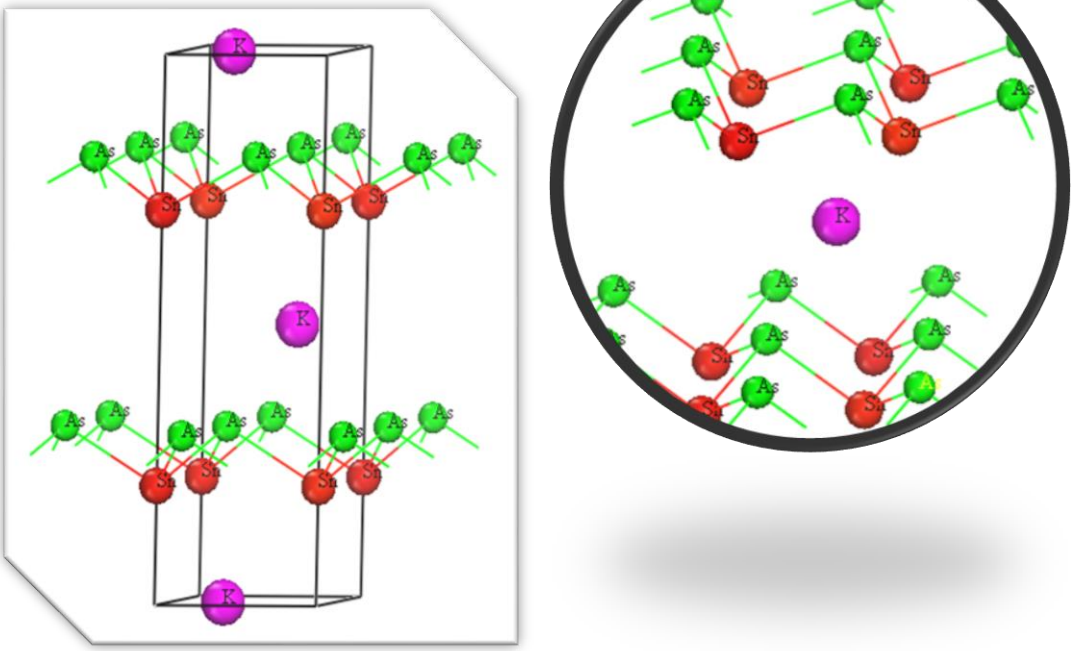

CHAPTER II
Previous Studies of Zintl Phase KAsSn

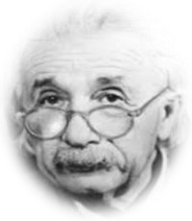

"Learn from yesterday, live for today, hope for tomorrow. The important thing is not to stop questioning"

Albert Einstein

Contents

Preface

In this chapter we present the theoretical and experimental study of physical properties of Zintl phases KAsSn. We expose, firstly the previous experimental works dealing with KAsSn compounds; especially those for structural properties of KAsSn, and then we displayed theoretical study about electronic properties. Furthermore we discuss our contribution which concentrates on the fundamental properties of Zintl phase KAsSn. In the end of this chapter we give a description of the calculated technics used in our work.

II.1 Introduction

Although about three quarters of all elements are metals or semimetals, the binary and ternary compounds of such elements have not attracted the same degree of attention. Chemists have, over many years, given an interest to compounds containing nonmetals. One of the major goals of solid state chemists has been to achieve a comprehensive understanding of the interrelationships among stoichiometry, crystal structure, and physical properties of solid state compounds [1-3]. Based on fundamental understanding of these relationships, we can create intermetallic materials which exhibit precisely designed crystal structures with properties specifically tuned for certain purposes. The synthesis of intermetallic compounds of the type A_xB_y, where A is an electropositive metal from group I or II and B is main group IV or V metal or semimetal, was initiated by Eduard Zintl and gave rise to a range of materials called Zintl phase. Zintl postulated that the stoichiometries and structures of these deeply intermetallic phases which sometimes have metallic luster can be interpreted by an ionic concept whereby the electropositive metals A lose their valence electrons to the semimetals B, which gain as many electrons as are necessary to complete their octets.

In recent years, new techniques have been developed to synthesize Zintl phases in the solid state. Since the X ray diffraction studies of Zintl et al [4-5], these members of the family of intermetallic compounds have been of special interest because some of their chemical properties are unusual for intermetallic phases. Many experimental investigations have been reported for binary and ternary compounds. Besides the crystal structure, the thermodynamic behavior, electrical conductivity, magnetic susceptibility, elastic constants have been studies.

Zintl phases are those intermetallic compounds which crystallize in typical non-metal crystal structures, one such example is Ternary Zintl phases KSnX (As, Sb) [6-7]. The crystal structures of KAsSn exhibit the same structure configuration as KSbSn , where it includes three-bonded pyramidally Sn and As atoms which consist of corrugated layers isostructural to elemental As with alternating Group IV and V elements. The potassium (K) cations were

located between them. KSnSb crystallizes in a hexagonal structure with two formula units in the unit cell, see Fig II.1 and II.2.

The resulting electronic configuration, ns_2np_3, indicates As^0 and Sn^- (pseudo element isostructural to arsenic). Due to the lower electronegativity of (Sn), the description of the distribution of formal oxidation states as $K^+Sn^-As^0$ appears unfounded. An alternative description of the electronic structure is based on the ionic approach to the Sn-As bond. With this extreme polarization, the electronic configurations are $4s^24p^6$ for As and $5s^25p^0$ for Sn. However, the slight difference between the electronegativities of tin (Sn) and arsenic (As) rules out the possibility of the ionic configuration $K^+Sn^{2+}As^{3-}$. The real distribution of oxidation states is intermediate between these two extreme schemes; the description K^+ (Sn As)$^-$ [8-9] is the most reasonable. Also the isostructural compound KSnSb can be represented as K^+ $(SnSb)^-$. These structures can be interpreted in terms of the Zintl concept [4,10,11] assuming a charge transfer of the valence electrons of the alkali/alkaline earth atoms to the Sn atoms, so giving anionic substructures $^2_\infty[SnAs]^-$ and $^2_\infty[SnSb]^-$ in which the elements follow the octet rule.

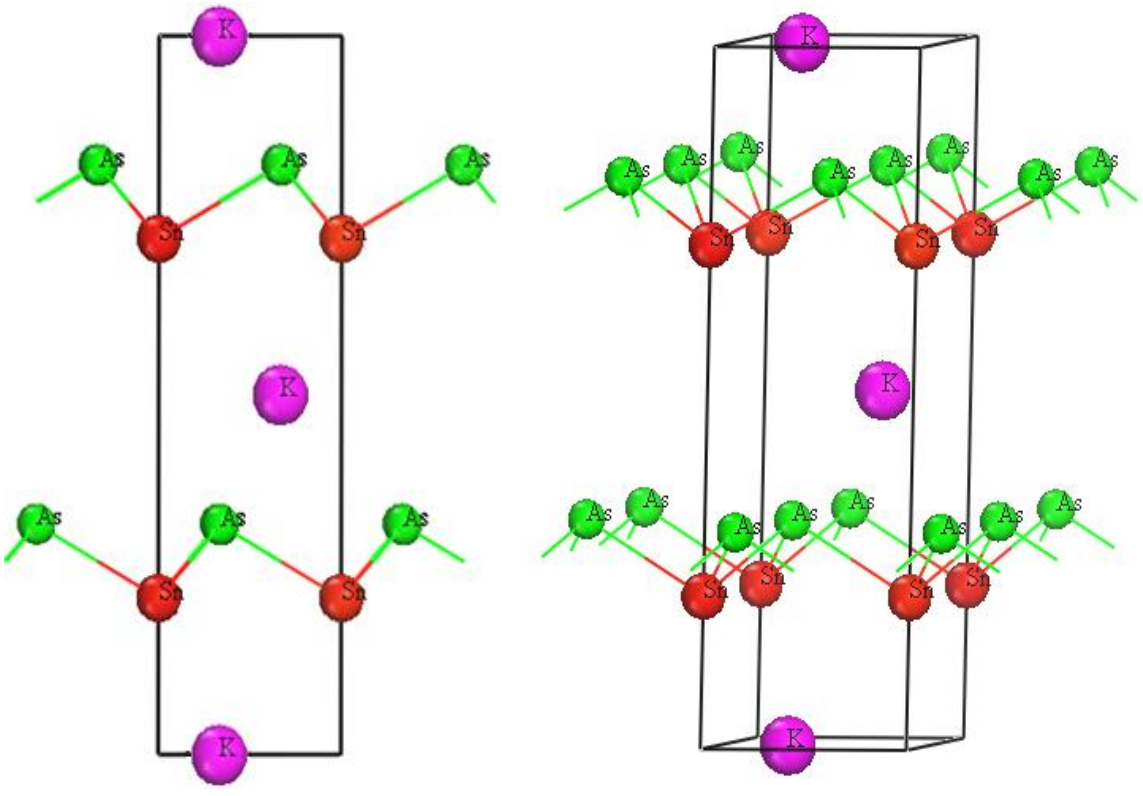

(a) (b)

Fig II.1 a- A perspective view of the KAsSn structure.

b- A projection of the KAsSn structure on to the $(11\bar{2}0)$ plane.

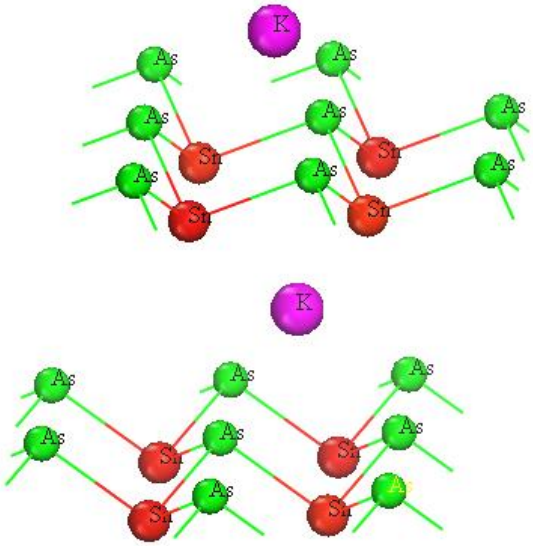

Fig II.2 Fragment of the crystal structure of KAsSn, the corrugated layers of Sn and As atoms separated by K atoms are shown.

II.2 Previous works

Several theoretical and experimental works which discussed the physical properties of KAsSn have been cited in the literature. We mention the most important contributions, as follows; Lii & Haushalter [8] and Asbrand et al [12] determinated the crystal structure of KAsSn and the distance between atoms by X ray powder diffraction. Schmidt et al [9] calculated the electronic properties of KAsSn included band structure and density of states using LDA approximation according to Hedin and Lundquist [13], and the ASW method [14]. We clarify the contributions of these authors, considering the structural and electronic structure properties of zintl phase KAsSn.

II.2.1 Practical experience

Structural properties of KAsSn were studied by Lii & Haushalter [8]. The compounds KAsSn was prepared in two steps.

1- KSn was prepared by reacting potassium metal with tin metal in an alumina crucible at about 280°C for 1 h under 1 atm He.
2- KAsSn was prepared by heating a mixture of KSn and As in an alumina crucible at 590°C for 24 h under 1 atm He.

Lii & Haushalter [8] found that KAsSn crystallized as shiny metallic plates. Therefore, the crystal structure and purity of the compounds was established by X-ray powder patterns using a Philips powder diffractometer and $Cu_{K\alpha 1}$ radiation [8]. Silicon powder was mixed with all samples for calculating the observed d-spacings and the unit cell parameters. The X-ray

powder diffraction investigations indicate that the tin and arsenic atoms in KAsSn are ordered in hexagonal structure, the tin and arsenic atoms were assumed to be at 2a and 2b special positions of the space group $P6_3mc$ (No.186) respectively [15]. The observed bond lengths d (Sn-As) (2.715 A°), d (As-As) = 2.517 A° [8] can be confirmed by the earlier findings in [16]. Various practical considerations associated with these techniques have been also considered in more detail by Klein & Eisenmann [15] and Asbrand et al [12] and carried out similar studies for determining the structure properties of Zintl phase KAsSn.

Tin 119 Mössbauer spectroscopy measurements recorded from Zintl phase KSnAs would be very informative either on the problem of disorder or in obtaining the experimental evidence of the oxidation states of Sn in this compound. Asbrand et al [12] studied the nature of the banding using Tin 119 Mössbauer spectroscopy [12]. He suggested that the shorter tin arsenic distances give raise to a more distorted octahedral array around tin of three pnictogen and three potassium neighbors. So he concluded that the bonding is more metallic in character.

The hexagonal unit cell parameters, the atomic positions and some selected interatomic distances are displayed in Table II.1.

The unit cell parameters	Interatomic Distance		Position parameters			
Hexagonal P63mc	Sn-As	2.715 A°	atom	x	y	z
a = 4.1032 A°	K'-As	4.227 A°	K	1/3	2/3	0
c = 12.845 A°	K'-Sn'	4.245 A°	Sn	0	0	0.2742
V = 187.30 A^3	K-As	3.230 A°	As	1/3	2/3	0.6709

TABLE II.1 The unit cell parameters for KAsSn

II.2.2 Theoretical aspect

Theoretically, few works were interested in the electronic properties of the Zintl phase KAsSn. They evaluate the band structure and density of the state at zero pressure.

II.2.2.1 Electronic properties

Schmidt et al [9] have used the local density functional approximation (LDA) [13]. According to Hedin and Lundquist [14], together with the augmented spherical wave (ASW) method (II) for the numerical computations to obtain the self-consistent energy band structures, the partial density of states and covalent, ionic contributions to the chemical bonds for ternary Zintl phase KAsSn.

II.2.2.1.1 Band structure, partial and total density of states of KAsSn

Schmidt et al. [9] calculated the partial and total density of states (DOS) of KAsSn on one hand and band structure on the other hand; the calculated results are shown in Fig II.3 and II.4.

In Fig II.4 we can see the band structure of the Zintl phase KAsSn. He found that the occupied valence bands below the Fermi energy E_F (s_{As} to P_{Sn-As}) are separated by a small band gap of about 0.1 eV from the unoccupied conduction bands, so it was concluded that this compound has small band gap with electron transfer from potassium to tin-arsenic.

As was pointed in his work, the nature of the energy bands can be deduced from the partial densities of states $n_{v,l}$ (E) which are shown for KSnAs in Fig. II.3. As it is remarked the two lowest lying valence bands labeled S_{As} correspond to the atomic 4s electrons of As, because the partial density of the 4s-like states $n_{As,s}$ (Fig. II.3.d) is the main contribution to n (E) for these states. While the two s_{As}-like bands are separated by an energy band gap of about 1.5 eV from the other valence bands. Both this energy separation and the dominance of nAs,s indicate that the s electrons of As do not contribute significantly to the chemical bond in KSnAs. The same finding holds for the bands above the s_{As}-like bands, which are the two 5s-like bands of Sn, labeled s_{Sn}.

Furthermore, we can observe from Figs (II.3. c) and (II.3 .d) that both $n_{Sn,p}$ and $n_{As,p}$ contribute significantly to the total density of states. As a result the maxima $n_{Sn,p}$ and $n_{As,p}$ are at the same energy values and the bonding mechanism corresponding to these energy bands can be described by strong covalent bonds between Sn and As.

From the calculated partial density of states (DOS) for the K atom, we can see from Fig. II.3b a small contributions of $n_{K,l}$(E) within the p_{Sn-s},-like bands, so no covalent or metallic bonds exist between K and Sn or As. The occupation of the 4s-like states of K is low and the potassium substructure should have cationic character. However, the ionic character is much less pronounced than in a typical ionic crystal, because the band gap between the valence and conduction bands is distinctly smaller than in ionic crystals.

Consequently, the mentioned studies yield fairly accurate band gap energies. It is noted that, for better study of the electronic properties it is very important to obtain best band structure.

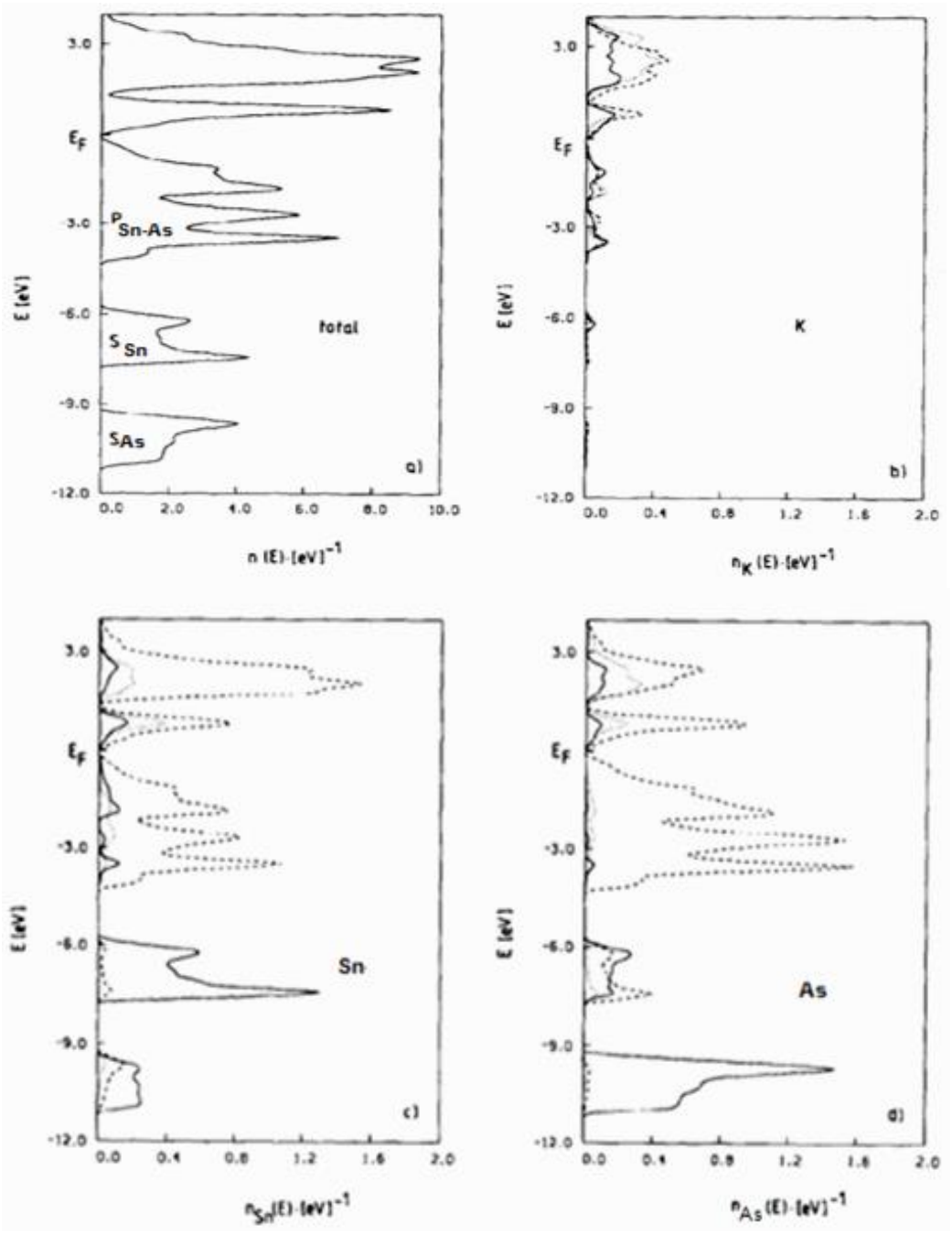

Fig II.3 Density of states as a function of *E* for the valence energy bands of KAsSn [9]

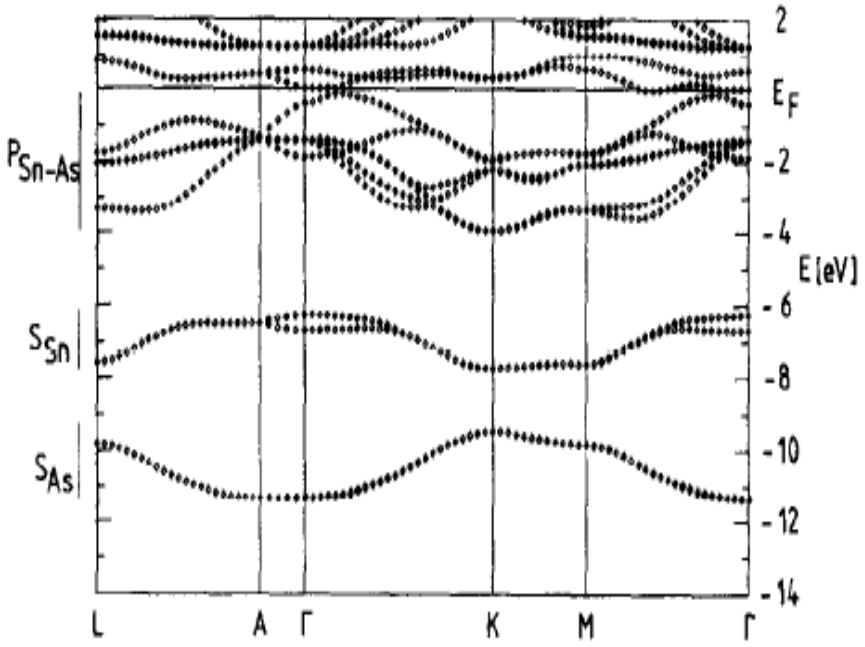

Fig II.4 Electronic band structure of the valence states of KSnAs [9]

The calculated results [9] will be compared with the results found for NaTI [17] and our obtained results for the electronic properties of Zintl phase KAsSn.

II.3 Comparison with NaTl

Schmidt et al [9] have compared the results for KAsSn with those found for NaTI in Reference [17], which is the prototype of the *B32*-type Zintl phases. He found that the density of states shows a sharp minimum at the Fermi level E_F. Furthermore, the partial density of states of Na is distinctly smaller than expected for covalent bonded sodium. Therefore in both cases, NaTI and KAsSn compounds have two common properties: a charge transfer from the alkali/ alkaline earth substructure to the more electronegative elements and, additionally, n/2 (almost) fully occupied valence bands separated from the $(n/2 + 1)^{th}$ energy band by (nearly) a band gap. It is concluded that there is no band gap between the occupied and unoccupied electronic states. He thought that this metallic character is due to interlayer interaction of the As atoms. Therefore the layer structure forms for large interlayer distances saturated bonds. The occupied and unoccupied *p*-like band states of As are separated, and the bonding mechanism is similar to the bonding mechanism in $[SnAs]^{2}_{\infty}$ layers.

II.4 Our contribution about physical properties of Zintl phase KAsSn

On the theoretical and experimental side, few works were interested in structural and electronic properties of this compound, our understanding of electronic properties and their behavior under external pressure effect is satisfactory and accurate.

To the best of our knowledge no experimental or theoretical studies are available in the literature for the elastic and optical properties of KAsSn compound.

Therefore, the goal of this work is to give an important information concerning fundamental properties of Zintl phase KAsSn, and then to show the effective use of this compound in technological applications especially in optoelectronic devices.

II.5 Calculation inputs

In our study first-principles calculations on KAsSn were performed by CASTEP code [18] within the framework of density functional theory (DFT). The exchange and correlation functional was treated by generalized gradient approximations developed by Wu-Cohen (GGA-WC) [19]. The interactions between ions and electrons are described by employing the Vanderbilt ultrasoft pseudo-potential [20]. All atomic positions in our model have been relaxed according to the total energy and force using the Broyden-Fletcher-Goldfarb-Shanno (BFGS) [21] scheme, based on the cell optimization criterion (the maximum ionic Hellmann–Feynman force within 0.01 eV.$Å^{-1}$, maximum stress of 0.02 GPa, maximum displacement of 5×10^{-4} Å and self-consistent convergence of the total energy of 5×10^{-6} eV/Atom. The K $3p^6$ $4s^1$, Sn $5s^2$ $5p^2$ and As $4s^2$ $4p^3$ electron states are explicitly treated as valence electron states.

In order to ensure convergence of the computed structures and energetics, the cut off energy of plane wave is set at 330 eV for KAsSn. The Brillouin zone integration uses Monkhorst–Pack scheme [22] method for hexagonal structure optimization of 12×12×4 mesh for optimizing the geometry, the elastic constants and the density of states (DOS), while 24×24×8 mesh is used for calculation of the optical properties. The elastic constants were determined by applying a set of given homogeneous deformation with a finite value and calculating the resulting stress with respect to optimizing the internal atomic freedoms [23].

II.6 Conclusion

We have cited in this chapter previous theoretical and experimental investigation concerning the fundamental properties of the Zintl phase KAsSn. In these previous works using the Zintl concept to interpret the chemical bonds in KAsSn, the arrangement of the atoms in this compound suggests that the almost free valence electrons of K are transferred to the Sn/ As

substructures to form saturated covalent bonds between Sn and As according to the octet rule. This compound can be understood within the Zintl formalism. If this picture is correct, we expect distinct nonmetal or semimetal behavior for this compound concerning properties like conductivity, magnetic susceptibility. The band structure results support these assumptions. First, the electronic valence states in the compounds are fully occupied energy bands separated by a small energy gap from the unoccupied energy bands. Second, a charge transfer is indicated by the finding that the partial density of states of Sn and As are exclusively the dominant contributions.

References

[1] J. H. Westbrook, R. L. Fleischer,. Intermetallic Compounds: Principles and Practice; John Wiley & Sons: West Sussex, Vol. 1-2, 1995.

[2] G. Sauthoff, Intermetallics; VCH Publishers Inc.: New York, 1995.

[3] T. You, Experimental and theoretical investigations in rare earth-triel-tetrel polar intermetallic systems: composition-structure-properties relationships, thesis, Iowa State University, 2008.

[4] E. Zintl, Brauer, G. Z. Phys. Chem. B20, 245, 1933.

[5] E. Zintl, Angew. Chem., 52, 1, 1939

[6] P. Doz., B. Eisenmann, J. Klein, Zintl-Phasen mit Schichtanionen: Darstellung und Kristallstrukturen der isotypen Verbindungen $SrSn_2As_2$ und $Sr_{0,87}Ba_{0,13}Sn_2As_2$ sowie eine Einkristallstrukturbestimmung von KSnSb, Zeitschrift für anorganische und allgemeine Chemie, 598/599, 93-102,1991.

[7] M. Asbrand, B. Eisenmann $K_3[SnSb_3]$, eine Zintl-Phase mit $_\infty^1[SnSb3]^{3-}$ Bändern Z. Anorg. Allg. Chem. 623, 561-564,1997.

[8]K.H. Lii, R. C. Haushalter, Journal of solid state chemistry, 67,374-378, 1987

[9] P. C. Schmidt, D. Stahl, B. Eisenmann, R. Kniep, Journal of solid state chemistry 97, (1992) 93-104.

[10] H. Schafer, B. Eisenmann, and W. Muller, Angew. Chem. Int. Ed. Engl. 12, 694, 1973

[11] H. Schafer, B. Eisenmann, Rev. Inorg. Chem. 3, 29, 1981

[12] M. Asbrand et al., bonding in some Zintl phases: A study by Tin-119 Mossbauer spectroscopy.

[13] L. Hedin and B. I. Lundquist, J. Phys. C 4, 2064, 1971

[14] A. R. Williams, J. Kübler, C. D. Gelatt, Phys. Rev. B 19, 6094, 1979.

[15] J. Klein, B. Eisenmann, Materials Research Bulletin, 23, 587- 594, 1988.

[16] N. N. Greenwood and A. Earnshaw, "Chemistry of the Elements," p. 643, Pergamon, Oxford, 1984.

[17] P. C. Schmidt, Phys. Rev. B 31, 5015, 1985.

[18] M.D. Segall, P.J.D. Lindan, M.J. Probert, C.J. Pickard, P.J. Hasnip, S.J. Clark, M.C. Payne, J. Phys.: Condens. Matter 14, 2717, 2002

[19] Z. Wu, R.E. Cohen, Phys. Rev. B 73, 235116, 2006.

[20] D. Vanderbilt, Phys. Rev. B 41, 7892, 1990

[21] T.H. Fischer, J. Almlof, J. Phys. Chem. 96, 9768, 1992.

[22] J.D. Pack, H.J. Monkhorst, Phys. Rev. B. 16, 1748, 1977.

[23] V. Milman, M.C. Warren, J. Phys.: Condens. Matter 13,241, 2001.

CHAPTER III
RESULTS AND DISCUSSION

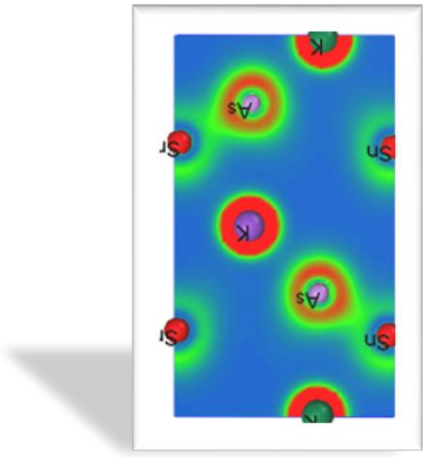

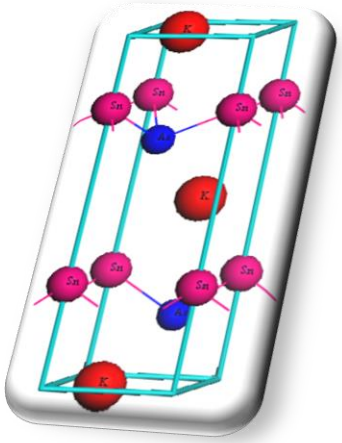

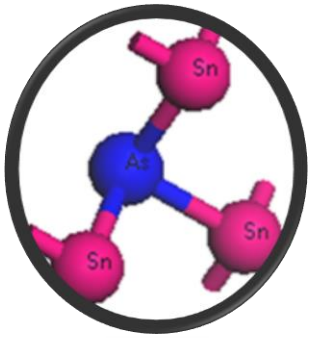

CHAPTER III
RESULTS AND DISCUSSION

Nothing amuses more harmlessly than computation and nothing is oftener applicable to real business or speculative enquiries. A thousand stories which the ignorant tell, and believe, die away at once, when the computist takes them in his grip.

Samuel Johnson

Contents

Preface

In this chapter, a first-principles study of ternary Zintl phase KAsSn compound using density-functional theory (DFT) method within the generalized gradient approximation developed by Wu-Cohen (GGA-Wc) has been performed. Based on the optimized structural parameter, the electronic structure, elastic and optical properties have been investigated. The calculated lattice constants agree reasonably with the previous results. The effect of high pressure on the structural parameters has been shown. The elastic constants were calculated and satisfy the stability conditions for hexagonal crystal. These indicate that this compound is stable in the studied pressure regime. The single crystal elastic constants (*C*ij) and related properties are calculated using the static finite strain technique, moreover the polycrystalline elastic moduli such as bulk modulus, shear modulus, micro-hardness parameter *Hv*, Young's modulus and Poisson's ratio were estimated using Voigt, Reuss and Hill's (VRH) approximations. The elastic anisotropy of the KAsSn was also analyzed. On another hand the Debye temperature was obtained from the average sound velocity. Electronic properties have been studied throughout the calculation of band structure, density of states and charge densities. It is shown that this crystal belongs to the semiconductors with a narrow gap of about 0.34eV. Furthermore, in order to clarify the optical transitions of this compound, linear optical functions including the complex dielectric function, refractive index, extinction coefficient, optical reflectivity, absorption coefficient and loss function were performed and discussed.

III.1 Crystal structure and lattice constants

III.1.1 Study at zero pressure

The ternary zintl compound potassium arsenide tin, KAsSn, has an KSrSn type structure and crystallizes in the hexagonal space group P 63/mc (No.186), with a=b=8.6374 Å and c=9.7209Å. Its structure has been determined through X-ray diffraction analysis [1]. As shown in Fig III. 1, the conventional unit cell of KAsSn contains 6 atoms (Z=2, K=2, Sn=2 and As =2), the K atoms occupy at 2b Wyckoff site (1/3, 2/3, 0), the Sn atoms at 2a site (0, 0, z_{Sn}), and As atoms on 2b site (1/3, 2/3, z_{As}). The structure is thus defined by two lattice parameters a and c, and the internal structural parameter z, for the Sn and As atoms respectively.

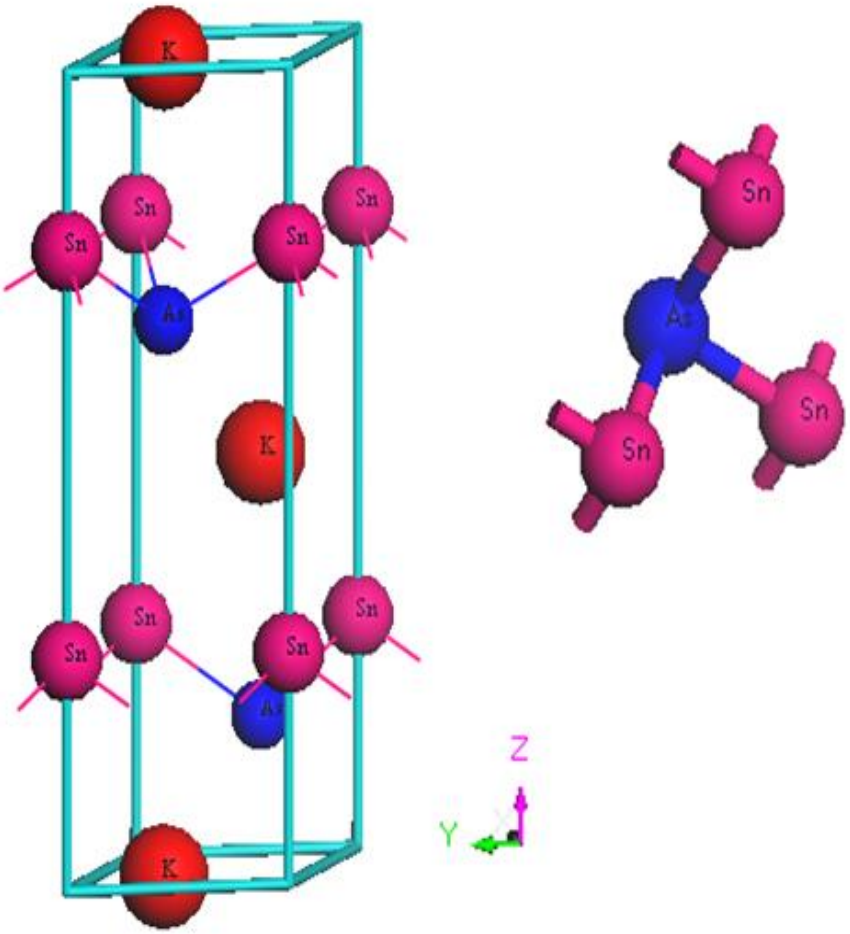

Fig III.1 The unit cell of the hexagonal KAsSn lattice.

The geometry optimized structural parameters at zero pressure (a_0, c_0, V_0, $(c/a)_0$, z_{0As}, z_{0Sn}), bulk modulus *B* and its pressure derivative *B'* were presented and compared with experimental data in Table III.1, where they are shown to agree with the available experimental values [1-2]. A small difference could be observed between calculated and experimental lattice parameters. The computed lattice constants a_0, c_0, V_0, z_0 (As), z_0 (Sn), on the other hand show a reduction of 0.87%, 1.63%, 0.06%, 0.51%, and 0.24% respectively. Our results show excellent agreement with previous experimental [1-2] data, which demonstrates the accuracy of our simulation.

KAsSn	Our work	Experiments
a_0 (Å)	4.138	4.103 [1] 4.102 [2]
c_0 (Å)	12.602	12.845 [1] 12.816 [2]
$(a/c)_0$	0.3283	0.319 [1] 0.320 [1]
V_0 (Å3)	186.886	187.30 [1] 186.76 [2]
Z_0(As)	0.676	0.6709 [1] 0.6795[2]
Z_0(Sn)	0.283	0.2742 [1] 0.2823[2]
B(GPa)	30.5	-
B'	3.08	-
Sn– As	2.745	2.715 [1] 271.0[2]
K-Sn	3.64	3.745 [1] 366.0[2]
K-As	3.246	3.230 [1] 330.2[2]

Table III. 1: Summary of calculated structural parameters (a_0, c_0, $(c/a)_0$, z_0 and V_0), bulk modulus *B* (GPa), as well as the pressure derivative *B′*(GPa) for KAsSn compared with available previous experiment and other theoretical results.

III.1.2 Study under pressure effect (equation of state construction)

The theoretical equilibrium bulk modulus *B* and its first order pressure derivative *B'* are determined by fitting the calculated unit cell volume at fixed values of applied hydrostatic pressure in the range from 0 to 20 GPa to the Birch–Murnaghan equation of state (EOS) [3]. However, no experimental or theoretical studies on the *B* and *B'* of this compound are available in the literature so far.

In Fig III.2 (a) we exhibit the pressure dependence of normalized lattice parameters (a/a_0, c/c_0) and volume V/V_0 for KAsSn. It can easily be seen that the relative parameters decrease with the pressure increasing from 0 GPa to 20 GPa. The changes of the ratios of $(c/a)_0$ for KAsSn keep almost constant with the pressure change. Therefore, it is seen that the c-axis is the most compressible and the a-axis is the least compressible under pressure actions, that is to say, the effect of pressure on c-axis is much more larger than a-axis.

The a/a_0, c/c_0 and the normalized cell volume V/V_0 as functions of pressure can be well described as third order polynomials: $\frac{X(P)}{X_0} = 1 + \beta x P + \sum_{n=2}^{3} K_n P^n$

$$\left(\frac{a}{a_0}\right) = 0.9994 - 0.0078P + 2.851 \times 10^{-4}P^2 - 4.140 \times 10^{-6}P^3$$

$$\left(\frac{c}{c_0}\right) = 1 - 0.0174P + 7.5136 \times 10^{-4}P^2 - 1.5934 \times 10^{-5}P^3$$

$$\left(\frac{V}{V_0}\right) = 0.9994 - 0.0324P + 0.001 \times 10^{-4}P^2 - 2.7954 \times 10^{-5}P^3$$

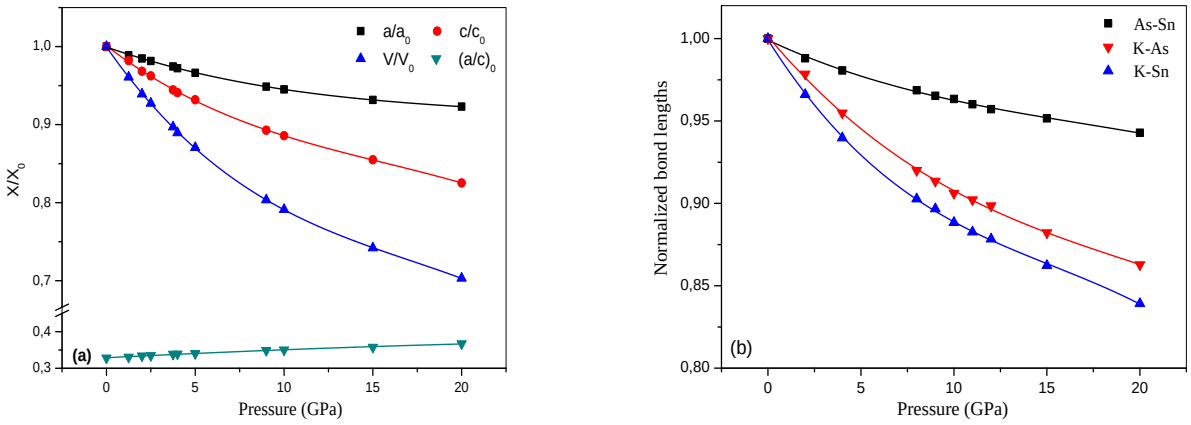

Fig III.2 (a) The normalized a/a_0, c/c_0, V/V_0 and the axial ratio $(a/c)_0$ as a function of pressure at T = 0.
(b) Variation of the normalized bond lengths between the atoms with pressure.

The bulk modulus for the hexagonal crystal may be estimated from the linear compressibilities *βx* along the a- and c-axes as follows *B*=1/ (2βa+β) [4]. Meanwhile using the volume compressibilities, the bulk modulus can be obtained by *B*=1/β. The calculated results are 32.25 GPa and 31.25 GPa respectively. These values are in good agreement with those obtained by Birch-Murnaghan equation of state (EOS).

Selected interatomic distances from KAsSn crystal structure under ambient conditions are also given in Table III.1. The observed bond lengths Sn-As, K-Sn and K-As can be successfully estimated based on previous experimental and theoretical data [1, 2, 5] by the following distances: 2.745Å, 3.64 Å and 3.246 Å for Sn-As, K-Sn and K-As respectively. In this structure the K atoms are coordinated by three Sn atoms and together by three As atoms in a distorted octahedral geometry, and it is of interest to compare bond lengths in these different environments [5]. Moreover, according to Fig III.2 (b), the normalized values of the bond lengths $L_{\text{Sn-As}}$, $L_{\text{K-Sn}}$ and $L_{\text{K-As}}$ have been plotted as function of pressure. By fitting the calculated data (L–P) to the third order polynomial, we obtain their relationships:

$$\left(\frac{L}{L_0}\right)_{\text{As-Sn}} = 0.99914 - 0.00529P + 2.02483 \times 10^{-4}P^2 - 3.96427 \times 10^{-6}P^3$$

$$\left(\frac{L}{L_0}\right)_{\mathrm{K-As}} = 1.00126 - 0.01343P + 4.89192 \times 10^{-4}P^2 - 8.17488 \times 10^{-6}P^3$$

$$\left(\frac{L}{L_0}\right)_{\mathrm{K-Sn}} = 0.99929 - 0.01789P + 8.75249 \times 10^{-4}P^2 - 1.90863 \times 10^{-5}P^3$$

Increasing pressure reduces the K-Sn bond length more than the K-As bond. However, The As–Sn bond length decreases gently under pressure. As a consequence, As–Sn bond is slightly less compressible than the K-As bond, whilst K-Sn bond has greater compressibility than K-Sn bond.

III.2 Elastic properties

III.2.1 Elastic constants (C_{ij}), bulk modulus (B) and shear modulus (G) at zero pressure

The elastic constants of solids provide a link between the mechanical, physical and dynamical behavior of crystals and give important information concerning the nature of the forces operating in solids. Elastic constants can be calculated by applying small strains to the equilibrium unit cell and determining the corresponding variations in the total energy. In order to study the mechanical properties of KAsSn, we have calculated the elastic constants C*ij*, bulk modulus *B*, shear modulus *G*, Young's modulus *E* and Poisson's ratio ν from the obtained elastic constants according to the Voigt–Reuss–Hill approximation [6-8].

Elastic properties of hexagonal KAsSn crystal can be described using five independent elastic constants (C_{11}, C_{12}, C_{13}, C_{33}, C_{44}) since $C_{66} = 0.5(C_{11} - C_{12})$. The calculated results at 0 K and zero pressure are illustrated in Table III.2. It can be seen that the value of C_{11} is higher than C_{33} and C_{13} is slightly smaller than C_{12}, this means that the resistance to the applied stress are high in the [1 0 0] direction than in the [0 0 1]. This signified that the KAsSn compound is more compressible along the c-axis than along the a-axis. This is in accord with the response of a and c under pressure, shown in Fig III.2 and discussed above in section III.1. At present, no experimental or theoretical data for the elastic constants of KAsSn are available to be compared to our present theoretical estimation.

Compound	C_{11}	C_{12}	C_{13}	C_{33}	C_{44}	C_{66}
KAsSn	59.11	19.49	18.60	46.60	16.21	19.80

Table III. 2: The calculated elastic constants (C_{ij} in GPa) for single cristal KAsSn at zero pressure.

The values of C_{12}, C_{66}, C_{13} and C_{44} are far smaller than that of C_{11}, which reflects the weak resistance to shear deformation for the crystal. Essentially the crystal is elastically anisotropic. The requirement of mechanical stability for hexagonal crystals leads to the following restrictions on the elastic constants [9]:

$$C_{11} > 0,\ (C_{11} - C_{12}) > 0,\ C_{44} > 0,\ (C_{11} + C_{12})\, C_{33} > 2C^2_{13} \qquad \text{(III.1)}$$

Within the pressure considered, the elastic constants obey these stability criteria indicating that KAsSn is mechanically stable. To the best of our knowledge, this study reports for the first time the elastic constant of this compounds. Once the single-crystal elastic constants are computed, the related properties of polycrystalline aggregates can be evaluated.

The bulk modulus, shear modulus, Young's modulus and Poisson's ratio are the most interesting elastic properties for applications and are often measured for polycrystalline materials while investigating their hardness.

The Voigt (*V*) and Reuss (*R*) bounds of the bulk modulus and shear modulus (B_V, B_R, G_V, G_R) in terms of the elastic constants *Cij*'s for an hexagonal structure are [10-11]:

$$Bv = \frac{2}{9}\left(C_{11} + C_{12} + \frac{C_{33}}{2} + 2C_{13}\right) \qquad \text{(III. 2)}$$

$$B_R = \frac{(C_{11} + C_{12})C_{33} - 2C_{13}^2)}{(C_{11} + C_{12} + 2\,C_{33} - 4C_{13})} \qquad \text{(III. 3)}$$

$$Gv = \frac{1}{30}(7C_{11} - 5C_{12} + 12C_{44} + 2C_{33} - 4C_{13}) \qquad \text{(III. 4)}$$

$$G_R = \frac{5}{2}\left\{\frac{[(C_{11} + C_{12})C_{33} - 2C_{13}^2]C_{44}C_{66}}{3BvC_{44}C_{66} + ((C_{11} + C_{12})\,C_{33} - 2C_{13}^2))(C_{44} + C_{66})}\right\} \qquad \text{(III. 5)}$$

The *VRH* mean values are obtained by $B_H = 1/2(B_V + B_R)$ and $G_H = 1/2\,(G_V + G_R)$.

The Young's modulus *E* is a measure of the stiffness of an elastic material and the Poisson ratio *v* reflects the stability of a crystal against shear. They can be obtained by using the bulk modulus and shear modulus [12]:

$$E = \frac{9BG}{3B + G} \qquad \text{(III. 6)}$$

$$v = \frac{3B - 2G}{2(3B + G)} \qquad \text{(III. 7)}$$

The calculated results are shown in Table III.3.

It should be noted that the calculated bulk moduli of KAsSn is in accordance with those obtained through the fit to a Birch Murnaghan *EOS*. It is seen that $B_H > G_H$, which indicates that the parameter limiting the stability of hexagonal KAsSn is the shear modulus.

Compound	B_R	B_V	B_H	G_R	G_V	G_H	G/B	E	v
KAsSn	30.50	30.91	30.71	17.44	17.66	17.55	0.57	44.22	0.26

Table III. 3: The elastic modulus *B* (GPa), shear modulus *G* (GPa), Young's modulus *E* (GPa) and *G/B*, Poisson's ratio (ν) for KAsSn using Voigt, Reuss and Hill's approximations.

The value of the Poisson's ratio is indicative of the degree of directionality of the covalent bonds. The value of the Poisson's ratio is small (v = 0.1) for covalent materials, whereas for ionic materials a typical value of v is 0.25 [13]. The calculated value of v for KAsSn is about 0.26 at 0 GPa, indicating a considerable ionic contribution in intra-atomic bonding. The calculated results demonstrate that KAsSn is more stable against shear owing to its smaller value of Poisson's ratio. The ductile or brittle nature of the materials may be distinguished on the basis of the Poisson's ratio [14]. For a material to be brittle v must be ≤ 0.33, else the material is ductile. It is observed from Table III.3 that our calculated value of v lies above critical value showing that our compounds are brittle at ambient conditions. Another index of brittle nature can also be known from the G_H/B ratio, which is presented in Table III.3. According to Pugh's criteria, the high (low) G_H/B ratio is associated with the brittle (ductile) nature of the materials [15]. The critical value separating ductility from brittleness is about 0.57. This ratio is around 0.571 for KAsSn which clearly implying the slightly brittle nature of this material. As well as the calculated value of G/B for KAsSn is 0.571, which also indicate that the ionic bonding is suitable for this compound.

III.2.2 Elastic constants, bulk modulus under pressure effect

We further study the high pressure elastic behavior of the KAsSn by computing the elastic constants *Cij*, bulk modulus *B* and their variations with pressure, as shown in Fig III.3.

The elastic constant C_{11} (C_{33}) represents the elasticity in length. The elastic constants C_{12} (C_{13}) and C_{44} (C_{66}) are related to the elasticity in shape. C_{11} can change with the longitudinal stain. It is found that, C_{11}, C_{33}, C_{12}, C_{13}, C_{44} are susceptible to pressure (Fig III.3). Also it can be seen that the elastic constants, C_{11}, C_{12}, C_{13}, C_{44} and C_{33}, increase monotonically with the increasing pressure, but with different slopes. As well it can be seen that $C_{33} < C_{11}$ in the whole range of pressure which implicates that the atomic bonds along the (1 0 0) planes between nearest neighbors are stronger than those along the (0 0 1) planes. As pressure

increases C_{11} varies largely under the effect of pressure as compared with the variation in C_{33}, C_{12}, C_{13}, C_{44} and B. So C_{11}, C_{33} and C_{44} are more sensitive to the change of pressure compared to B, C_{12} and C_{13}.

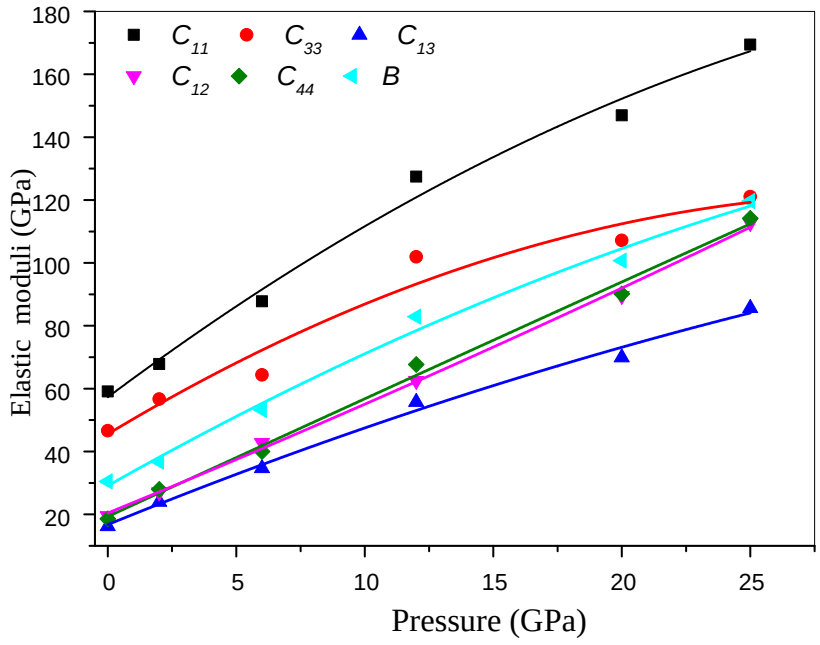

Fig III.3 Elastic constants C_{ij}, bulk modulus B versus pressure for KAsSn

Noticeably, Fig III.3 exhibits a quasi linear dependence between the elastic constants and hydrostatic pressure as the applied hydrostatic pressure ranges from 0 to 25 GPa. The second order polynomials describing the pressure dependence of the elastic constants and bulk modulus for KAsSn are given by the following expressions:

$$C_{11} = 57.28396 + 6.12493P - 0.06891P^2$$

$$C_{33} = 45.54261 + 4.92599P - 0.07907P^2$$

$$B = 29.113 + 4.6235P - 0.0425P^2$$

$$C_{44} = 19.2998 + 3.7635P - 0.00157P^2$$

$$C_{12} = 20.4358 + 3.34615P - 0.01159P^2$$

$$C_{13} = 16.7479 + 3.32917P - 0.025427P^2$$

III.2.3 Anisotropy factor (*A*), hardness (*Hv*)

It is important to calculate elastic anisotropy in brittle materials in order to hopefully find the mechanisms which will improve their durability. The elastic anisotropy arises from both shear anisotropy and the anisotropy of linear bulk modulus. The shear anisotropic factors on

different crystallographic planes supply a measure of the degree of anisotropy in atomic bonding in different planes. The shear anisotropic factors for hexagonal structure are written as follows [16-17] $A_1 = A_2 = 4C_{44}/(C_{11}+C_{33}-2C_{13})$ for the (100) (010) plane directions and similarly due to the crystal symmetry, $A_3=4C_{66}/(C_{11}+C_{22}-2C_{12})$ for the (001) direction ($C_{66}=(C_{11}-C_{12})/2$). For an isotropic crystal, the factors A_1, A_2 and A_3 should be equal 1, while any deviation from 1 indicates the degree of the shear anisotropy. The shear anisotropic factors obtained from our theoretical studies are also listed in Table III.4. KAsSn is elastically isotropic for the (001) shear plane and weak elastically anisotropic for the (100) (010) shear planes.

compound	C_{13}/C_{12}	C_{33}/C_{11}	C_{44}/C_{66}	A_B (%)	A_G (%)	A_1	A_2	A_3	A^U	A_{Bc}	A_{Ba}
KAsSn	0.954	0.788	0.818	0.66	0.62	0.94	0.94	1	0.07	0.67	1

Table III.4: The shear anisotropic factors *Ai* with *i*=1,2,3, the anisotropies linear bulk modulus A_{Bc} , A_{Ba}, the percentage of anisotropy in the compression A_B and shear A_G (%) and universal elastic anisotropy index A^U.

The universal anisotropy index A^U that represents a measure to quantify the single crystal elastic anisotropy can be written as [18]: $A^U=5(G_V/G_R)+(B_V/B_R)-6$. A^U is zero for locally isotropic single crystal. The deviation of A^U from zero reflects the extent of single crystal anisotropy. Table III.4 indicates that the hexagonal KAsSn is slightly anisotropic. In addition to evaluate the elastic anisotropy of KAsSn, we calculated the percentage of anisotropy in compression and shear [19] for polycrystalline material, which are defined as $A_B=(B_V-B_R)/(B_V+B_R)$ and $A_G=(G_V-G_R)/(G_V+G_R)$, respectively. Table III.4 lists also the percentage of anisotropy in compression and shear for KAsSn and also the anisotropy factors. It can be seen that this material exhibits small anisotropy in shear and compression. Interestingly, A_B shows that KAsSn has better isotropy in compression, while A_G indicates that is more isotropic in shear. We also investigated the contribution of linear bulk modulus to the elastic anisotropy A_{Ba}, A_{Bc}, and the results are displayed in Table III.4. The anisotropy of the bulk modulus along the a- and c- axes with respect to the b-axis can be written as [17-20]:

$$A_{Ba} = \frac{B_a}{B_b}\ , A_{Bc} = \frac{B_c}{B_b} = \frac{1}{\beta}\ = \frac{(C_{33}-C_{13})}{(C_{11}+C_{12}-2\,C_{13})} \qquad \text{(III. 8)}$$

$$B_a = a\frac{dp}{da} = \frac{\Lambda}{2+\beta}\ , B_c = c\frac{dp}{dc} = \frac{B_a}{\beta} \qquad \text{(III. 9)}$$

Where $\Lambda = 2(C_{11} + C_{12}) + 4C_{13}\beta + C_{33}\beta^2$

ß is defined as the relative change of the c-axis as a function of the deformation of the a-axis. A_{Bc} is calculated to be 0.67, which indicates that the compressibility for KAsSn along c-axis is smaller than along a-axis. We can conclude that the atomic bonding strength along the a-axis is stronger than that along c-axis from the large C_{13}/C_{12} and small C_{33}/C_{11} anisotropic parameters values.

In order to get a better understanding of stiffness for the KAsSn, the micro-hardness parameter *Hv* has been calculated. However, there are many correlations between Vickers hardness (*Hv*) and bulk, shear, Young's moduli, Poisson's ratio and *G/B* to obtain the value of micro-hardness parameter *H*, as following [21-22]:

$$Hv = \frac{(1-2v)E}{6(1+v)} \quad \text{(III. 10)}$$

$$H_v = 0.1475G \quad \text{(III. 11)}$$

$$H_v = 0.0608\ E \quad \text{(III. 12)}$$

$$H_v = 0.0963B \quad \text{(III. 13)}$$

$$H_v = 2((G/B)^2 G)^{0.585} - 3 \quad \text{(III. 14)}$$

The calculated *Hv* values are listed in Table III.5. It is found that Eq. (14) and (13) obtain the lowest and the highest values, respectively. Therefore, the Vickers hardness of KAsSn should be near 2.7 GPa.

Compound	Eq. (10)	Eq. (11)	Eq. (12)	Eq. (13)	Eq.(14)
KAsSn	2.80	2.588	2.688	2.957	2.53

Table III. 5: The microhardness parameter *Hv* (in GPa) for the KAsSn

III.2.4 Acoustic wave velocities, Debye temperature

Acoustic wave velocities in a material can be obtained from the Cristoffel equation [23]. Moreover, the velocities of the longitudinal (v_l) and transversal waves (v_{T1} and v_{T2}) along [1 0 0], [0 0 1] and [1 2 0] directions have been calculated for hexagonal crystal using the elastic constants *Cij*, and following the relations:

$$v_L^{[100]} = v_L^{[120]} = \sqrt{\frac{C_{11}}{\rho}}\ , v_{T1}^{[100]} = v_{T1}^{[120]} = \sqrt{\frac{(C_{11}-C_{12})}{2\rho}}\ , v_{T2}^{[100]} = v_{T2}^{[120]} = \sqrt{\frac{C_{44}}{\rho}} \quad \text{(III.15)}$$

$$v_L^{[001]} = \sqrt{\frac{C_{33}}{\rho}}\ ,\quad v_{T1}^{[001]} = v_{T2}^{[001]} = \sqrt{\frac{C_{44}}{\rho}} \quad \text{(III.16)}$$

Where ρ is the density of material, *T* and *L* represent transverse and longitudinal wave polarization. The values of acoustic wave velocities for KAsSn reproduced from the elastic constants C*ij* at zero pressure along [1 0 0], [1 2 0] and [0 0 1] directions are listed in Table III.6.

Compound	$\nu_L^{(100,120)}$	$\nu_{T1}^{(100,120)}$	$\nu_{T2}^{(100,120)}$	$\nu_L^{(001)}$	$\nu_{T1}^{(001)}$	$\nu_{T2}^{(001)}$
KAsSn	3780	2188	1979	3356	1979	1979

Table III. 6: Acoustic wave velocities (in m/s) for different propagation directions for KAsSn compound

We can observe that there is nuance between the values of the longitudinal velocities along the a-axis and c-axis. Furthermore the longitudinal wave along the [1 0 0] direction travel faster than shear wave since the square root of C_{33} is generally larger than C_{44} and C_{11}.
Debye temperature θ_D may be estimated from the average wave velocity v_m using the following equation [24-25]

$$\theta_D = \frac{h}{k_B}\left[\frac{3n}{4\pi}\frac{N_A\rho}{M}\right]^{\frac{1}{3}} v_m \qquad \text{(III. 17)}$$

Where *h* is the Plank's constant, k_B is the Boltzmann's constant, *n* is the number of atom in a molecule, N_A is the Avogadro's number, ρ is the density and *M* is the molecular weight. The sound velocity v_m is given by [26-27]:

$$v_m = \left[\frac{1}{3}\left(\frac{2}{v_t^3} + \frac{1}{v_l^3}\right)\right]^{\left(\frac{1}{-3}\right)} \qquad \text{(III. 18)}$$

Where v_l and v_t are the longitudinal and shear elastic wave velocities, respectively, which can be obtained from [28]:

$$v_l = \left[\left(\frac{3B + 4G}{3\rho}\right)\right]^{\left(\frac{1}{2}\right)} \qquad v_t = \left(\frac{G}{\rho}\right)^{1/2} \qquad \text{(III. 19)}$$

The calculated wave velocities, Debye temperature as well as the density of KAsSn at zero pressure are given in Table III.7. As far as we know, there are no experimental data available for comparison.

compound	ρ	ν_L	ν_T	ν_m	θ_D
KAsSn	4.135	3610	2060	2289	216

Table III. 7: The calculated density ρ (g/cm^3), density longitudinal, transverse and average wave velocity (v_l, v_t, v_m in m/s) and the θ_D (unit in K)

III.3 Electronic properties

III.3.1 Electronic band structure

The calculated electronic band structure of the crystal KAsSn at zero pressure along the principal symmetry directions of the Brillouin zone are shown in Fig III.4. The top of the valence band whose mostly formed by the combination of As-s, Sn-s, p (Sn-As) states is chosen to be the Fermi level (E_F = 0 eV), while the bottom of the conduction bands is mainly derived from the p Sn (5s+5p) and As (4s+4p) states and small contribution from K-3p states. The upper valence band maximum and the lower conduction band minimum occur at G point, making KAsSn a direct band narrow gap material; it appears along the Gv-Gc direction with energy of 0.341 eV. As there is no experimental data for the band gap therefore the calculated value is close to the previous ones obtained by LDA (*Eg*=0.1eV) [29]. However, the indirect band gap appears at (G-L), (G-K), (G-H) transitions are 0.93eV, 1.31eV, 1.18eV respectively. Our results elucidate that KAsSn is a semiconductor with narrow band gap.

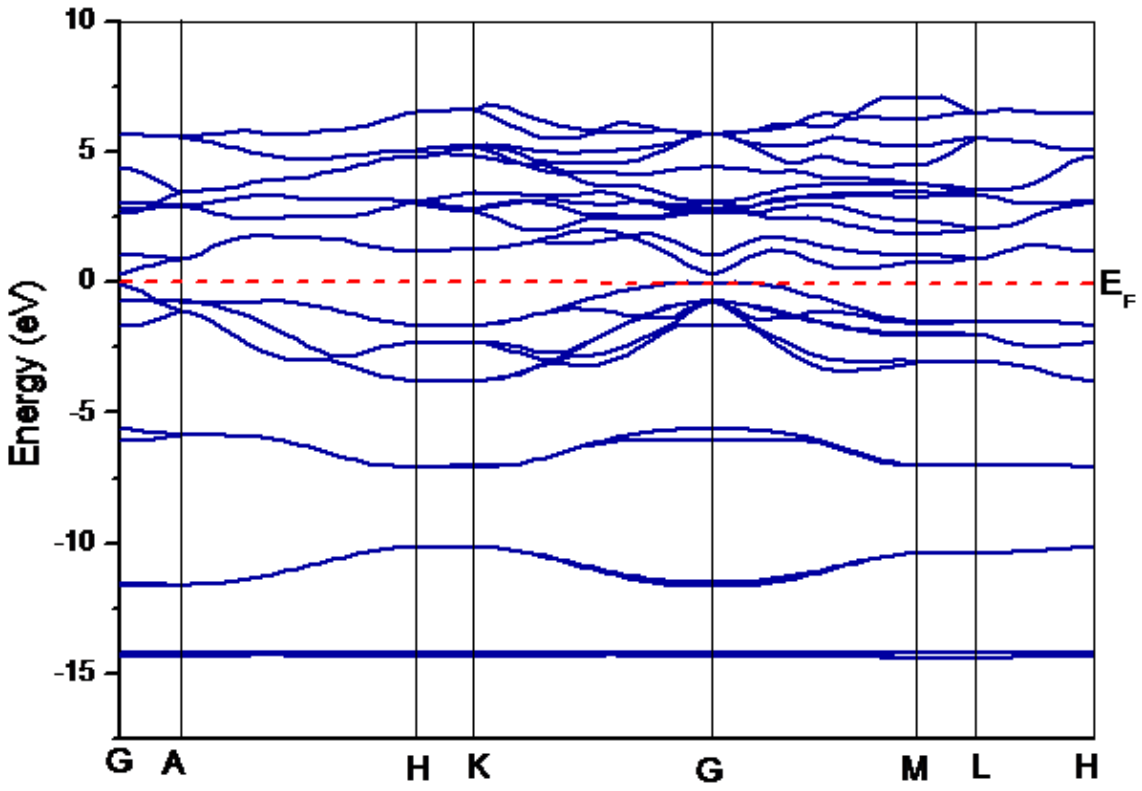

Fig III.4 Bande structure of KAsSn

III.3.2 Total and partial density of states

For the sake of clarity and ease of guidance, the total density of states TDOS is also plotted in Fig III.5 along with the PDOS densities of states diagrams at ambient pressure. It is shown that the total density of states extended from about -35 eV to 10 eV. In the total DOS curve of KAsSn there are six main peaks (A, B, C, D, E and F). Evidently, the peaks A and B in the lower energy part of the TDOS curve are derived from K-3s and 3p states respectively, which are localized and contribute little to the bonding of KAsSn. For the peak C, the TDOS mainly made of the occupied Sn-5s states with less contribution from As-4p mixing with a minor presence of As-4s. The energy decreased in total TDOS at the peak C implies that there are s-p interactions in As. Moreover, the peak D, originates from As-4s hybridize with Sn -5p mixing with a small existence of Sn-5s states. Furthermore, for the peak E, the Sn-5p states strongly hybridize with the As-4p states, together with small contributions from As-4s states. Crossing the peaks E and F, the strong hybridization of the Sn-5p and As-4p can lower the energy of the bonding states and increase the energy of anti-bonding states, which produce the presence of a valley near the Fermi level, and this is referred to as a narrow gap. Above the

Fermi level, anti-bonding As-4p states dominate with hybridizations bonding between Sn-5p and fewer contributions from K-3p states.

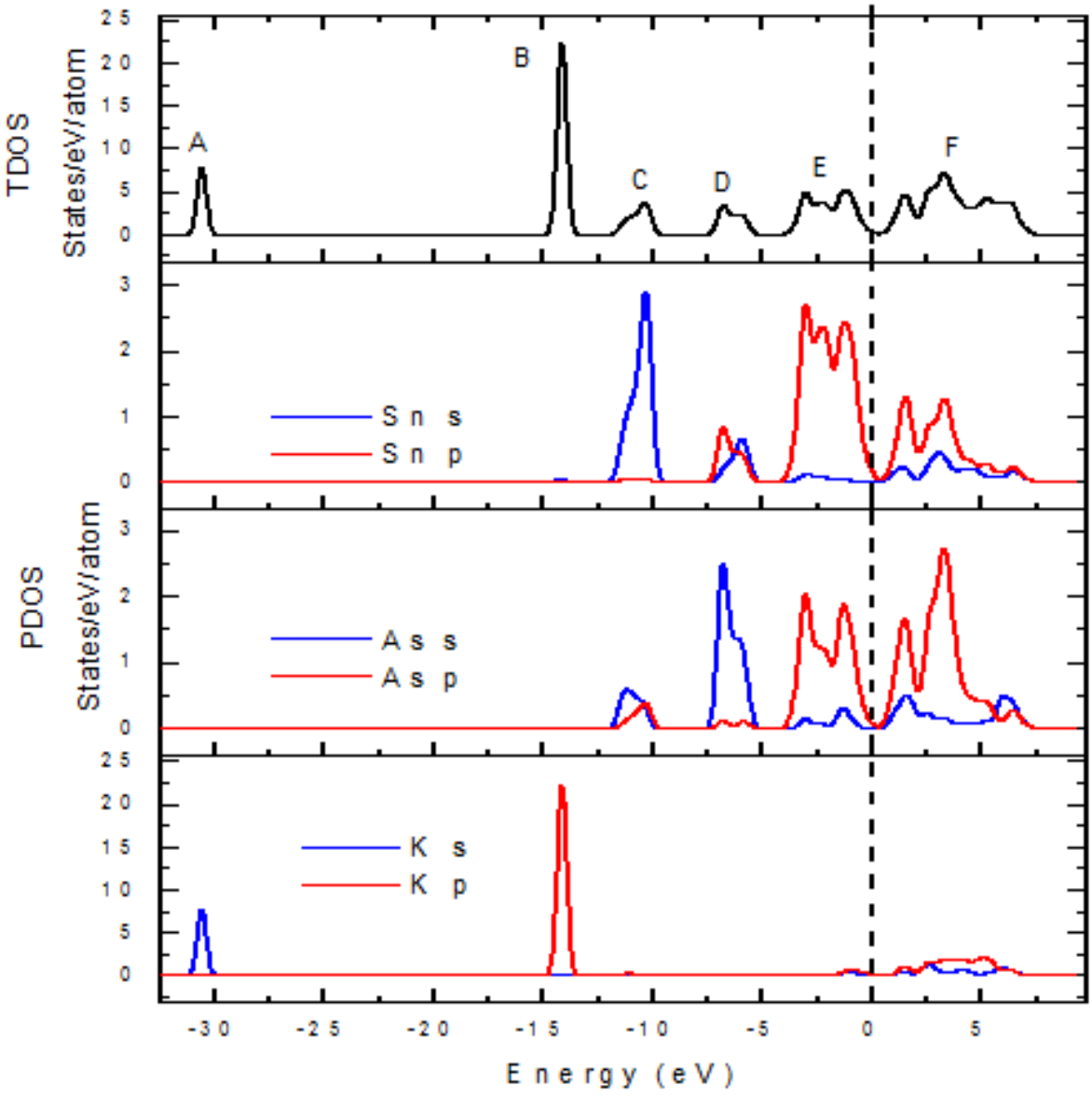

Fig III.5 Calculated total and partial densities of states (TDOS and PDOS)

III.3.3 Bond length, Mulliken population

To further understand interatomic bonding behaviors of this crystal, the calculated atomic populations, bond length and charges via the Mulliken population analysis are listed in Table III.8. Generally, a high value of positive population indicates a high degree of covalency in the bond [30]. As seen from Table III.8, two different bonding characters take place in the atomic interactions of the considered systems, As–Sn, K-K bonds are covalent and K–As, K–

Sn, Sn–Sn, As–As are ionic. We may observe also that the bond population of the K–Sn bond is clearly much larger than that of the K–As and As–Sn.

Band	Mulliken Population	Bond length
As - Sn	2.73	2.74555
K - As	-1.92	3.24617
K - Sn	-0.96	3.64336
Sn - Sn	-0.12	6.30121
K - K	2.39	6.73892
As - As	-0.54	6.73892

Table III. 8: Mulliken atomic population and Bond lengths of KAsSn

Now, we report the calculated Mulliken atomic population for KAsSn. The Mulliken charges are determined to be 0.32e for K atoms, -0.25e for As atoms, and -0.07e for Sn atoms, respectively. We can see that electrons run from K to As and Sn with gaining a total of 0.32 electrons per atom, these propose a valence state of $K^{+0.32}(As^{-0.25})$ $(Sn^{-0.07})$. The value of K Mulliken charges is representative of the concurrent ionic and covalent bonding in KAsSn.

To visualize the nature of the bonding character of the solids, we have obtained the charge density distributions map for KAsSn in Fig III.6.

For the sake of simplicity, only the charge density distribution for a slice of the (1 1 0) plane is plotted with a contour lines from 0 to 0.39 eV/$Å^3$. Higher density region corresponds to the core electron distribution of K, As and Sn atoms, and it contributes relatively little to the bonding. Moreover the value of the charge density between As-K and Sn-K is larger than that between As-Sn, so As–Sn bonding is relatively stronger than the Sn-K and K-As bonding in KAsSn. The figure reveals that a significant overlapping can be observed between Sn and As bonding due to As-4p and Sn-5p hybridization, indicating covalent bonding between As and Sn, while the bonding between K–Sn and K-As atom is mainly ionic. Then, also, due to the difference in the electronegativity between the comprising elements, some ionic character can be expected.

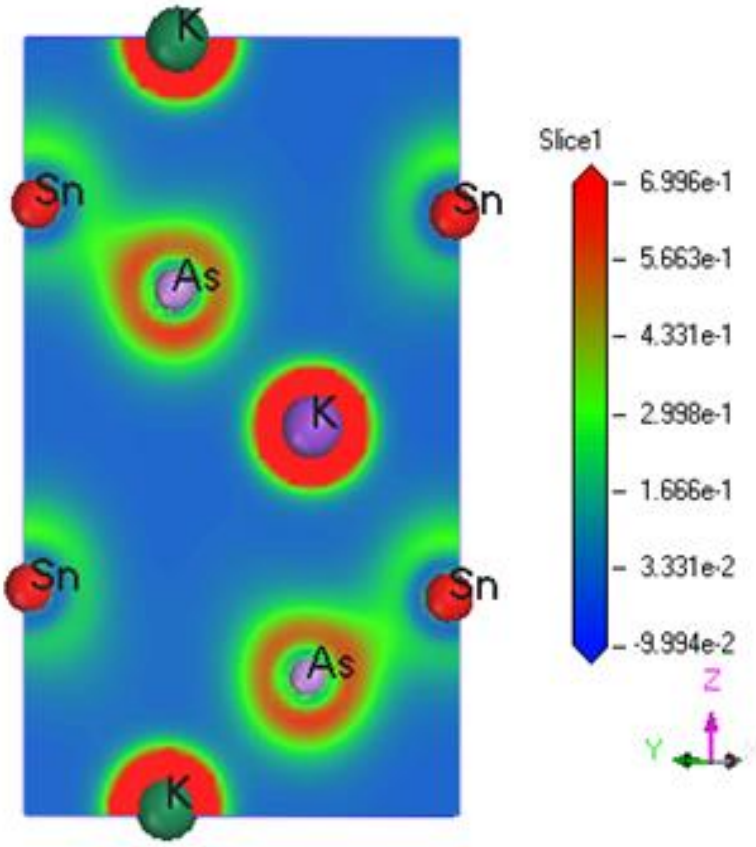

Fig III.6 The bonding charge density plots in the (110) plane of the KAsSn

III.3.4 Energy band gap

Fig III.7 shows the variation of the direct band gap energy G-G with applied hydrostatic pressure in the range 0-19 GPa. As one can see, the band gap manifests an unusual increase with pressure initially up to 2 GPa and then decreases nonlinearly when the pressure is enhanced. More interestingly, when the application pressure is greater than 19.01 GPa, the band gap almost disappears and the resultant compound becomes metallic. The calculated values for the band gaps are fitted to the third order function:

$$E_g = 0.347+0.0565P-0.0117P^2+ 4.9552\times10^{-4}P^3$$

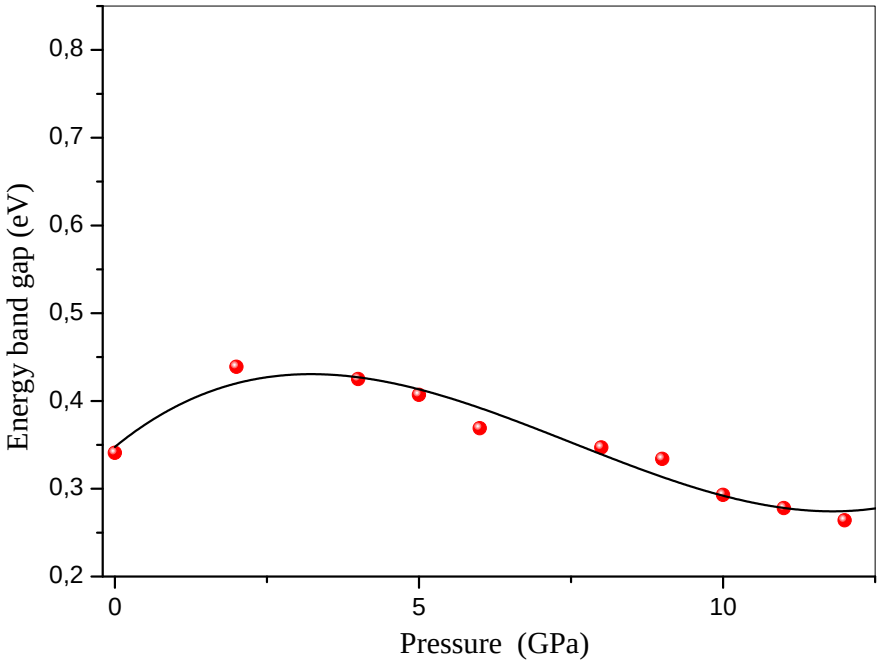

Fig III.7 Energy band gap of KAsSn versus the pressure

III.4 Optical properties

Generally, the optical properties are mainly studied through many physical parameters including the refractive index $n(\omega)$, extinction coefficient $k(\omega)$, optical reflectivity $R(\omega)$, absorption coefficient $\alpha(\omega)$, and energy-loss spectrum $L(\omega)$. It is known that the optical response can be described by a complex frequency dependent dielectric function ε(ω): $\varepsilon(\omega)=\varepsilon_1(\omega)+i\,\varepsilon_2(\omega)$ which is mainly connected with the electronic structures. The imaginary part of the dielectric function $\varepsilon_2(\omega)$ which arises from interband transitions, depends on density of states can be calculated from the momentum matrix elements and by considering all the possible transitions between the occupied and unoccupied electronic states with the equation [31-33]:

$$\varepsilon_2(\omega) = \frac{2e^2\pi}{\Omega\varepsilon_0}\sum_{k,c,v}\int|\Psi_k^c < \hat{u}r > \Psi_k^v|^2\delta(E_k^c\text{-}E_k^v - E) \qquad \text{(III. 20)}$$

Where the integral is over the first Brillouin zone, ω is the frequency, e is the electronic charge, $\Omega \propto m^2\,\omega^2$, m is the electron effective mass, Ψ_k^c and Ψ_k^v are the conduction and valence band wave functions at k, ε_0 is the dielectric function of free space. The real part $\varepsilon_1(\omega)$ can be attracted from Kramers-Kroning relationship [34-36]

$$\varepsilon_1(\omega) = 1 + \frac{2}{\pi} M \int_0^{\infty} \frac{\omega' \varepsilon_2(\omega')}{\omega'^2 - \omega^2} d\omega' \quad \text{(III. 21)}$$

Where *M* is the principal value of the integral. Other optical constants such as the absorption coefficient $\alpha(\omega)$, the electron energy loss spectrum $L(\omega)$, the refractive index $n(\omega)$, extinction coefficient $k(\omega)$ and optical reflectivity $R(\omega)$ can be computed from the complex dielectric function $\varepsilon(\omega)$, through the following relations [31-32]:

$$n(\omega) = \left[\sqrt{\varepsilon^2{}_1(\omega) + \varepsilon^2{}_2(\omega)} + \varepsilon_1(\omega)\right]^{\frac{1}{2}} / \sqrt{2} \quad \text{(III. 22)}$$

$$k(\omega) = [\sqrt{\varepsilon^2{}_1(\omega) + \varepsilon^2{}_2(\omega)} - \varepsilon_1(\omega)]^{1/2} / \sqrt{2}$$

$$R(\omega) = \left| \frac{\left(\varepsilon(\omega)^{\frac{1}{2}} - 1\right)}{\left(\varepsilon(\omega)^{\frac{1}{2}} + 1\right)} \right|^2 \quad \text{(III. 23)}$$

$$L(\omega) = \frac{\varepsilon_2(\omega)}{\varepsilon^2{}_1(\omega) + \varepsilon^2{}_2(\omega)}$$

$$\alpha(\omega) = \sqrt{2}\omega[\sqrt{\varepsilon_1(\omega) + \varepsilon^2{}_2(\omega)} - \varepsilon_1(\omega)]^{1/2}$$

From here, some of the optical properties at the equilibrium lattice constant have been computed and are plotted (Figs III. 8-10) in the energy range 0-20 eV. To date there are no experimental or theoretical optical spectra available for this compounds.

III.4.1 Dielectric function, Refractive index

The real and imaginary parts of dielectric function curves are presented in Fig III.8. It can be seen that in a high energy area, the values of the imaginary part are very small, while the real part changes very little. The curve of $\varepsilon_2(\omega)$ indicate that the main peak around 2.85 eV originates predominantly from the direct optical transitions along the (G–G) direction between the highest valence electrons (Sn-5p states) and the lowest first conduction band (As-4p states). The static dielectric constant ε_1 (0) which is the electronic part, strongly depends on the bandgap and is given by the low energy limit of dielectric function $\varepsilon_1(\omega)$ and is equal to 12.75. All the components of dielectric tensor for the hexagonal crystals are anisotropic ($\varepsilon_x = \varepsilon_y \neq \varepsilon_z$) so the KAsSn exhibits birefringence.

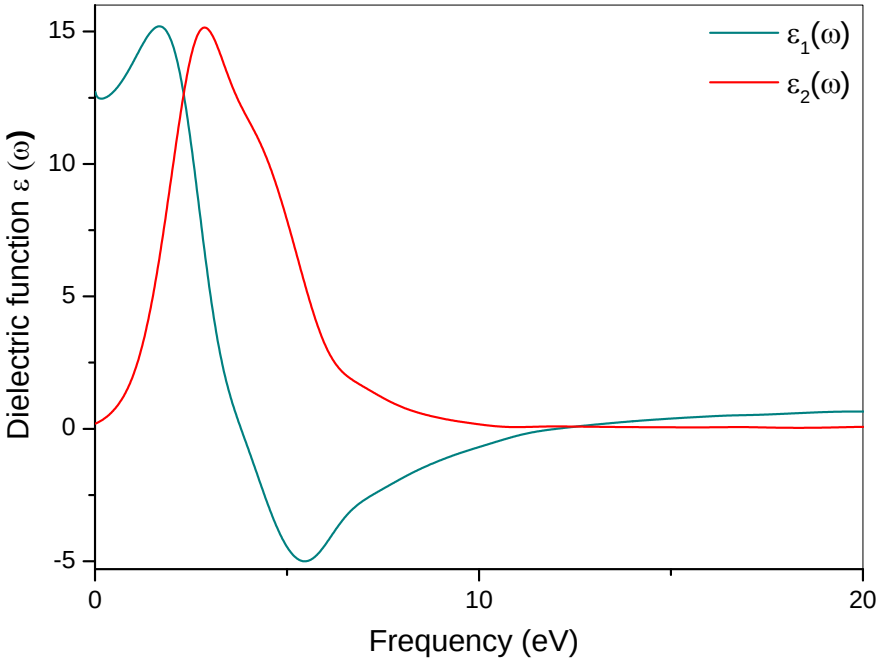

Fig III.8 Real part ε_1 (ω) and imaginary part ε_2 (ω) of the dielectric function for kAsSn

A calculated spectrum of refractive index and extinction coefficient for kAsSn are displayed in Fig III.9 is also related to ε(0) by the relation $n(0) = \sqrt{Re\varepsilon(0)}$. From the real dielectric function the calculated refractive index is 3.57. While from Fig III. 9, the static refractive index is found to have the value 3.52, this value increases with increasing energy and reaches peak in the visible region at about 1.87eV. It then decreases to a minimum level at 10.8 eV with a value 0.057. For the extinction coefficient the maximum arises at 4.87 eV.

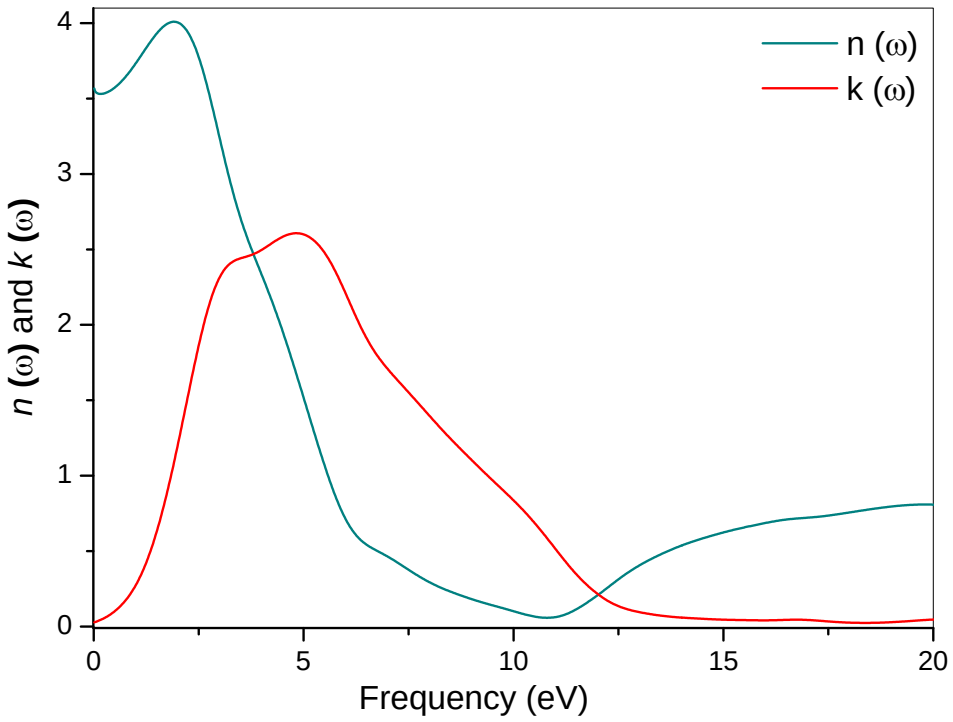

Fig III.9 The calculated refractive index and extinction coefficient for KAsSn

III.4.2 Extinction coefficient, optical reflectivity, absorption coefficient and energy-loss spectrum

Fig III.10 (a), (b) and (c) show the calculated results of the linear absorption spectrum α(ω), reflectivity function $R(\omega)$ and electron energy loss function $L(\omega)$ for KAsSn. The energy loss of a fast electron traversing the material is manifested in the energy loss spectrum. The prominent peaks in energy loss spectra represent the characteristic associated with the plasma frequency ω_p. In the energy loss spectrum (Fig III.10 (c)), we see that the plasma frequency ωp corresponds to the abrupt reduction of the reflection spectra and appears at about 12 eV. Also this figure shows the absorption spectrum with a large broaden peak between 5 and 6.5 eV (5.52) which rises and then decreases rapidly in the high energy region. The absorption edge start from the energy value of 0.34eV, which could possibly be due to transitions across the direct band gap at G point, this arises from Sn-5p/As-4p electronic transitions. The figure also shows some structures in the ultraviolet region at 20.24 eV and 16.9 eV respectively.

As can be seen in Fig III.10 (a), the absorption spectrum started at 1.09 eV and decreased rapidly in the low energy region. In the range from 0 to 1.09 eV, the reflectivity is lower than 35%, which indicates that KAsSn material is transmitting for frequencies less than 1.09 eV. From Fig III.10 (c), the maximum reflectivity occurs in the energy of 10.7 and has a value of approximately 85 % in the ultraviolet region.

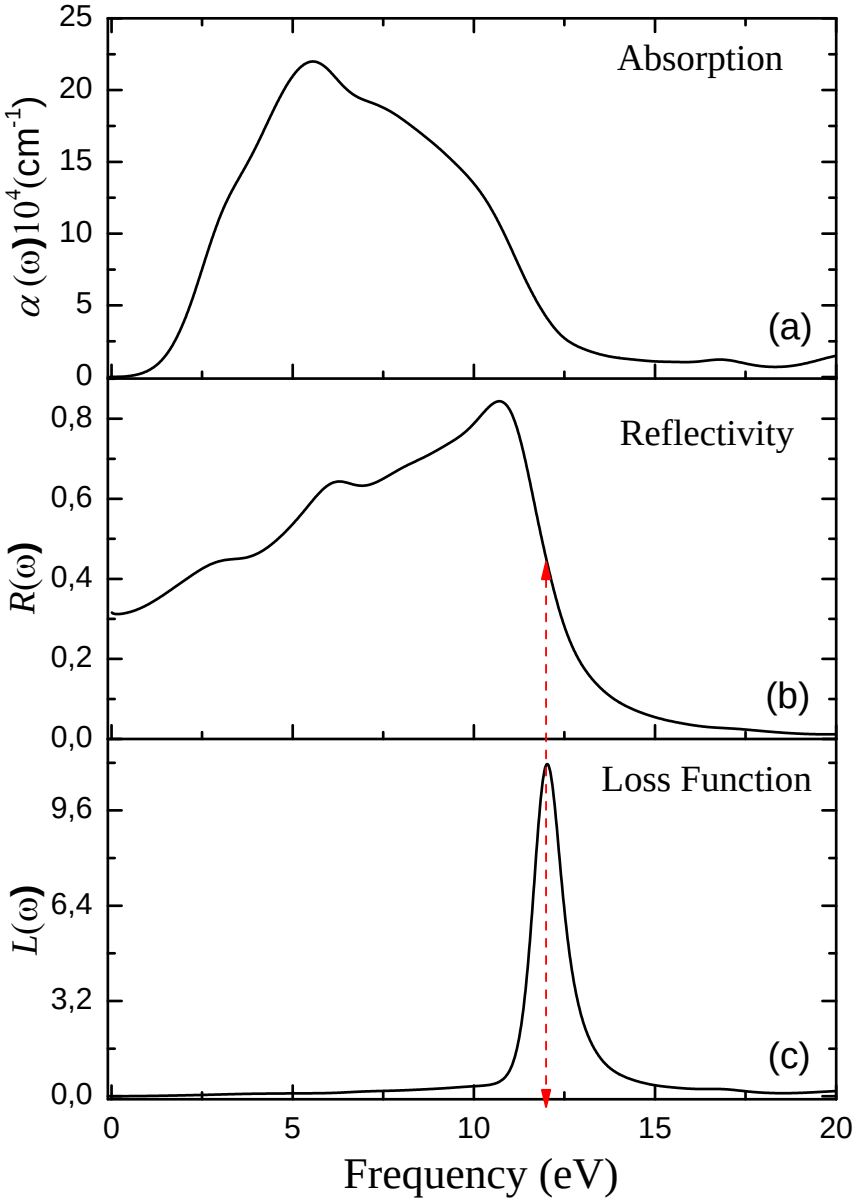

Fig III.10 Reflectivity, Absorption and electron energy-loss function of KAsSn under 0 GPa.

III.4.3 Pressure dependence of the static dielectric constant

The pressure dependence of the static dielectric constant and the static refractive index of the KAsSn compound are plotted in Fig III.11. We remark that these parameters decrease monotonically with increasing pressure in the range from 0 to 20 GPa. The pressure coefficients displayed in Fig III.11 are obtained by fitting the calculated values to a quadratic polynomial as follows:

$$n(0) = 3.54418 - 0.02871P + 0.00128P^2$$

$$\varepsilon_1(0) = 12.61816 - 0.21258P + 0.00939P^2$$

Where P is the pressure in GPa unit.

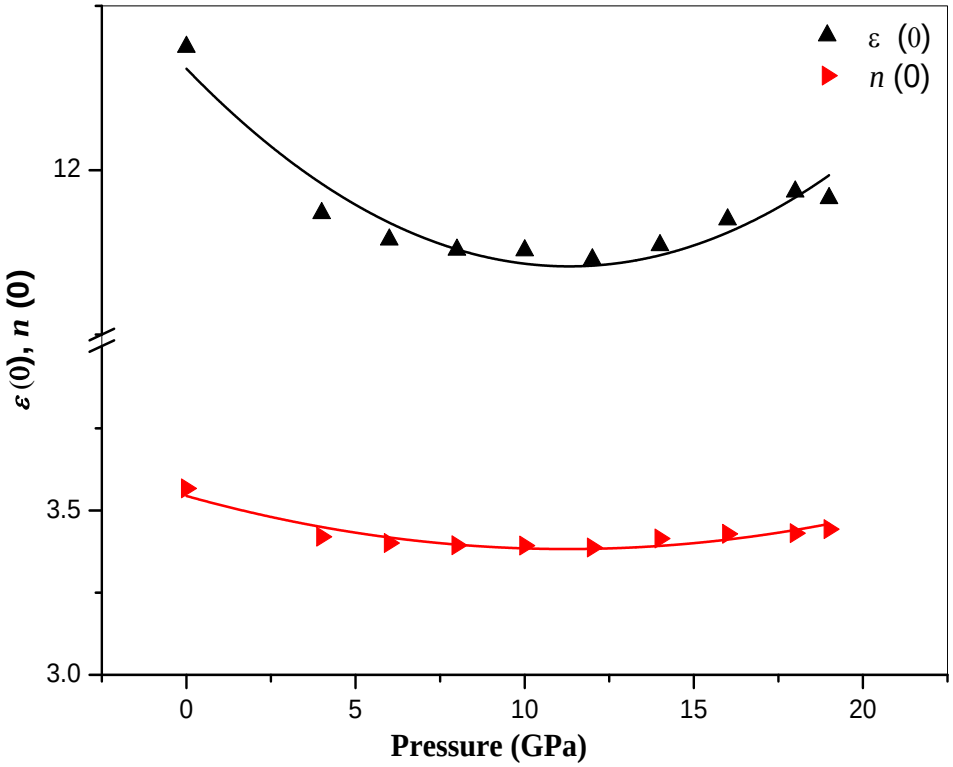

Fig III.11 Pressure dependence of the static dielectric constant $\varepsilon_1(0)$ and static refractive index $n(0)$ for KAsSn

References

[1] K.H. Lii, R. C. Haushalter, Journal of solid state chemistry, 67 (1987)374-378.

[2] J. Klein, B. Eisenmann, Materials Research Bulletin, 23 (1988) 587- 594.

[3] F. Birch, Phys. Rev. 71 (1947) 809.

[4] V. Milman, M.C. Warren, J. Phys.: Condens. Matter 13 (2001) 5585.

[5] P. C. Schmidt, D. Stahl, B. Eisenmann, R. Kniep, Journal of solid state chemistry 97, (1992) 93-104.

[6] W. Voigt, Lehrbuch der Kristallphysik (Taubner, Leipzig, 1928).

[7] A. Reuss, Z. Angew, Math. Mech. 9 (1929) 55.

[8] R. Hill, Proc. Phys. Soc., London, Sect. A 65 (1952) 349.

[9] B. Kong, X-R. Chen, L-C. Cai, G-F. Ji, Compt. Mat. Sci. 50 (2010) 105.

[10] S. Aydin, M. Simsek, J. Alloys Compd. 509 (2011) 5219.

[11] Z.J.Wu, E.-j. Zhao, H.-p. Xiang, X.-f. Hao, X.-j. Liu, J. Meng, Phys. Rev. B 76 (2007) 054115.

[12] J. Haines, J.M. Leger, G. Bocquillon, Ann. Rev. Mater. Res. 31 (2001) 1.

[13] V.V. Bannikov, I.R. Shein, A.L. Ivanovskii, Phys. Status Solidi RRL 1 (2007) 89– 91.

[14] I.N. Frantsevich, F.F. Voronov, S.A. Bokuta, in: I.N. Frantsevich (Ed.), Elastic Constants and Elastic Moduli of Metals and Insulators Handbook, Naukova Dumka, Kiev, 1983, pp. 60–180.

[15] S.F. Pugh, Philos. Mag. 45 (1954) 823.

[16] Y. Mo, M. Pang, W. Yang, Y. Zhan, Compt. Mat. Sci. 69 (2013) 160

[17] M.M. Wua, L. Wen, B.Y. Tang, L. M. Peng, W.J. Ding, Journal of Alloys and Compounds 506 (2010) 412–417

[18] S.I. Ranganathan, M. Ostoja-Starzewski, Phys. Rev. Lett. 101 (2008) 55504

[19] M.X. Zeng, R.N. Wang, B.Y. tang, L.M. Peng, W.J. Ding, Modelling Simul. Mater,Sci. Eng. 20 (2012) 035018.

[20] C. Li, Z. Wang, C. Wang, Intermetallics 33 (2013) 105-112

[21] L. Nie, W. Zhou, Y. Zhan, Computational and Theoretical Chemistry, 1020 (2013) 51–56.

[22] A.L. Ivanovskii, Int. J. Refract. Met. Hard Mater, 36 (2013) 179–182.

[23] Robert E. Newnham, Properties of materials; Anisotropy, Symmetry, Structure, Oxford University Press, New York, 2005.

[24] Y.J.Hao,X.R.Chen,H.L.Cui,Y.L.Bai,Physica B382(2006)118.

[25] P. Wachter, M. Filzmoser, J. Rebizant, Physica B 293 (2001) 199.

[26] O.L. Anderson, J. Phys. Chem. Solids 24 (1963) 909.

[27] H.Wang, Y. Zhan, M. Pang, Computational Materials Science 58 (2012) 17–23.

[28] E. Schreiber, O.L. Anderson, N. Soga, Elastic Constants nd their Measurements, McGraw-Hill, New York, 1996.

[29] M. Asbrand, F.J. Berry, B. Eisenmann, R. Kniep, L.E. Smart, R.C. Thied, Journal of Solid State Chemistry, 118 (1995) 397–401.

[30] N. Kanoun-Bouayed, M.B. Kanoun, S. Goumri-Said, Cent. Eur. J. Phys. 9 (2011) 205.

[31] D. Jana, C. L.Sun, L.C. Chen, Progress in Materials Science 58 (2013) 565–635

[32] F. Wooten, Optical Properties of Solids, Academic New york, 1972

[33] G. Wang, S. Wu, Z.H. Geng, S.Y. Wang, L.Y. Chen, Y. Jia, Opt. Commun. 283 (2010) 4307–4309.

[34] N. Korozlu, K. Colakoglu, E. Deligoz, Y.O. Ciftci, Opt. Commun. 284 (2011), 1863–1867.

[35] M. Yang, B. Chang, G. Hao, J. Guo, H. Wang, M. Wang, Optik 125 (2014) 424– 427.

[36] Q. J. Liu, N. C. Zhang, F. S. Liu, H.Y. Wang, Z. T. Liu, Optical Materials 35 (2013) 2629–2637

GENERAL CONCLUSION

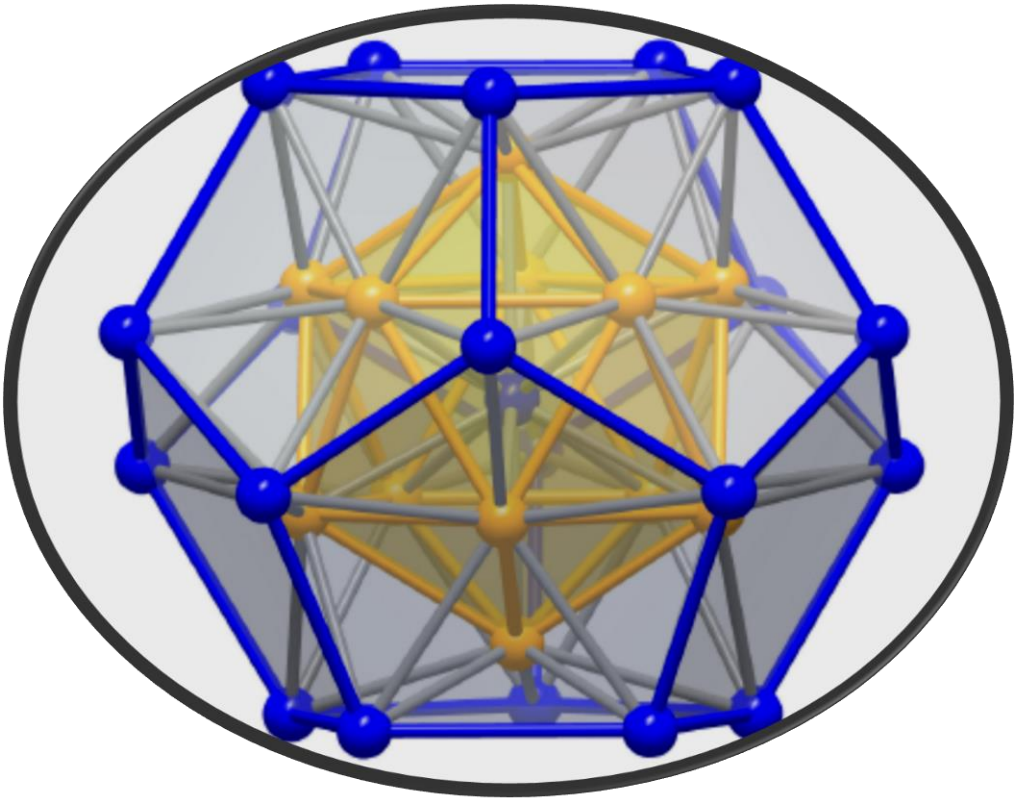

GENERAL CONCLUSION

We have studied in this thesis, the properties of the hexagonal zintl phase KAsSn using the first principles pseudo-potential method based on the density functional theory, within the generalized gradient approximation developed by Wu-Cohen (GGA-Wc). On the basis of the reasonable structural results, the electronic structures, elastic, optical properties, and the relationship among these properties we can conclude that:

1. The calculated structural characteristics including equilibrium lattice constants and bond length agree well with the available experimental and other theoretical data. The bulk modulus *B* of about 30.5 GPa is obtained by fitting the computed P–V relation to the Birch–Murnaghan equation of state.
2. The calculation provides an excellent description of the band structures of KAsSn, which could be useful for further theoretical investigation. Analysis of the DOS revealed that the conduction band is mainly composed of p-Sn (5s+5p) and As (4s+4p) states, whereas the valence band is essentially dominated by As-s, Sn-s and p (Sn-As) states. The calculated band gaps of this zintl phase suggested that this crystal belongs to the semiconductors with narrow gap of about 0.34eV.
3. The calculation of the complete set of zero pressure elastic constants has been performed and satisfied the mechanical stability criteria, highlighting the fact that the KAsSn structure is mechanically stable. The polycrystalline elastic parameters (*B, G, E, A* and *v*) have been further calculated within the scheme of Voigt–Reuss–Hill (VRH) approximation. The ductility and plasticity, especially elastic anisotropies including the shear anisotropy factors, percentage of bulk and shear anisotropies and the linear bulk modulus, micro-hardness parameter *Hv* are discussed in details. Our analysis of the predicted elastic moduli shows that KAsSn is predicted to be brittleness and characterized by a weak elastic anisotropy. Furthermore, we have derived the sound velocity and the Debye temperature for the KAsSn.
4. Mulliken charge population analyses show the charge transfer during the geometry optimization and the presence of concurrent ionic and covalent bonding in the KAsSn structure. Moreover the analysis of the Mulliken charge populations and bond length population shows that K–Sn bond possesses the stronger covalent bonding strength than K-As and As–Sn bonds.
5. The imaginary and real parts of the dielectric function of this compound have been calculated. From this the other optical properties such as refractive index, extinction

coefficient, optical reflectivity, absorption coefficient and loss function are derived in a wide energy range. Using the band structure, we have analyzed the interband contribution to the optical response functions. The direct band gap and high absorption power in the ultraviolet energy range show the effective use of this compound in the optoelectronic devices.

We hope that our results are reliable reference to further experimental and theoretical investigations.

APPENDIX
DENSITY FUNCTIONAL THEORY

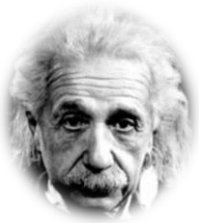

"If you can't explain it simply, you don't understand it well enough."
Albert Einstein

Contents

Preamble

The purpose of this appendix is to explain in a mathematical way what density functional theory is and what it is used for. A brief introduction is to be made of problems in quantum mechanics and the formally exact solution provided by the Kohn-Sham formulation of density functional theory. Therefore DFT is characterized by the use of functionals of the electron density and is among the most popular and versatile methods available in condensed matter physics. The plane wave pseudo-potential method of performing DFT calculations was discussed. *Ab-initio* techniques, such as the CASTEP method, attempt to solve the quantum mechanical equations of systems composed of up to thousand of atoms. In practice, the exact solution of these equations is an unsolvable analytic problem and several approximations must be made. These approximations are described and justified in the description of CASTEP code.

A.1 Introduction and Basics

Atomic scale computational materials sciences have become an interdisciplinary subject that straddles physics, chemistry, biology, and geophysics. One of the basic problems in theoretical physics and chemistry is the description of the structure and dynamics of many-electron systems. These systems comprise single atoms, the most elementary building blocks of ordinary matter, all kinds of molecules, ranging from dimers to proteins, as well as mesoscopic systems, for example clusters or quantum dots, and solids, including layered structures, surfaces and quasi-crystals [1].

The quantum mechanical wave function contains, in principle, all the information about a given system. For the case of a simple 2D square potential or even a hydrogen atom we can solve the Schrödinger equation exactly in order to get the wave function of the system. We can then determine the allowed energy states of the system. Unfortunately it is impossible to solve the Schrödinger equation for an *N*-body system. Evidently, we must involve some approximations to render the problem soluble albeit tricky.

Density functional theory (DFT) provides a powerful tool for computations of the quantum state of atoms, molecules and solids, and of ab-initio molecular dynamics. It was conceived in its initial naïve and approximative version by Thomas and Fermi immediately after the foundation of quantum mechanics, in 1927. In the middle of the sixties, Hohenberg, Kohn and Sham on one hand established a logically rigorous density functional theory of the quantum ground state on the basis of quantum mechanics, and on the other hand, guided by this

construction, introduced an approximative explicit theory called the local-density approximation, which for computations of the quantum ground state of many-particle systems proved to be superior to both Thomas-Fermi and Hartree-Fock theories. From that time on, density functional theory has grown vastly in popularity, and a flood of computational work in molecular and solid state physics has been the result. Motivated by its success, there has been always a tendency to widen the fields of application of density functional theory, and in these developments, some points which were left somewhat obscure in the basic theory, were brought into focus from time to time. This led in the early eighties to a deepening of the logical basis, essentially by Levy and Lieb, and finally Lieb gave the basic theory a form of final mathematical rigor. Since that treatment, however, is based on the tools of modern convex functional analysis, its implications only gradually became known to the many people who apply density functional theory [2].

The original density functional theory has been generalized to deal with many different situations: spin polarized systems, multi-component systems such as nuclei and electron hole droplets, superconductors with electronic pairing mechanisms, relativistic electrons, time-dependent phenomena and excited states, molecular dynamics, etc.

A.2 Schrödinger equation

The Schrödinger equation was discovered in 1926 by Erwin Schrödinger, it is an important equation that is fundamental to quantum mechanics. Many of the physical and chemical phenomena surrounding us today are governed by this equation. Indeed, the Schrödinger equation can be viewed as a form of the wave equation applied to matter waves. The Schrödinger equation has two 'forms', one in which time explicitly appears, and so describes how the wave function of a particle will evolve in time. In general, the wave function behaves like a wave, and so the equation is often referred to as the time dependent Schrödinger wave equation. The other is the equation in which the time dependence has been 'removed' and hence is known as the time independent Schrödinger equation and is found to describe, amongst other things, what the allowed energies are of the particle. These are not two separate, independent equations – the time independent equation can be derived readily from the time dependent equation.

The fundamental equation governing a quantum system is the time dependent Schrödinger equation [4]:

$$\widehat{H}\psi(r,t) = i\hbar\frac{\partial}{\partial t}\,\psi(r,t) \tag{A.1}$$

where i is the imaginary unit, $\hbar$ is the Planck constant divided by 2π, the symbol $\partial/\partial t$ indicates a partial derivative with respect to time t, Ψ is the wave function of the quantum system, and $\hat{H}$ is the Hamiltonian operator .

Very important special case of the Schrödinger equation is the situation when the potential energy term does not depend on time. As the name implies, this is the situation when the potential depends only on position (It is only used when the Hamiltonian itself is not dependent on time). The time independent Schrödinger equation is the equation describing stationary states (wave functions can form standing waves, called orbitals, as in atomic orbitals or molecular orbitals).

The properties of any time independent quantum system can be determined by solving the Schrödinger equation [5]:

$$\hat{H}\psi(r_1, r_2, \dots, r_N) = E\,\psi(r_1, r_2, \dots, r_N) \tag{A.2}$$

Where $\hat{H}$, $\psi(r_1, r_2, \dots, r_N)$ and E are the Hamiltonian, many body wave function and total energy of the system. Matter consists of electrons and nuclei interacting with each other coulombically, consequently the Hamiltonian for any such system is given by:

$$\hat{H} = -\sum_{i=1}^{M}\frac{\hbar^2}{2m_{Z_i}}\nabla_{\mathrm{Ri}}^2 - \sum_{i=1}^{N}\frac{\hbar^2}{2m_e}\nabla_{\mathrm{ri}}^2 + \frac{1}{4\pi\epsilon_0}\sum_{i}^{M}\sum_{j>i}^{M}\frac{Z_i Z_j}{|R_i - R_j|} - \frac{1}{4\pi\epsilon_0}\sum_{i=1}^{N}\sum_{j=1}^{M}\frac{Z_j e}{|r_i - R_j|} + \frac{1}{4\pi\epsilon_0}\sum_{i}^{N}\sum_{j>i}^{N}\frac{e^2}{|r_i - r_j|} \tag{A.3}$$

Where M and N are the number of nuclei and electrons in the system, m_Z, Z and R are the mass, charge and position of the nuclei, m_e and e are the mass and charge of an electron, and r represents the position of the electrons.

The first two terms in (A.3) are the kinetic energy contributions from the nuclei and the electrons respectively, and the rest are Coulombic potential energy terms arising from the ion-ion repulsion, ion-electron attraction and the electron-electron repulsion respectively.

Though in principle everything is known exactly, the Schrödinger equation (A.2) with this Hamiltonian is simply too difficult to solve directly. Hence, the quantum many-body problem is centered up on finding intelligent approximations to the Hamiltonian (A.3) and the many body wave function ψ, which retain the correct physics and are computationally tractable to solve.

A. 3 Theoretical background

A.3.1 Born-Oppenheimer Approximation

The Born-Oppenheimer approximation [6] is a way to simplify the complicated Schrödinger equation for a molecule. The nucleus and electrons are attracted to each other with the same magnitude of electric charge, thus they exert the same force and momentum. While exerting the same kind of momentum, the nucleus, with a much larger mass in comparison to electron's mass, will have a very small velocity that is almost negligible. Born-Oppenheimer takes advantage of this phenomenon and makes the assumption that since the nucleus is way heavier in mass compared to the electron, its motion can be ignored while solving the electronic Schrödinger equation; that is, the nucleus is assumed to be stationary while electrons move around it. The motion of the nuclei and the electrons can be separated and the electronic and nuclear problems can be solved with independent wave functions.

By means of this approximation the total wave function can be decoupled in two parts, one concerning the electrons $\psi_{electrons}$ of the system and second one ψ_{nuclei} that deal merely with nuclei description:

$$\psi_{system} = \psi_{electrons} \otimes \psi_{nuclei}$$

This involves the following assumptions:

- The electronic wave function depends upon the nuclear positions but not upon their velocities, i.e., the nuclear motion is so much slower than electron motion that they can be considered to be fixed.
- The nuclear motion (e.g., rotation, vibration) sees a smeared out potential from the speedy electrons.

Within this approximation the complexity of the full many-body Hamiltonian (A.3) reduces to that of an electronic Hamiltonian:

$$\widehat{H} = -\sum_{i=1}^{M} \frac{\hbar^2}{2m_e} \nabla_i^2 - \frac{1}{4\pi\epsilon_0} \sum_{i=1}^{N} \sum_{j=1}^{M} \frac{Z_i e}{|r_i - R_j|} + \frac{1}{4\pi\epsilon_0} \sum_{i}^{N} \sum_{j>i}^{N} \frac{e^2}{|r_i - r_j|} \qquad (A.4)$$

The Born Oppenheimer approximation is certainly not universally valid. It is well known that the Born Oppenheimer approximation will break down when there are multiple potential energy surfaces close to each other in energy or crossing each other (dissociative adsorption of molecules on metal surfaces). More caution must be exerted when dealing with systems such as those of [7-9].

Devising accurate schemes to approximate the many electron problems has been an important goal since the founding of quantum mechanics in the early 1900s. Several notable advances have been made, initially Thomas and Fermi (TF) in the 1920s suggested describing atoms as uniformly distributed electrons around nuclei in a six dimensional phase space (momentum and coordinates). This is an enormous simplification of the actual many body problems. It is instructive to consider the basic ideas of the TF approximation before starting with a more accurate theory: the DFT. In1930 came Hartree-Fock theory [10,11] which builds upon the single-particle approximation proposed earlier by Hartree [12]. A significant leap in electronic structure theory was made in 1964 with the remarkable theorems of density functional theory (DFT), proved by Hohenberg and Kohn [13]. DFT allows the ground-state properties of a many-electron system to be determined exactly through the electron density n(r), and therefore in a computationally tractable manner, however DFT is only a proof of existence, it does not give details of how this can be achieved in practice. In 1965 Kohn and Sham [14] devised an ingeniously practical single-particle scheme for performing DFT calculations, which is still exact, in principle. The price to be paid for the benefits of Kohn-Sham DFT is that the single-particle Hamiltonian is only partly known in practice - approximations must be made for a single unknown component that accounts for electron many-body effects, known as exchange and correlation.

A.3.2 Thomas Fermi Theory

Thomas-Fermi theory marks a change in approach from Hartree and Hartree-Fock theory, as it was the first method to propose using the electronic charge density as its fundamental variable instead of the wave function. It is thus the earliest form of density functional theory. Although the charge density is that of a non-uniform electron gas, the number of electrons in a given element, dr, can be expressed as $n(r)dr$, where $n(r)$ is the charge density for a uniform electron gas at that point. It is then possible to express the total energy of a system as a functional $E^{TF}[n(r)]$ [15-16].

$$E^{TF}[n(r)] = A_{\mathrm{k}} \int n(r)^{5/3} dr + \int n(r) v_{ext}(r) dr + \frac{1}{2} \iint \frac{n(r)n(r')}{|r - r'|} \, dr dr' \qquad (A.5)$$

The Thomas-Fermi energy functional is composed of three terms, the first term is the electronic kinetic energy associated with a system of non interacting electrons in a homogeneous electron gas. This form is obtained by integrating the kinetic energy density of a homogeneous electron gas $t_0[n(r)]$ [17-18].

$$T^{TF}[n(r)] = \int t_0[n(r)] dr \qquad (A.6)$$

Where t_0 [$n(r)$] is obtained by summing all of the free electron energy states $\varepsilon = k^2/2$, up to the Fermi wave vector $k_{F=}[3\pi^2 n(r)]^{1/3}$,

$$t_0\ [n(r)] = \frac{2}{(2\pi)^3}\int \frac{k^2}{2} n_k dk = \frac{1}{2\pi^2}\int_0^{kF} k^4\, dk \qquad (A.7)$$

Where n_k is the density of allowed states in reciprocal space, and the coefficient $A_k = \frac{3}{10}(3\pi^2)^{2/3}$. The power-law dependence on the density can also be established on dimensional grounds [19].

The second term is the classical electrostatic energy of attraction between the nuclei and the electrons, where $v_{ext}\ (r)$ is the static Coulomb potential arising from the nuclei,

$$v_{ext}\ (r) = -\sum_{j=1}^{M} \frac{Z_j}{|r - R_j|} \qquad (A.8)$$

The third term in (A.5) represents the electron-electron interactions of the system, and in this case is approximated by the classical Coulomb repulsion between electrons, known as the Hartree energy.

To obtain the ground state density and energy of a system, the Thomas-Fermi equation (A.5) must be minimised subject to the constraint that the number of electrons is conserved. This type of constrained minimisation problem, which occurs frequently within many body methods, can be performed using the technique of Lagrange multipliers. In general terms, the minimisation of a functional F [f], subject to the constraint C [f], leads to the following stationary condition,

$$\sigma(F[f] - \mu C[f] = 0) \qquad (A.9)$$

μ is a constant known as the Lagrange parameter. Incorporates this in the equation (A.6) leads to the Thomas Fermi equations that can be solved directly to obtain the ground state density,

$$\frac{5}{3}A_k n(r)^{2/3} + v_{ext}(r) + \int \frac{n(r')}{|r - r'|}\, dr' - \mu = 0 \qquad (A.10)$$

This approach is extremely simple, and is qualitatively correct for atoms. However it does not give a binding energy for molecules, and the proof is not rigorous [20-22]. To overcome these problems it is necessary to move on to the work of Hohenberg, Kohn and Sham.

A.3.3 Hartree-Fock Theory:

Hartree was one of the first scientist who attempted to solve this problem by simplifying the problem by making an assumption [12]: the form of the N-electron wave function ψ is just the

product of a set of *N* single particle orbitals, $\psi_i(r_i\, s_i)$, which would take the form of simple plane waves in a homogeneous system:

$$\Psi(r_1 s_1, r_2 s_2, \dots, r_N s_N) = \frac{1}{\sqrt{N}}\Psi_1(\mathrm{r_1 s_1})\Psi_2(\mathrm{r_2 s_2}) \dots \dots \Psi_{\mathrm{N}}(\mathrm{r_N s_N}) \qquad (A.11)$$

Where ψ_i $(r_i s_i)$ is composed of a spatial function $\phi_i(r_i)$, and an electron spin function $\sigma(si)$ such that:

$$\Psi_{\mathrm{i}}(r_i) = \phi_i(r_i)\sigma(s_i) \qquad (A.12)$$

and $\sigma = \alpha, \beta$ represent up-spin and down-spin electrons respectively. However, the Hartree approximation does not account for exchange interactions since (A.12) does not satisfy Pauli exclusion Principle [23]:

$$\Psi(r_1 s_1, \dots, r_i s_i, \dots, r_j s_j, \dots . r_N s_N) = -\Psi(r_1 s_1, \dots, r_j s_j, \dots r_i s_i, \dots r_N s_N) \qquad (A.13)$$

Unfortunately, the Hartree approximation does not give particularly good results since, for example, it predicts that in a neutral uniform system there will be no binding energy holding the electrons in the solid.

An improvement over the Hartree's framework is the Hartree-Fock's (HF) approach [10-12] in that the *N*-electron wave function is constructed from the single-electron wave function is required to be antisymmetric.

The Hartree-Fock wave function ψ_{HF} amounts to a linear combination of the terms in (A.12), which includes all permutations of the electron coordinates with the corresponding weights ±1, i.e.

$$\Psi_{\mathrm{HF}} = \frac{1}{\sqrt{N!}}[\Psi_1(\mathrm{r_1 s_1})\Psi_2(\mathrm{r_2 s_2}) \dots \dots \Psi_{\mathrm{N}}(\mathrm{r_N s_N}) - \Psi_1(\mathrm{r_2 s_2})\Psi_2(\mathrm{r_1 s_1}) \dots \Psi_{\mathrm{N}}(\mathrm{r_N s_N}) \ \dots] \qquad (A.14)$$

Instead of using a simple product wave function, a Slater [11] determinant is used,

$$\Psi_{HF} = \frac{1}{\sqrt{\mathrm{N!}}}\begin{vmatrix} \Psi_1(\mathrm{r_1 s_1}) \cdots \cdots \cdots \Psi_1(\mathrm{r_N s_N}) \\ \vdots \qquad\qquad \vdots \qquad\qquad \vdots \\ \Psi_{\mathrm{N}}(\mathrm{r_1 s_1}) \cdots \cdots \cdots \Psi_{\mathrm{N}}(\mathrm{r_N s_N}) \end{vmatrix} \qquad (A.15)$$

Where the orbitals are subject to the orthonormal constraint,

$$\int \Psi_{\mathrm{i}}^{*}(r)\Psi_{\mathrm{j}}(\mathrm{r})\mathrm{dr} = \langle \Psi_{\mathrm{i}}/\Psi_{\mathrm{j}} \rangle = \delta_{ij} \qquad (A.16)$$

The Slater determinant can also be written in shorthand notation as,

$$\Psi_{\mathrm{HF}} = \frac{1}{\sqrt{N!}}\det[\Psi_1(\mathrm{r_1 s_1})\Psi_2(\mathrm{r_2 s_2}) \dots \dots \Psi_{\mathrm{N}}(\mathrm{r_N s_N})] \qquad (A.17)$$

Thanks to this new assumption the Hamiltonian equation (A.4) for the system can be deduced through the variational principle:

$$E_{HF} = \sum_{i}^{N} \int \Psi_i^* (r)(-\frac{1}{2}\nabla^2 + v_{ext}(r))\Psi_i(\mathrm{r})\mathrm{dr} + \frac{1}{2}\sum_{i}^{N}\sum_{j}^{N} \iint \frac{|\Psi_i(\mathrm{r})|^2|\Psi_i(\mathrm{r}')|^2}{|r-r'|}\, drdr'$$

$$-\frac{1}{2}\sum_{i}^{N}\sum_{j}^{N} \iint \frac{\Psi_i^*(r)\Psi_i(\mathrm{r}')\Psi_j^*(r)\Psi_j(\mathrm{r}')}{|r-r'|}\, \delta_{sisj}\, drdr' \qquad (A.18)$$

The last term is of significant interest since it arises from the anti-symmetric nature of the Hartree-Fock wave function, it vanishes when $s_i \neq s_j$, which is an artefact of the Pauli principle.

The Hartree-Fock approximation corresponds to the conventional single electron picture of electronic structure: the distribution of the *N* electrons is given simply by the sum of one electron distributions $|\psi|^2$. But it must be remembered that this is an artifact of the initial ansatz and that in some systems modifications are required to these ideas. Hartree-Fock theory, by assuming a single determinant form for the wave function, neglects correlation between electrons. The electrons are subject to an average non local potential arising from the other electrons, which can lead to a poor description of the electronic structure. Although qualitatively correct in many materials and compounds, Hartree-Fock theory is insufficiently accurate to make accurate quantitative predictions.

A.3.4 Density Functional Theory (DFT)

In recent years Density Functional Theory (DFT) has become the most popular method in quantum chemistry, accounting for approximately 90% of all calculations today. The reason for this preference is the extreme computational cost required to obtain chemical accuracy with multiple determinant methods. This difference in speed is heightened by the fact that multiple determinant calculations require very large basis sets, with high momentum basis functions, whereas DFT can produce accurate results with relatively small basis sets.

Density functional theory (DFT) is primarily a theory of electronic ground state structure, couched in terms of the electronic density distribution $n(r)$. It has become increasingly useful for the understanding and calculation of the ground state density, $n(r)$, and energy, E, of molecules, clusters, and solids any system consisting of nuclei and electrons with or without applied static perturbations. It is an alternative, and complementary, approach to the traditional methods of quantum chemistry which are couched in terms of the many electron wave function $\psi(r_1,...,r_N)$.

An early density functional theory was proposed by Thomas and Fermi. This took the kinetic energy to be a functional of the electron density, but in common with the Hartree and Hartree-Fock methods, only incorporated electron-electron interactions via a mean field potential: as such it neglected both exchange and correlation; a subsequent proposal by Dirac [46], formulating an expression for the exchange energy in terms of the electron density failed to significantly improve the method. Both Thomas-Fermi and Hartree-Fock-Slater methods can be regarded as ancestors of modern DFT. But whereas those theories are intrinsically approximate, modern DFT is in principle exact. Probably the most widely used theory for quantitative prediction in condensed matter physics is the density functional theory (DFT), originally developed by Hohenberg and Kohn. This theory has the advantage that it does not require adjustable parameters from experiments, in principle only fundamental constants as the speed of light in vacuum, Planck's constant, electron charge, etc. are taken from the experiment. DFT allows calculating the ground state properties of materials: total energy, ground-state lattice constants, electronic structure etc. Authoritative and comprehensive discussions of DFT can be found in a range of excellent review articles [24-25] and text books [26-27].

A.3.4.1 Hohenberg-Kohn Theorems

Modern density-functional theory was born in 1964 with the paper of Hohenberg and Kohn [13]. The two key results of this paper are: (i) a one to one mapping between external potential and electron density was established; (ii) it was shown that the ground state density can be found by using a variational principle.

***Theorem* 1:**

The Hohenberg-Kohn theorem [13] states that if *N* interacting electrons move in an external potential v_{ext} (*r*), the ground state energy is a unique functional of the density *n*(r). Thus the ground state electron density is sufficient to construct the full Hamilton operator and hence to calculate - in principle - any ground state property of the system without the knowledge of the many electron wave functions. Alternatively formulated, this means that any ground state property can be expressed in terms of the ground state electron density *n*(r).

The energy functional *E* [*n*(r)] alluded to in the first Hohenberg-Kohn theorem can be written in terms of the external potential v_{ext} *(r)* in the following way,

$$E[n(r)] = \int n(r) v_{ext}(r) dr + F[n(r)] \qquad (A.19)$$

Where F [$n(r)$] is a universal functional of the electron density $n(r)$ only, and the minimum value of the functional E is E_0 the exact ground-state electronic energy.

Correspondingly, a Hamiltonian for the system can be written such that the electron wave function ψ that minimizes the expectation value gives the ground state energy (assuming a non-degenerate ground state),

$$E[n(r)] = \langle \Psi | \hat{H} | \Psi \rangle \quad \text{(A. 20)}$$

Such that,

$$\hat{H} = \hat{F} + \hat{V}_{ext} \quad \text{(A. 21)}$$

Where $\hat{F}$ is the electronic Hamiltonian consisting of a kinetic energy operator $\hat{T}$ and an interaction operator $\hat{V}ee$,

$$\hat{F} = \hat{T} + \hat{V}_{ee} \quad \text{(A. 22)}$$

The electron operator $\hat{F}$ is the same for all N electron systems, so that the $\hat{H}$, and hence the ground states are completely defined by the number of electrons N, and the external potential $v_{ext}(r)$.

Proof by *reductio ad absurdum* assume that a second external potentials, $v'_{ext,}$ (r) give rise to the same density n_0 (r). The corresponding Hamiltonians and ground state energy for wave functions, ψ and ψ' are $\hat{H}$ and $\hat{H'}$ and E, E', respectively. It is at this point that the Hohenberg-Kohn theorems, and therefore DFT, apply rigorously to the ground state only. As ψ' is not the ground state of $\hat{H}$, we can say that [28]:

$$E\langle \Psi | \hat{H} | \Psi \rangle = \langle \Psi' | \hat{H'} | \Psi' \rangle + \langle \Psi' | \hat{H} - \hat{H'} | \Psi' \rangle = E' + \int n_0(r)[v_{ext}(r) - v'_{ext}(r)]dr \quad \text{(A. 23)}$$

So we have

$$E < E' + \int n_0(r)[v_{ext}(r) - v'_{ext}(r)]dr \quad \text{(A. 24)}$$

If the unprimed and primed indices are reversed, we also have:

$$E' < E + \int n_0(r)[v'_{ext}(r) - v_{ext}(r)]dr \quad \text{(A. 25)}$$

Addition of equations (A.24) and (A.25) leads to the result:

$$E + E' < E' + E$$

Which is a contradiction, and as a result the ground state density uniquely determines the external potential $v_{ext}(r)$.

***Theorem* 2:**

The total energy of a system, which is a functional of the ground state electron density through the first theorem, is minimised for the correct ground state energy.

The proof of the second theorem is also straightforward: as just shown, *n(r)* determines $v_{ext}(r)$, *N* and $v_{ext}(r)$ determine $\hat{H}$ and therefore ψ. This ultimately means ψ is a functional of *n*(*r*) , and so the expectation value of $\hat{F}$ is also a functional of *n(r)*, i.e.

$$F[n(r)] = \langle \Psi | \hat{F} | \Psi \rangle \qquad (A.26)$$

A density that is the ground state of some external potential is known as *v*-representable. Following from this, a *v*-representable energy functional $E_v[n(r)]$ can be defined in which the external potential *v(r)* is unrelated to another density *n'(r)*,

$$E_v[n(r)] = \int n'(r) v_{ext}(r) dr + F[n'(r)] \qquad (A.27)$$

So, it follows from the variational principle that:

$$\langle \Psi' | \hat{H} | \Psi' \rangle = \langle \Psi' | \hat{F} | \Psi' \rangle + \langle \Psi' | \widehat{V_{ext}} | \Psi' \rangle > \langle \Psi | \hat{F} | \Psi \rangle + \langle \Psi | \widehat{V_{ext}} | \Psi \rangle \qquad (A.28)$$

Where *ψ* is the wave function associated with the correct ground state *n*(*r*). This leads to,

$$\int n'(r) v_{ext}(r) dr + F[n'(r)] > \int n(r) v_{ext}(r) dr + F[n(r)] \qquad (A.29)$$

Consequently the variational principle of the second Hohenberg-Kohn theorem is obtained,

$$E_v[n'(r)] > E_v[n(r)] \qquad (A.30)$$

Therefore the total energy functional gives the exact ground state energy only for the exact ground state density. If the universal functional *F* [*n*(*r*)] is known, then the total energy can be minimised with respect to *n(r)* and the exact ground state electron density and total energy would be found. Simple yet powerful as the Hohenberg-Kohn theorems are, they do not provide a route to construct functionals or a method to calculate the ground state density.

Almost exactly a year after the Hohenberg-Kohn theorems were published, Kohn and Sham published [14] an approach that makes DFT feasible.

A.3.4.2 Kohn-Sham Formulation

The Kohn-Sham ansatz is that the exact ground state density can be written as the ground state density of a fictitious system of non interacting particles. This then gives us a set of independent particle equations that can be solved numerically. Through the Hohenberg-Kohn theorems, these independent particle equations have their own ground state energy functional. We write the variational problem for the Hohenberg Kohn density functional, introducing a Lagrange multiplier μ to constrain the number of electrons to be *N*:

$$\sigma\left[F[n(r)] + \int v_{ext}(r)n(r)dr - \mu\left(\int n(r)dr - N\right)\right] = 0 \qquad (A.31)$$

$$\Rightarrow \mu = \frac{\delta F[n(r)]}{\delta n(r)} + v_{ext}(r)$$

Kohn and Sham separated F [$n(r)$] into three distinct parts, the first two of which are known exactly and constitute the majority of the energy, the third being a small unknown quantity,

$$F[n] = T_s[n] + \frac{1}{2}\int \frac{n(r)n(r')}{|r-r'|}drdr' + E_{XC}[n] \qquad (A.32)$$

In the condensed from equation (A. 25) has the following expression:

$$F[n(r)] = T_s[n(r)] + E_H[n(r)] + E_{XC}[n(r)] \qquad (A.33)$$

Ts [$n(r)$] is the kinetic energy of a non interacting electron gas of density n(r), E_H [$n(r)$] is the classical electrostatic (Hartree) energy of the electrons, and E_{XC} [$n(r)$] is an implicit definition of the exchange correlation energy which contains the non classical electrostatic interaction energy and the difference between the kinetic energies of the interacting and non interacting systems. The aim of this separation is that the first two terms can be dealt with simply, and the last term, which contains the effects of the complex behavior, is a small fraction of the total energy.

Consequently, equation (A. 26) can be rewritten:

$$\mu = \frac{\delta T_s[n(r)]}{\delta n(r)} + v_{KS}(r) \qquad (A.34)$$

Where

$$v_{KS}(r) = v_{ext}(r) + v_H(r) + v_{XC}(r) \qquad (A.35)$$

and

$$v_H(r) = \frac{\delta E_H[n(r)]}{\delta n(r)} = \int \frac{n(r')}{|r-r'|}dr' \qquad (A.36)$$

In which the exchange-correlation potential $v_{XC}(r)$ is

$$v_{XC}(r) = \frac{\delta E_{XC}[n(r)]}{\delta n(r)} \qquad (A.37)$$

Crucially, *non interacting* electrons moving in an external potential v_{KS}(r) would result in the same equation(A. 26). To find the ground state energy, E_0(r), and the ground state density, n_0(r), the one electron Schrödinger equation

$$\left[-\frac{1}{2}\nabla^2 + v_{KS}(r)\right]\psi_i(r) = \psi_i(r)\varepsilon_i \qquad (A.38)$$

ε_i are Lagrange multipliers corresponding to the orthonormality of the N single particle states ψi(r).

should be solved self-consistently with,

$$n(r) = \sum_{i=1}^{N} |\psi_i(r)|^2 \qquad (A.39)$$

and equations (A. 34) and (A. 37). A self-consistent solution is required due to the dependence of v_{KS}(r) on n (r).

The non-interacting kinetic energy TS [n(r)] is therefore given by,

$$T_{TS}[n(r)] = -\frac{1}{2}\sum_{i=1}^{N} \psi_{i_i}^{*}(r)\,\nabla^2\psi_i(r)dr \qquad (A.40)$$

An implicit definition of exchange-correlation functional $\mathrm{E_{XC}}$[n(r)] can be given through (A. 34) as,

$$E_{XC}[n(r)] = T[n(r)] - T_S[n(r)] + E_{ee}[n(r)] - E_H[n(r)] \qquad (A.41)$$

Where $T[n(r)]$ and $E_{ee}[n(r)]$ are the exact kinetic and electron-electron interaction energies respectively.

Since v_{KS}(r) depends on the density through the exchange-correlation potential, relations (A. 37), (A. 40) and(A. 41), which are known as the Kohn-Sham equations, must be solved self-consistently as in the Hartree-Fock scheme [1].

The above equations provide a theoretically exact method for finding the ground state energy of an interacting system provided the form of $E_{XC}[n(r)]$ is known. Unfortunately, the form of $E_{XC}[n(r)]$ is in general unknown and its exact value has been calculated for only a few very simple systems. In electronic structure calculations $E_{XC}[n(r)]$ is most commonly approximated within the local density approximation or generalised-gradient approximation.

A.3.4.3 Exchange-Correlation Functionals

Density functional theory is in principle exact! But, in practice approximations have to be made."

W. Kohn

To use the Kohn-Sham equations we must know what the form of the exchange- correlation energy functional is. However, the exact form of *Exc* is not known and may never be known. Thus since the birth of DFT some sort of approximations for *Exc* have been used. By now

there is an almost endless list of approximations with varying levels of complexity. Rather recently a useful way for categorizing the many and varied E_{xc} functionals that exist has been proposed by Perdew [29]. In this scheme functional are grouped according to their complexity on rungs of a ladder which lead from the Hartree approximation on "earth" to the exact exchange-correlation functional in «heaven". A briefly discussion is to be made of the first few rungs of this ladder as a means to introduce some of the most common types of exchange-correlation functionals in widespread use:

1- Local Density Approximation (LDA):

The simplest approximation is to assume that the density can be treated locally as an uniform electron gas; the exchange correlation energy at each point in the system is the same as that of an uniform electron gas of the same density. This approximation was originally introduced by Kohn and Sham [13] and holds for a slowly varying density. The LDA is only dependent on the local density, and the total energy is commonly written as,

$$E_{XC}^{LDA}[n(r)] = \int n(r)\epsilon_{XC}\,[n(r)]dr \qquad (A.42)$$

The exchange correlation potential v_{XC}(r) then takes the form

$$v_{XC}^{LDA}[n(r)] = \frac{\delta E_{XC}^{LDA}}{\delta n(r)} = \epsilon_{XC}\big(n(r)\big) + n(r)\frac{\partial \epsilon_{XC}(n)}{\partial n}\Big|_{n=n(r)} \qquad (A.43)$$

Where $\epsilon_{XC}[n(r)]$ is the exchange correlation energy density per particle of an uniform electron gas of density $n(r)$. The exchange correlation energy can be decomposed into exchange and correlation contributions, $\varepsilon_{XC}[n(r)] = \varepsilon_X[n(r)] + \varepsilon_c[n(r)]$

$\varepsilon_X[n(r)]$ is given by the Dirac functional

$$\varepsilon_X[n(r)] = -\frac{3}{4}\left(\frac{3}{\pi}\right)^{\frac{1}{3}} n(r) \qquad (A.44)$$

While accurate values for $\varepsilon_c[n(r)]$ is determined from an interpolation formula [30,31] that connects the known limiting form of $\epsilon_C[n(r)]$ in the high [32] and low density limits [33]. A commonly used correlation formula is that of Perdew and Zunger [30] which uses accurate Quantum Monte Carlo (QMC) calculations of the homogeneous electron gas.

The LDA is often surprisingly accurate and for systems with slowly varying charge densities generally gives very good results. Its use is justified *a posteriori* by its surprising success at predicting physical properties in real systems. The failings of the LDA are now well established: it has a tendency to favor more homogeneous systems and over binds molecules and solids.

2. The Generalised Gradient Approximation:

As the LDA approximates the energy of the true density by the energy of a local constant density, it fails in situations where the density undergoes rapid changes such as in molecules. An improvement to this can be made by considering the gradient of the electron density, the so called *Generalized Gradient Approximation* (GGA) which is currently the most popular exchange correlation functional in condensed matter physics. Symbolically this can be written as:

$$E_{xc} = E_{xc}[n(r), \nabla n(r)] \qquad (A.45)$$

The vital steps that lead to the GGA were principally made by Perdew and co-workers [29] who devised a cutoff procedure. As a result of this procedure the GGA can be conveniently written in terms of an analytic function known as the enhancement factor, $F_{\mathrm{XC}}[n(\mathrm{r}), \nabla\, n(\mathrm{r})]$, that directly modifies the *LDA* energy density,

$$E_{XC}^{GGA}[n(r)] = \int n(r)\epsilon_{XC}^{hom}\,[n(r)]F_{XC}[n(r), \nabla n(r)]dr \qquad (A.46)$$

Despite the crudeness of the real space cutoff procedure, the GGA gave improvement over the LDA in several instances. The most notable outcome was the significant reduction in the LDA over binding error for solids and molecules.

While there is only one LDA there are several different parameterizations of the GGA. Some of these are semi-empirical, in that experimental data is used in their derivation. Others are found entirely from first principles. A commonly used functional is the PW91 functional, due to Perdew and Yang [34].

Thus GGAs are "semi-local" functionals, comprising corrections to the LDA while (again) ensuring consistency with known sum rules. For many properties, for example geometries and ground state energies of molecules, GGAs can yield better results than the LDAs. Although for the properties of metals and their surfaces, GGA results are not necessarily superior to LDA results. The most widely used GGAs in surface physics are the PW91 functional, and its close relative PBE [35].

PW91 is determined from exact quantum-mechanical relations. The exchange enhancement factor has the form,

$$F_X^{PW91}(s) = \frac{1 + 0.19645s\ sinh^{-1}(7.7956s) + (0.2743 - 0.15084e^{-100s^2}}{1 + 0.19645s\ sinh^{-1}(7.7956s) + 0.004s^4} \qquad (A.47)$$

Until recently, PW91 was the sole GGA used by the physics community. It has now probably been superseded by a modified form devised by Perdew, Burke and Ernzerhof known as PBE [35], which uses a much simplified exchange enhancement factor of the form:

$$F_X^{PBE}(s) = 1 + k - \frac{k}{1 + \mu s^2/k} \quad (A.48)$$

Where u=0.21951 and k=0.804 . PBE was designed to give a simpler functional form by retaining only the most energetically important conditions satisfied by PW91**.**

3. The meta-GGAs (MGGA): These are the third generation functionals and use the second derivative of the density, $\nabla^2 n$(r), and or kinetic energy densities, as additional degree of freedom. In gas phase studies of molecular properties meta-GGAs [36, 37] have been shown to offer improved performance over LDAs and GGAs. However, aside from some benchmark studies of bulk materials, these functionals have not yet been exploited to any great extend in the solid state.

4. The hybrid functionals: These fourth generation functionals add "exact exchange" from Hartree-Fock theory to some conventional treatment of DFT exchange and correlation. The most widely used, particularly in the quantum chemistry community, is the B3LYP [38, 40].

A.4 Plane-Waves and Pseudopotentials

One way of implementing the Kohn-Sham formulation of DFT is the plane wave pseudo potential method. As with the wave function based methods, when it comes to the practical application of DFT issues such as basis sets need to be considered. In calculations of solids or condensed matter, plane-wave basis set is a very common choice. In many cases, combined with plane-wave is the pseudo potential approach for treating the strong interactions between core electron and nuclei.

A.4 .1 Bloch's Theorem

Thus far, the quantum mechanical approaches to solving the many body problems have been discussed. However, the correlated nature of the electrons within a solid is not the only obstacle to solving the Schrödinger equation for a condensed matter system: for solids, one must also bear in mind the effectively infinite number of electrons within the solid. One may appeal to Bloch's theorem in order to make headway in obviating this latter problem.

Bloch's theorem [41] shows that the wave function of an electron $\psi_{j,k}$, within a periodic potential, can be expressed as a combination of a lattice periodic part $u_j\,(r)$and a wavelike part $e^{ik.r}$,

$$\psi_{j,k}(r) = u_j\,(r)e^{ik.r} \quad (A.49)$$

Where the subscript *j* indicates the band index and *k* is a continuous wave-vector that is confined to the first Brillouin zone of the reciprocal lattice [41]. This leads us to choose a plane wave basis set to describe the wave function within the periodic cell. Since u_j (r) is a periodic function, we may expand it in terms of a Fourier series:

$$u_j(r) = \sum_G c_{j.} G e^{iG.r} \qquad (A.50)$$

Where the G is reciprocal lattice vectors defined through $G.R = 2\pi m$G, *m* is an integer, *R* is a real space lattice vector and the $c_j.G$ are plane wave expansion coefficients. The electron wave functions may therefore be written as a linear combination of plane waves:

$$\psi_{j,k}(r) = \sum_G c_{j,k} + Ge^{i(G+k).r} \qquad (A.51)$$

Bloch's theorem allows us to take an infinite system but only calculate a finite number of electronic wave functions

In practice, we need only to choose a sample of k-points as the wave function varies slowly over small regions of k-space. The electronic wave functions at k-points that are close will be nearly identical. Therefore a region of k-space can be represented by the wave function at a single k-point. Efficient k-point sampling schemes have been developed, such as the one given by Monkhorst and Pack [42]. The symmetry of the lattice can be used to reduce the number of k-points required. The Brillouin zone can be made irreducible by applying the point group symmetries of the lattice, leaving no k-points related by symmetry.

Plane waves are a simple way of representing electron wave functions. They offer a complete basis set that is independent of the type of crystal and treats all areas of space equally.

A.4 .2 Pseudo potentials approach

It is well established that most physically interesting properties of solids are determined by the valence electrons rather than the core electrons. Meanwhile, the deeply bound core electrons within plane-wave basis sets require a huge amount of basis functions for their description. Thus this leads to a contradiction that the less important core electrons will consume a lot of computational cost. To alleviate this problem, the pseudopotential approximation [43-46] replaces the strong ionic potential with a weaker pseudopotential.

In general, there are two main purposes of the pseudopotential formalism. First, to use a much weaker pseudopotential to replace core electrons which due to their deep potential need to be described by many plane-wave basis functions. Second, to eliminate the rapid oscillations of the valence electron wave function in the core region. These lead to large kinetic energies hence the need for large numbers of plane waves. Also a large number of plane waves are

needed to describe the tightly bound core states [47]. These issues are shown in Figure A.1. From this Figure, we can see the pseudo-potential approximation replaces the strong ionic potential v_{ion} (r) in the core region, by a weaker pseudo-potential v^{PS}_{ion} (r). The corresponding set of pseudo wave functions ψ^{PS} (r) and the all-electron wave functions ψ^{AE} (r) are identical outside a chosen cutoff radius r_c and so exhibit the same scattering properties, but ψ^{PS} (r) does not possess the nodal structure that cause the oscillations inside r_c, which means they can now be described with a reasonable number of plane waves.

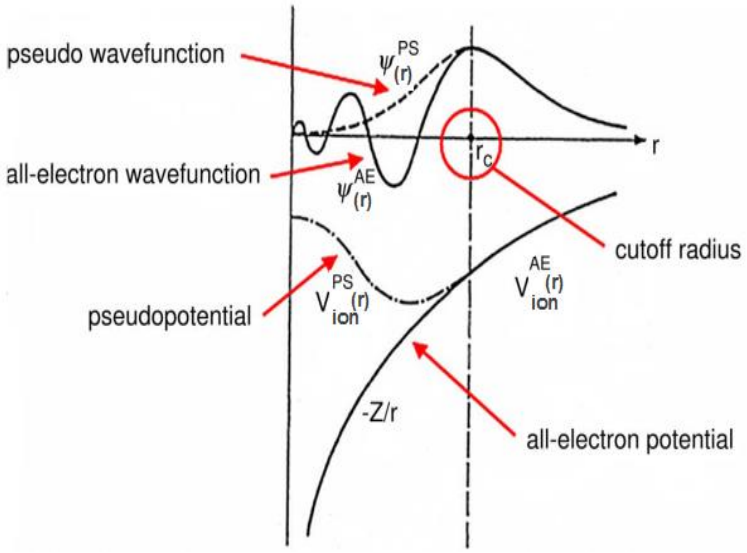

Figure A.1: Schematic illustration of the pseudopotential concept. The solid lines show the all-electron wave function, ψ^{AE} (r) , and ionic potential, v^{AE}_{ion} (r), while the dashed lines show the corresponding pseudo-wave function, ψ^{PS} (r), given by the pseudopotential, v^{PS}_{ion} (r) . All quantities are shown as a function of distance, *r*, from the atomic nucleus. The cutoff radius r_c marks the point beyond which the all-electron and pseudo quantities become identical.

To ensure that a pseudo-potential calculation reproduces the same energy differences as an all-electron calculation it is necessary for the pseudo-wave functions to be identical to the all-electron wave functions outside the core. This condition is called `norm-conservation'.

There are a number of different methods for generating pseudo-potentials. The two most widely used methods are the norm conserving approach of Kleinman and Bylander [48] and the ultrasoft approach of Vanderbilt [49]. Norm-conservation refers to the constraint that the charge within the core radius for the true system is equal to the charge within the core radius for the pseudo wavefunction. With ultrasoft pseudopotentials this constraint is relaxed and therefore a more slowly varying pseudopotential can be chosen, further reducing the number

of plane waves required. Ultrasoft pseudopotentials also show better transferability between different condensed matter systems [49].

A.4 .2.1 Ultrasoft Pseudo-potentials (USP)

The idea of ultrasoft pseudopotentials (USP) as put forward by Vanderbilt [49] is that the relaxation of the norm conserving condition can be used to generate much smoother (softer) potentials. Therefore the pseudo-wave functions are allowed to be as soft as possible within the core region, so that the cutoff energy can be reduced dramatically. The total valence density *n*(*r*) is partitioned into so-called hard and soft contributions,

$$n(r) = \sum_n |\emptyset_n(r)|^2 + \sum_{ij} Q_{ij}(r)\langle\emptyset_n|\beta_j\rangle\langle\beta_i|\emptyset_n\rangle \qquad (A.52)$$

Where β_i are projector functions that depend on the ionic positions and the augmentation function $Q_{ij}(r)$ is given by

$$Q_{ij}(r) = \psi_i^*(r)\psi_j(r) - \emptyset_i^*(r)\,\emptyset_j(r) \qquad (A.53)$$

$\psi_i(r)$ are the all-electron wave functions, and $\emptyset_i(r)$ are ultrasoft wavefunctions constructed without satisfying the norm conservation condition .

Typically, the cutoff energy E_{cut} when using ultrasofts is about half that of conventional norm-conserving pseudopotentials, for simple estimates the number of plane-waves scales as $E_{cut}^{3/2}$, therefore approximately one third less plane waves are required in a given calculation.

A.4 .2.2 Norm-conserving pseudopotentials

The main requirement of the pseudo-potential approach is that it reproduces the valence charge density associated with chemical bonds. It has been shown [50] that for pseudo and all-electron wave functions to be identical beyond the core radius, *rc*, it is necessary for the integrals of squared amplitudes of the two functions be the same. This is equivalent to requiring norm-conservation from pseudo wave functions, i.e. that each of them should carry exactly one electron. This condition ensures that the scattering properties of the pseudo potential are reproduced correctly.

Kleinman-Bylander pseudo potentials are norm-conserving, that is, outside the core, the real and pseudo wave functions generate the same charge density. This can be expressed formally as:

$$\int_0^{rc} \psi_{AE}^*(r)\psi_{AE}(r)dr = \int_0^{rc} \psi_{ps}^*(r)\psi_{ps}(r)dr \qquad (A.54)$$

Where $\psi_{AE}(r)$ is the all electron wave function (*i.e.* the Kohn-Sham orbital that would be obtained from a calculation involving all electrons), and $\psi_{ps}(r)$ is the pseudo wave function [51]. Relaxation of the norm conservation condition leads to Vanderbilt ultrasoft potentials [49]; instead, a generalised eigenvalue formalism is adopted. A non-local overlap operator is defined through

$$s = 1 + \sum_{ij} Q_{ij} \, |\beta_i\rangle\langle\beta_i| \tag{A.55}$$

Where β_i are projector functions depending upon ionic positions and the Q_{ij} are the matrix elements

$$Q_{ij} = \langle\psi_i|\psi_j\rangle - \langle\emptyset_i|\emptyset_j\rangle \tag{A.56}$$

Where ψ are the all-electron wave functions, whilst ϕ are pseudo wave functions. The norm-conservation condition is recovered when $Q_{ij} = 0$. The non-local potential may then be written as:

$$V_{non-local} = \sum_{ij} B_{ij} + \epsilon_i Q_{ij} \, |\beta_i\rangle\langle\beta_i| \tag{A.57}$$

B is the matrix whose elements are formed from

$$\mathrm{B_{ij}} = \langle\phi_\mathrm{i}|\chi_\mathrm{j}\rangle \tag{A.58}$$

and χ is a local wave function. The ϕ_i are then solutions of the generalised eigenvalue problem

$$(\mathrm{H}-\epsilon_\mathrm{i}\mathrm{S}| - \emptyset_\mathrm{j}\rangle \tag{A.59}$$

So
$$\langle\emptyset_\mathrm{i}|\mathrm{S}|\emptyset_\mathrm{j}\rangle = \langle\psi_\mathrm{i}|\psi_\mathrm{j}\rangle \tag{A.60}$$

and thus the pseudo and all electron wave function amplitudes are the same beyond the cut-off radius value. Relaxation of the norm conserving condition allows smoother wave functions, and hence lower cut-off energies. This is advantageous in reducing the size of the plane wave basis set used, and it is for this reason that Vanderbilt ultra-soft pseudo potentials are amongst the most widely used in the condensed matter community.

A.4 .3 Pseudo-potential Generation

Pseudo-potentials are usually generated from all-electron calculations by self-consistently solving the all-electron Schrödinger equation:

$$\left(-\frac{1}{2}\nabla^2 + \mathrm{V}\right)\psi_\mathrm{l}^{\mathrm{AE}} = \epsilon_\mathrm{l}\psi_\mathrm{l}^{\mathrm{AE}} \tag{A.61}$$

Where $\psi_\mathrm{l}^{\mathrm{AE}}$ is the all-electron wave function with angular momentum quantum number *l*. The resulting valence eigenvalues are then substituted back into the Schrödinger equation, but

with a parameterised pseudo wave function. Inversion of the Kohn-Sham equations with this pseudo wave function then yields the pseudo potential.

Pseudo-potential is not unique: however, it must obey certain criteria:

- The pseudo wave function must be the same as the all-electron wave function outside a radius r_{cut}.
- The core charge produced by both sets of wave functions must be the same. This norm conservation requirement can be relaxed though, as discussed earlier.
- The pseudo wave functions must be continuous at the cut-off radius, as must be the first and second derivatives.
- The valence all-electron and pseudo-potential eigenvalues must be equal.

A.5 Computational Physics: Empirical versus *ab initio* Methods

In order to investigate theoretically systems as complicated as molecular crystals, it is necessary to model the interactions as accurately as possible, whilst ensuring that the calculations remain computationally feasible. The simplest and crudest approaches to this problem rely upon the usage of empirical potentials; that is potentials which are obtained by fitting to various experimentally obtained properties, such as the lattice constant and bulk modulus. However, although empirical potentials can be of use, they are limited by the accuracy of the parameterisation, and correspondingly, their transferability to other environments can be poor. Further, empirical potentials optimised to accurately obtain quantities such as the lattice parameter accurately, may be inadequate for other properties such as lattice dynamical properties, for which they were not designed, leading to further problems of transferability.

In order to derive an empirical potential, it is usual for some assumption to be made concerning the electronic structure of the system under consideration and the bonding mechanisms present. Modeling interactions with no a priori knowledge of the bonding present requires the use of sophisticated *ab initio* or *first principles* methodologies, in which one attempts to solve the Schrödinger equation governing the electronic dynamics. The methodology of choice for such calculations is the density functional theory (DFT). The *ab initio* approach, although more computationally intensive, does possess the advantage of being completely transferable, requiring only that the atomic constituents of the system under consideration be specified. It is thus more intellectually appealing, but moreover, this ensures that it may be used to calculate the properties of systems about which no a priori knowledge exists.

By solving the electronic structure of the system, a deeper understanding of the system's behavior may be gleaned; furthermore, knowledge of the electronic structure then allows a range of properties from equilibrium geometries to thermodynamic properties and equations of state to be obtained without recourse to experimental input. One may also use the output of high quality *ab initio* calculations to parameterise classical potentials allowing the computational restrictions associated with *ab initio* methods to be circumvented. It is for these reasons that in this work an *ab initio* approach is preferred to an empirical one.

A.5.1 CASTEP Code

The CASTEP programme [52-53] is a first principles quantum mechanical code for performing electronic structure calculations. Within the density functional formalism it can be used to simulate a wide range of materials including crystalline solids, surfaces, molecules, liquids and amorphous materials; the properties of any material that can be thought of as an assembly of nuclei and electrons can be calculated with the only limitation being the finite speed and memory of the computers being used. This approach to simulation is extremely ambitious, given that the aim is to use no experimental (empirical) data, but to rely purely on quantum mechanics.

The calculations and methods developed in this thesis were performed using, and implemented in, CASTEP. CASTEP (CAmbridge Serial Total Energy Package) is a package for performing *ab-initio* quantum mechanical atomistic simulations. It employs density functional theory, pseudo-potentials and a plane-wave basis set. Electron-ion interactions are evaluated using ultra-soft (Vanderbilt) pseudo-potentials and the exchange-correlation energy was calculated using the GGA functional.

CASTEP uses special k-points sampling for integration over the Brillouin zone, fast Fourier transforms (FFT) to evaluate matrix elements, and wave function summarization for crystals with point group symmetry higher than P_1. For metallic systems CASTEP introduces partial occupancies for levels close to the Fermi energy (de Vita, 1992).

A.5.2 CASTEP functionality

CASTEP offers the following functionality: solve DFT equations for a given structure; calculate forces on atoms and stress tensor; optimize geometry of a given system, including cell relaxation; calculate electronic structure, including density of states and dispersion along high symmetry directions; calculate optical properties that are due to inter-band electronic transitions; calculate electron density difference maps; display 3D isosurfaces or contour plots

of density, density difference, electrostatic potential, orbitals, etc. CASTEP can treat metals, semiconductors, or insulators, can be used to study charged systems or to perform spin-polarized calculations.

A.6 Conclusion

Density functional theory provides us with a relatively efficient and unbiased tool with which to compute the ground state energy in realistic models of bulk materials and their surfaces. The reliability of such calculations depends on the development of approximations for the exchange-correlation energy functional. Significant advances have been made in recent years in the quality of exchange correlation functional as dependence on local density gradients, and nonlocal exchanges functional have been introduced.

The local density approximation (LDA) is a very simple and remarkably reliable for the structure, elastic moduli, and relative phase stability of many materials but is less accurate for binding energies and details of the energy surface away from equilibrium geometries. The GGA has since become the accepted functional in DFT calculations within condensed matter physics.

CASTEP is a leading code for calculating the properties of materials from first principles. Using density functional theory, it can simulate a wide range of properties of materials proprieties including energetics, structure at the atomic level, vibrational properties, electronic response properties etc. In particular it has a wide range of spectroscopic features that link directly to experiment, such as infra-red and Raman spectroscopies, NMR, and core level spectra.

References

[1] H. Eschrig., The Fundamentals of Density Functional Theory, Edt am Gutenbergplatz, pp 8, 2003.

[2] E. Engel, R. M. Dreizler, Density Functional Theory, Theoretical and Mathematical Physics, An Advanced Course, Springer-Verlag Berlin Heidelberg, 2011 pp 2.

[3] D. Sholl, J. Steckel, density functional theory a practical introduction , john wiley & sons, inc., pp1-7, 2009.

[4] E. Schrödinger. Ann. Physik, 79:361, 1926.

[5] R. Shankar, Principles of Quantum Mechanics, 2nd edition, Kluwer Academic Plenum Publishers, New York, 1994.

[6] M. Born and R. Oppenheimer. Zur Quantentheorie der Molekeln. Ann. Phys. (Leipzig) 84 (20), 457, 1927

[7] J. Behler, B. Delley, S. Lorenz, K. Reuter, and M. Sche_er, Phys. Rev. Lett. 94, 036104, 7, 2005.

[8] J. Behler, K. Reuter, and M. Sche_er, Phys. Rev. B 77, 115421,7, 2008

[9] A. C. Luntz, M. Persson, and G. O. Sitz, J. Chem. Phys. 124, 091101,2006

[10] V. Fock. Z. Phys., 61:126, 1930.

[11] J. C. Slater. Phys. Rev., 81:385, 1951.

[12] D. R. Hartree. Proc. R. Soc. London, A113:621, 1928.

[13] P. Hohenberg and W. Kohn. Phys. Rev., 136:864B, 1964.

[14] W. Kohn and L. J. Sham. Phys. Rev., 140:1133A, 1965.

[15] L. H. Thomas. Proc. Cambridge Philos. Soc., 23:542, 1927.

[16] E. Fermi. Z. Phys., 48:73, 1928.

[17] R. O. Jones and O. Gunnarsson. Rev. Mod. Phys., 61:689, 1989.

[18] G. D. Mahan. Many-Particle Physics. Plenum Press, New York and London, 1990.

[19] R. G. Parr and W. Yang. Density Functional Theory of Atoms and Molecules.Oxford University Press, New York, 1989.

[20] E. Teller. Rev. Mod. Phys., 34:627, 1962.

[21] N. Balázs. Phys. Rev., 156:42, 1967.

[22] E. H. Lieb and F. Y. Wu. Phys. Rev. Lett., 31:681, 1968.

[23] W. Pauli, Z. Physik. 31, 765, 1925.

[24] T. Ziegler, Chem. Rev. 91, 651, 22, 1991.

[25] P. Geerlings, F. D. Proft, and W. Langenaeker, Chem. Rev. 103, 1793, 22, 2003

[26] R. G. Parr and W. Yang, Density-Functional Theory of Atoms and Molecules (Oxford University Press, New York, 22, 1989.

[27] M. R. Dreizler and E. K. U. Gross, Density Functional Theory: An Approach to the Quantum Many-Body Problem (Springer, Berlin, 1990). 22

[28] L. I. Schiff. Quantum Mechanics. McGraw-Hill, 1986.

[29] J. P. Perdew and K. Schmidt, in Density Functional Theory and Its Application to Materials, edited by V. Van Doren (AIP Press, Melville, New York, 2001). 2, 26

[30] J. Hubbard. Proc. R. Soc. London Ser. A, 243:336, 1957.

[31] D. Pines and P. Nozières. Benjamin, Reading, Mass., 1966.

[32] W. J. Carr and A. A. Maradudin. Phys. Rev., 133:A371, 1964

[33] E. Wigner. Phys. Rev., 46:1002, 1934.

[34] J. P. Perdew, J. A. Chevary, S. H. Vosko, K. A. Jackson, M. Pederson, D. J. Singh, and C. Fiolhais. Phys. Rev. B, 46:6671, 1992.

[35] J. P. Perdew, K. Burke, and M. Ernzerhof. Phys. Rev. Lett., 77:3865, 1996.

[36] S. K. Ghosh and R. G. Parr. Phys. Rev. A, 34:785, 1986.

[37] A. D. Becke and M .R. Roussel. Phys. Rev. A, 39:3761, 1989.

[38] A. D. Becke, J. Chem. Phys. 98, 5648 (1993). 27, 75

[39] C. Lee, W. Yang, and R. G. Parr, Phys. Rev. B 37, 785 (1988). 27, 75

[40] N. W. Ashcroft and N. D. Mermin, Solid State Physics, Holt Saunders, Philadelphia, p. 113 (1976).

[41] N. W. Ashcroft and N. D. Mermin. Solid State Physics, Harcourt College Publishers, 1976

[42] H. J. Monkhorst and J. D. Pack, Phys. Rev. B 13, 5188 (1976).

[43] J. C. Phillips, Phys. Rev. 112, 685, 1958.

[44] J. C. Phillips and L. Kleinman, Phys. Rev. 116, 287, 1959.

[45] M. L. Cohen and V. Heine, Solid State Physics 24, 37, 1970.

[46] W. E. Pickett. Pseudopotential methods in condensed matter applications, Comp. Phys. Rep. 9 (3), 115, 1989

[47] M. C. Payne, M. P. Teter, D. C. Allan, T. A. Arias and J. D. Joannopoulos, Rev. Mod. Phys. 64, 1045, 1992.

[48] L. Kleinman and D. M. Bylander, Phys. Rev. Lett. 48, 1425 (1982).

[49] D. Vanderbilt, Phys. Rev. B 41, 7892 (1990).

[50] D. R. Hamann, M. Schlüter, and C. Chiang. Phys. Rev. Lett., 43:1494, 1979.

[51] L. Kleinman and D. M. Bylander Phys. Rev. Lett. 48, 1425, 1982.

[52] Segall, M. D.; Lindan, P. J. D.; Probert, M. J.; Pickard, C. J.; Hasnip, P. J.; Clark, S. J.; Payne, M. C.: First-principles simulation: ideas, illustrations and the CASTEP code. J. Phys. Cond. Matter. 14 , 2717–2744,2002.

[53] Payne, M. C.; Teter, M. P.; Allan, D. C.; Arias, T. A.; Joannopoulos J. D.: Iterative minimization techniques for abinitio totalenergy calculations - molecular-dynamics and conjugate gradients. Rev. Mod. Phys. 64, 1045–1097, 1992.

APPENDIX
DENSITY FUNCTIONAL THEORY

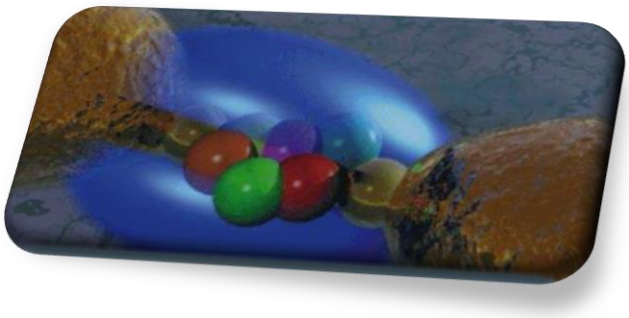

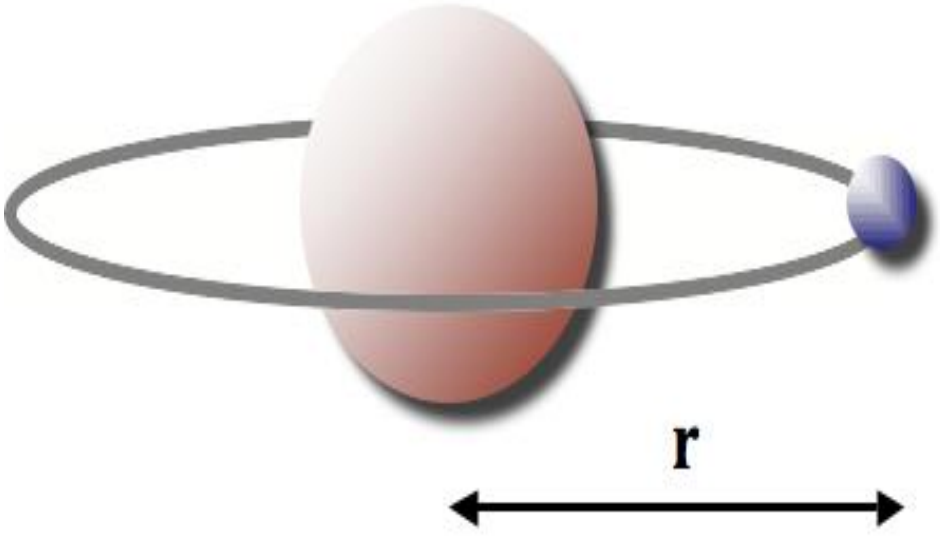

الأطروحة : **دراسة الخصائص البصرية والإلكترونية والهيكلية للمركب زنتل فيزس** KAsSn

اللقب: **قشي** الإسم: **عبلة** المؤطر: **مرابط عبد العالي**

ملخص:

موضوع الأطروحة كان حول الدراسة النظرية للخصائص الهيكلية وفيزيائية للمركب Zintl phase KAsSn. واستندت هده الحسابات على نظرية دالية الكثافة الإلكترونية مع تقريب الانحدار المعمم باستعمال البرنامج CASTEP بغية حساب الخواص البنيوية, ثابت الشبكة عند التوازن المتحصل عليهم مع وجود فجوة أقل من0.87 % ,1.63% و 0.06% (V, c ,a) على التوالي . قمنا بدراسة تأثير الضغط علي الخصائص البنيوية للمركبات المدروسة من أجل T=0 و ضغوط بين 0 GPa 20 .بالمثل تم حساب الثوابت المرونية (Cij) و وحدات مرونة الكريستالات (G) (B), وقدرت على أسس تقريبية من فويت, رويس و هيل. حساباتنا تشير أن هيكل الفرقة الالكترونية لهده المركبات هي أشباه الموصلات مع وجود فجوة مباشرة زائفة تقدر ب 0.34 الكترون فولط. تباين مختلف المعايير البصرية مثل :الدالة العازلة,الامتصاص البصري ,معامل الانكسار, معامل الانقراض , دالة الفقدان البصري و الانعكاسية عند ضغط معدوم لمركباتنا قد تم دراستها. الفجوة الفرقة المباشرة وقوة امتصاص عالية في الطاقة فوق البنفسجية تظهرفعالية الاستخدام لهذا المركب في الأجهزة البصرية الالكترونية.

كلمات مفتاحية: KAsSn زنتل فيزس, كاستب ,التوليف الضغط العالي, الخصائص البصرية, اللالكترونية, البنيوية.

Thesis: **Study of optical, electronic and structural properties of Zintl phase KAsSn**

First name: **GUECHI** Last name: **Abla** Directed by: **Merabet Abdelali**

Abstract:

The thesis has been the subject of theoretical study on the structural and physic al properties of compound Zintl phase KAsSn. The structural, electronic, elastic and optical properties of KAsSn compound have been investigated by employing first principles method using the density-functional theory (DFT) method within the generalized gradient approximation developed by Wu-Cohen (GGA-Wc). The equilibrium geometries of the studied materials have been optimized at 0 K for different pressure values between 0 and 20 GPa by using the CASTEP package. The calculated lattice constants are in good agreement with experiments with a deviation less than 0.87%, 1.63% and 0.06% for a, c and *V* respectively. The single crystal elastic constants (*C*ij) and related properties are calculated using the static finite strain technique, moreover the polycrystalline elastic moduli such as bulk modulus, shear modulus, were estimated using Voigt, Reuss and Hill's (VRH) approximations. Electronic properties have been studied throughout the calculation of band structure, density of states and charge densities. It is shown that this crystal belongs to the semiconductors with a pseudo gap of about 0.34eV. Furthermore, in order to clarify the optical transitions of this compound, linear optical functions including the complex dielectric function, refractive index, extinction coefficient, optical reflectivity, absorption coefficient and loss function were performed and discussed. The direct band gap and high absorption power in the ultraviolet energy range show the effective use of this compound in the optoelectronic devices.

Key words: KAsSn, Zintl phase, high pressure synthesis, CASTEP, optic, electronic, structural properties.

Thèse : **Etude des propriétés optique structural et electronique de phase Zintl KAsSn**

Nom: **GUECHI** Prénom: **Abla** Encadreur: **Merabet Abdelali**

Résumé :

Le travail de thèse a fait l'objet d'une étude théorique sur les propriétés structurales et physiques du composé phase zintl KAsSn. Les propriétés structurales, électroniques, élastiques et optiques du composé phase zintl KAsSn ont été étudiées. Les calculs ont été effectués par la méthode de calcul des ondes planes (PP-PW) avec l'approximation du gradient généralisé de Wu-Cohen (GGA-Wc) implémentée dans le code CASTEP qui se base sur La théorie de la fonctionnelle de la densité (DFT). Les géométries d'équilibres des systèmes étudiés ont été optimisées à T = 0 K pour des pressions entre 0 et 20 GPa via CASTEP. Les paramètres des mailles calculés sont en bon accord avec les expériences avec un écart inférieur à 0.87%, 1.63% et 0.06% pour a, c et V respectivement. De même, les constantes élastiques (Cij) ont été calculées et les modules d'élasticité polycristalline (B et G) ont été estimés en fonction des approximations de Voigt, Reuss et Hill. Nos calculs de la structure de bandes électroniques suggèrent que ce composé est un semi-conducteurs de faible bande gap de l'ordre 0.34eV. La variation des différents paramètres optiques tels que: la fonction diélectrique, l'absorption optique, l'indice de réfraction, le coefficient d'extinction, la fonction de perte optique et la réflectivité à 0 GPa, pour nos composés, a été étudiée. La variation des différents paramètres optiques tels que: la fonction diélectrique, l'absorption optique, l'indice de réfraction, le coefficient d'extinction, la fonction de perte optique et la réflectivité à 0GPa ont été étudiée. La bande interdite directe et le pouvoir d'absorption élevé dans l'ultraviolet montrent l'utilisation efficace de ce composé dans les dispositifs optoélectroniques.

Mots clés :KAsSn, phase Zintl, synthèse a haute pression, CASTEP, propriétés optique, électronique, structurale